

Electronic Thesis and Dissertation Repository

---

8-6-2020 10:00 AM

## A Hybrid PET/MRI Brain Connectivity Approach for Improving Epilepsy Surgical Evaluation

Stefan E. Poirier, *The University of Western Ontario*

Supervisor: Anazodo, Udunna C., *Lawson Health Research Institute*

Co-Supervisor: Thiessen, Jonathan D., *Lawson Health Research Institute*

A thesis submitted in partial fulfillment of the requirements for the Master of Science degree in Medical Biophysics

© Stefan E. Poirier 2020

Follow this and additional works at: <https://ir.lib.uwo.ca/etd>



Part of the [Medical Biophysics Commons](#)

---

### Recommended Citation

Poirier, Stefan E., "A Hybrid PET/MRI Brain Connectivity Approach for Improving Epilepsy Surgical Evaluation" (2020). *Electronic Thesis and Dissertation Repository*. 7164.  
<https://ir.lib.uwo.ca/etd/7164>

This Dissertation/Thesis is brought to you for free and open access by Scholarship@Western. It has been accepted for inclusion in Electronic Thesis and Dissertation Repository by an authorized administrator of Scholarship@Western. For more information, please contact [wlsadmin@uwo.ca](mailto:wlsadmin@uwo.ca).

## **Abstract**

Hybrid PET/MRI can non-invasively improve epileptic focus (EF) localization prior to surgical resection in drug-resistant epilepsy (DRE), especially when MRI is negative. In this thesis, we developed an  $^{18}\text{F}$ -fluorodeoxyglucose (FDG) PET-guided diffusion tractography (PET/DTI) approach to assess white matter (WM) integrity in MRI-negative DRE and evaluated its potential impact on epilepsy surgical planning. To validate the potential of PET/MRI, we first evaluated the diagnostic competence of PET/MRI in DRE and found that PET/MRI provides similar diagnostic information as PET/CT (current clinical standard). For the PET/DTI approach, we used asymmetry index (AI) mapping of FDG-PET to guide WM fiber tractography around glucose hypometabolic brain regions (potential EF). Fiber tractography was repeated in the contralateral brain region (opposite to EF), which served as a control for this study. WM fibers were quantified by calculating the fiber count, mean fractional anisotropy (FA), mean fiber length, and mean cross-section of each fiber bundle. WM integrity was assessed through fiber visualization and by normalizing ipsilateral fiber measurements to contralateral fiber measurements. The added value of PET/DTI in clinical decision-making was assessed by an experienced epileptologist. In over 60% of the patient cohort ( $n = 14$ ), AI mapping findings were concordant with clinical reports on seizure-onset zone. Mean FA, fiber count, and mean fiber length were decreased in 14/14 (100%), 13/14 (93%), and 12/14 (86%) patients, respectively. PET/DTI improved diagnostic confidence in 10/14 (71%) patients and indicated surgical candidacy be reassessed in 3/6 (50%) patients who had not undergone surgery. FDG-PET coupled with diffusion tractography can be a powerful tool for detecting EF and assessing WM integrity around EF in MRI-negative epilepsy. PET/DTI could further enhance clinical decision-making in epilepsy surgery.

## **Keywords**

PET/MRI, PET/CT, drug-resistant epilepsy, fluorodeoxyglucose, MRI-based attenuation correction, standardized uptake value, asymmetry index, diffusion tractography

## Summary for Lay Audience

Drug-resistant epilepsy (DRE) is a serious neurological condition affecting approximately one in three epilepsy patients. Surgical resection of the seizure-onset zone in the brain can alleviate seizure occurrence and improve quality of life. However, about 50% of DRE patients continue to have seizures after surgery. Poor surgical outcomes can occur when the seizure-onset zone and its relationships with surrounding brain regions are not properly characterized. Furthermore, absence of a clear structural lesion in the brain can further decrease a patient's chances of achieving long-term seizure freedom after surgery. Recent advances in medical imaging have seen the increased use of MRI and PET to non-invasively map out brain structure and function in epilepsy. Specifically, multimodal brain imaging combining PET and MRI (hybrid PET/MRI) can improve detection of the seizure-onset zone prior to surgical resection and could potentially improve surgical outcomes, especially in MRI-negative epilepsy. In this thesis, we developed a hybrid PET/MRI approach combining PET and diffusion tractography to non-invasively assess structural integrity around seizure-onset zones in MRI-negative DRE and then evaluated the potential clinical impact of this PET/MRI approach on epilepsy surgical planning. To validate the potential of PET/MRI, we first assessed the diagnostic competence of PET/MRI in DRE and found that PET/MRI provides similar diagnostic information as PET/CT (current clinical standard). For the PET/MRI approach, we used PET to detect seizure foci as brain regions showing decreased PET activity and then used diffusion tractography to assess structural integrity around seizure foci. The added value of the PET/MRI approach in guiding clinical decision-making was evaluated by a senior neurologist. Our PET/MRI approach revealed structural alterations around seizure foci and improved diagnostic confidence in the majority of our DRE patient cohort. Furthermore, the PET/MRI approach indicated surgical candidacy be reassessed in some patients who had not undergone surgery. PET/MRI can be a powerful tool for detecting seizure foci and assessing structural integrity around seizure foci in DRE. Our hybrid PET/MRI approach could be used to further enhance clinical decision-making in epilepsy surgery.

## Co-Authorship Statement

This thesis contains two manuscripts, the first has been submitted for publication in a scientific journal, the second has been published in a scientific journal. Details regarding authors' contributions to each manuscript are provided below.

**Chapter 2** is an original research article entitled "*An evaluation of the diagnostic competence of hybrid PET/MRI in clinical management of drug-resistant epilepsy*" and has been submitted for publication in "*American Journal of Neuroradiology*" in June 2020 and is currently under review (Manuscript ID: AJNR-20-00760). This manuscript was co-authored by Stefan E Poirier, Benjamin YM Kwan, Michael T Jurkiewicz, Lina Samargandy, Maryssa Iacobelli, David A Steven, Victor Lam Shin Cheung, Gerald Moran, Frank S Prato, R Terry Thompson, Jorge G Burneo, Udunna C Anazodo, and Jonathan D Thiessen. My contributions to the manuscript included analyzing and interpreting the data, and writing the manuscript. Udunna C Anazodo and Benjamin YM Kwan conceived and designed the study. Benjamin YM Kwan, Michael T Jurkiewicz, Lina Samargandy, David A Steven, and Jorge G Burneo provided clinical insight and interpretation. Victor Lam Shin Cheung collected the clinical data. Maryssa Iacobelli assisted in data analysis. Udunna C Anazodo and Jonathan D Thiessen provided supervisory guidance, assisted with data analysis, and edited the manuscript. All the other authors assisted with data interpretation and reviewed the manuscript. All authors read and approved the submitted manuscript draft.

**Chapter 3** is an original research article entitled "*<sup>18</sup>F-FDG PET-guided diffusion tractography reveals white matter abnormalities around the epileptic focus in medically refractory epilepsy: implications for epilepsy surgical evaluation*" and has been published in "*European Journal of Hybrid Imaging*, Volume 4, Article 10" in 2020 (<https://doi.org/10.1186/s41824-020-00079-7>). This manuscript was co-authored by Stefan E Poirier, Benjamin YM Kwan, Michael T Jurkiewicz, Lina Samargandy, David A Steven, Ana Suller-Marti, Victor Lam Shin Cheung, Ali R Khan, Jonathan Romsa, Frank S Prato, Jorge G Burneo, Jonathan D Thiessen, and Udunna C Anazodo. My contributions to the manuscript included developing the image analysis pipeline, analyzing and interpreting the data, and writing the manuscript. Udunna C Anazodo and Benjamin YM Kwan conceived and



designed the study. Benjamin YM Kwan, Michael T Jurkiewicz, Lina Samargandy, David A Steven, and Jorge G Burneo provided clinical insight and interpretation. Victor Lam Shin Cheung and Ana Suller-Marti collected the clinical data. Udunna C Anazodo and Jonathan D Thiessen provided supervisory guidance, assisted with data analysis, and edited the manuscript. All the other authors assisted with data interpretation and reviewed the manuscript. All authors read and approved the final manuscript.

## **Acknowledgments**

First, I would like to thank my supervisors, Dr. Udunna Anazodo and Dr. Jonathan Thiessen, for their ongoing guidance, support, and mentorship in my research studies. Thank you for taking me under your wing as an Undergraduate Student and allowing me the opportunity to grow and develop as a researcher (I cannot believe it has already been four years since I first joined Jonathan's lab! Time flies!). Thank you both for providing a very positive research experience and I cannot wait to see what the future holds.

Thank you to my fellow lab members, past and present, for supporting me and my research endeavours. You were always there if I needed help with work or just needed to chat! I really enjoyed the infamous "Lawson coffee break walks" we took to get away from the office and recharge our minds.

Thank you also to Dr. Michael Jurkiewicz and Dr. Ali Khan for serving on my advisory committee. Your valuable feedback, insight and support was much appreciated, especially when I presented my research at the monthly Epilepsy Imaging Meetings.

I would also like to thank the various clinical collaborators I had the pleasure of working with on this epilepsy project. I would like to thank Dr. Michael Jurkiewicz, Dr. Benjamin Kwan and Dr. Lina Samargandy for allowing me to observe them read patient data and for providing valuable clinical feedback on my project. Thank you Dr. David Steven for allowing me to observe you and your team perform epilepsy surgery so I could gain new insight into epilepsy treatment. Thank you Dr. Jorge Burneo for allowing me to present my Master's work at the CNS epilepsy rounds where I received valuable clinical feedback. Additionally, thank you Dr. Burneo for taking the time out of your busy schedule to meet with me to evaluate the potential clinical impact of my epilepsy research, a meeting that was fundamental in shaping my first published manuscript.

Finally, I would like to thank my family – the most important people in my life. Thank you Mom, Dad, and my dog Sunshyne for always being there for me and supporting me with your unconditional love, especially in the most challenging of times. No words can express my gratitude and how much I appreciate all that you have done for me. Thank you.

# Table of Contents

Abstract .....	ii
Summary for Lay Audience .....	iii
Co-Authorship Statement .....	iv
Acknowledgments.....	vi
Table of Contents.....	vii
List of Tables .....	x
List of Figures.....	xi
List of Abbreviations.....	xv
<b>Chapter 1</b> .....	<b>1</b>
1 Introduction to Epilepsy Imaging.....	1
1.1 Background and Motivation.....	1
1.2 Positron Emission Tomography .....	4
1.2.1 Glucose Hypometabolism in Epilepsy .....	4
1.2.2 Visual PET Assessment .....	5
1.2.3 Quantitative PET Analysis .....	6
1.2.3.1 Statistical Parametric Mapping Analysis .....	6
1.2.3.2 Asymmetry Index Mapping.....	8
1.3 Diffusion Tensor Imaging.....	10
1.3.1 Water Diffusion .....	10
1.3.2 The Diffusion Tensor Model .....	10
1.3.3 Diffusion Tractography.....	12
1.3.4 Diffusion MRI Image Analysis Pipeline.....	15
1.4 Hybrid PET/MRI in Epilepsy Imaging.....	16
1.5 Thesis Objectives .....	17

1.6	References.....	19
<b>Chapter 2</b>	.....	<b>25</b>
2	An evaluation of the diagnostic competence of hybrid PET/MRI in clinical management of drug-resistant epilepsy .....	25
2.1	Introduction.....	25
2.2	Materials and Methods .....	27
2.2.1	Patients .....	27
2.2.2	Data Acquisition .....	28
2.2.3	Qualitative Image Analysis .....	29
2.2.4	Region-Based Quantitative Assessment of PET <sub>MRAC</sub> and PET <sub>CTAC</sub> .....	30
2.2.5	Statistical Analysis.....	31
2.3	Results.....	31
2.4	Discussion.....	39
2.5	Conclusions.....	41
2.6	Acknowledgements .....	41
2.7	References.....	43
<b>Chapter 3</b>	.....	<b>47</b>
3	<sup>18</sup> F-FDG PET-guided diffusion tractography reveals white matter abnormalities around the epileptic focus: implications for epilepsy surgical evaluation.....	47
3.1	Introduction.....	47
3.2	Materials and Methods .....	50
3.2.1	Patients .....	50
3.2.2	Data Acquisition .....	51
3.2.3	DWI Preprocessing.....	52
3.2.4	PET Data Analysis.....	53
3.2.5	PET/MR Image Reading.....	54
3.2.6	PET-Guided Diffusion Tractography (PET/DTI).....	54

3.2.7	Clinical Assessment of PET/DTI Findings .....	56
3.3	Results.....	57
3.3.1	AI Mapping of FDG-PET for EF Localization and Lateralization in MRE .....	57
3.3.2	PET/DTI – Tracking WM Around Glucose Hypometabolic Regions (Suspected EF).....	61
3.3.3	Clinical Assessment of PET/DTI Findings .....	63
3.4	Discussion and Conclusions.....	64
3.5	Supplementary Tables .....	72
3.6	Acknowledgements .....	75
3.7	References.....	75
<b>Chapter 4</b>	.....	<b>83</b>
4	Conclusions and Future Directions .....	83
4.1	Conclusions.....	83
4.2	Future Directions.....	84
4.3	References.....	86
Appendix A:	Empirical evaluation of diffusion tractography pipeline using whole-brain tractograms from a white matter phantom.....	87
Appendix B:	Permission for Reproduction of Scientific Articles and Figures .....	90
Curriculum Vitae	.....	95

## List of Tables

Table 2.1: Study patient demographics and surgical outcomes.....	28
Table 2.2: Qualitative and quantitative regional assessments of diagnostic competency between PET <sub>MRAC</sub> and PET <sub>CTAC</sub> .....	34
Table 2.3: Qualitative and quantitative assessments of diagnostic competency between modalities .....	38
Table 3.1: Patient demographics and clinical profile.....	51
Table 3.2: EEG, PET, and surgical findings .....	60
Table 3.3: Clinical assessment of PET/DTI findings.....	64

## List of Figures

- Figure 1.1: IC-EEG brain monitoring. Electrodes are placed on the surface of the patient’s brain to record seizure events. Image courtesy of Dr. David Steven (Chief/Chair, Neurosurgery, Western University). ..... 2
- Figure 1.2: Visual FDG-PET assessment shows a clear hypometabolic PET ROI (yellow circle), indicative of a potential EF, in the right temporal lobe of an MRI-negative epilepsy patient. Image is displayed using the radiological convention. This patient was confirmed to have right temporal lobe focal epilepsy, determined based on all available diagnostic information. .... 5
- Figure 1.3: SPM analysis can reveal metabolic abnormalities in the brains of epilepsy patients through statistical comparison of FDG-PET images between patients and healthy controls. In this MRI-negative temporal lobe epilepsy cohort, FDG-PET hypometabolism (bright regions using patients < controls) is seen in the middle temporal gyrus. Colorbar represents t-values ( $p < 0.001$  was considered statistically significant). Adapted from Shang et al., Am J Neuroradiol (2018).<sup>20</sup> Image used with permission from the American Society of Neuroradiology. .... 7
- Figure 1.4: Flowchart of a typical AI mapping analysis pipeline. The PET image ( $BP_{ND}$ ) is spatially normalized, smoothed, and then thresholded to account for inter-subject variability in patient anatomy. The thresholded PET image ( $V_{BP}$ ) is flipped about the sagittal plane to generate an AI map ( $V_{AI}$ ). Adapted from Didelot et al., J Nucl Med (2010).<sup>40</sup> ..... 9
- Figure 1.5: Isotropic and anisotropic diffusion tensor ellipsoids with the three eigenvalues labelled. Adapted from Tromp, The Winnower (2016).<sup>50</sup> ..... 12
- Figure 1.6: Schematic representation of streamlines tractography. *Left:* Fiber tractography is initiated using a user-defined seed point (red arrow) and this seed point is used to link voxels with similar diffusion orientation (likely to be connected by a WM fiber pathway). *Right:* Streamlines are propagated along the fiber orientation path at an incremental distance called the step size (mm). Too large of a step size (white dots) can cause the streamline to deviate

off-course, leading to inaccurate fiber reconstruction. Adapted from Mori & Tournier (2013).<sup>59</sup> Image used with permission from Elsevier..... 14

Figure 1.7: Diffusion MRI image analysis pipeline. DWI data were preprocessed using a variety of different image processing software packages to generate an FA map and images that can be used to visualize WM fiber pathways in the brain using diffusion tractography.. 15

Figure 1.8: Raw DWI data from an epilepsy patient preprocessed using our in-house diffusion MRI image analysis pipeline to generate WM fiber pathways in the brain via diffusion tractography. .... 16

Figure 2.1: Comparison of visual PET assessment between PET<sub>MRAC</sub> and PET<sub>CTAC</sub> in an MRI-negative epilepsy patient (patient #2). A) SUV images are well matched between PET<sub>MRAC</sub> and PET<sub>CTAC</sub>. B) Z-score maps show exaggerated regional hypometabolism (especially in the left temporal lobe) in PET<sub>MRAC</sub>. C) Slices of percent difference SUV ( $\Delta$ SUV) map show low quantitative bias between PET<sub>MRAC</sub> and PET<sub>CTAC</sub>. .... 32

Figure 2.2: Association between PET<sub>MRAC</sub> and PET<sub>CTAC</sub> across all brain regions in 18 DRE patients. A) Regression plots show a tight correlation in mean SUV ( $r = 0.99$ ,  $p < 0.001$ ) and mean  $Z_{db}$  ( $r = 0.92$ ,  $p < 0.001$ ) between modalities. B) Bland-Altman plots reveal close agreement in SUV (bias: -0.23 to 0.93) and  $Z_{db}$  (bias: -1.31 to 1.21) between PET<sub>MRAC</sub> and PET<sub>CTAC</sub>. .... 33

Figure 2.3: Mean SUV and  $Z_{db}$  values ( $n=18$ ) in thirty-six *a priori* brain regions often interrogated in DRE. MRAC and CTAC produce similar mean SUV,  $Z_{db}$  and in most cases matched outliers (black dots) across all brain regions ( $p > 0.05$ ). .... 35

Figure 2.4: Group percent difference in SUV (*left*) and absolute difference in  $Z_{db}$  (*right*) between PET<sub>MRAC</sub> and PET<sub>CTAC</sub> in thirty-six *a priori* brain regions often interrogated in DRE. Error bars indicate standard deviation. Mean MRAC SUV and  $Z_{db}$  biases across all thirty-six *a priori* brain regions were  $-4.02 \pm 2.03\%$  and  $0.35 \pm 0.27$ , respectively. Most brain regions have  $<5\%$  SUV<sub>MRAC</sub> bias or  $<0.5$   $Z_{db}$ -MRAC bias except regions in lateral aspects at the base of the skull (denoted with an \*). Abbreviations: cb, cerebellum; front, frontal lobe; fg, fusiform gyrus; gr, gyrus rectus; Hg, Heschl’s gyrus; hipp, hippocampus; itg, inferior



temporal gyrus; ins, insula; mtl, mesial temporal lobe; mtg, middle temporal gyrus; occ, occipital lobe; phg, parahippocampal gyrus; par, parietal lobe; stg, superior temporal gyrus; temp, temporal lobe; tp:mtg, temporal pole: middle temporal gyrus; tp:stg, temporal pole: superior temporal gyrus; thal, thalamus. .... 36

Figure 2.5: Visual assessment reveals similar A) attenuation correction, B) SUV, C)  $Z_{db}$  and D)  $Z_{AI}$  maps ( $L < R$ ) between  $PET_{MRAC}$  and  $PET_{CTAC}$  in one DRE patient (patient #11). .... 38

Figure 3.1: 2D representation of the 3D procedure for tracking WM regions around the EF in one MRE patient (patient #9). A) EF (detected by AI mapping of FDG-PET) overlaid onto structural MRI. B) EF overlaid onto a WM probability map. Because the EF is located in a cortical area (left hippocampus), WM tracking was performed at three distances away from the EF: 3 mm, 9 mm, and 15 mm. The coloured regions around the EF represent WM areas covering the three distances. These WM regions were used as seed ROIs to initiate neural fiber bundle tracking in Fibernavigator..... 56

Figure 3.2: Images from a 45 year old female MRE patient (patient #9) with a clinical hypothesis of left temporal lobe focal epilepsy: A) PET SUV map; B) Anatomical MRI; C) PET fused with MRI; D) Z-score map from computer-assisted diagnosis of PET data (Siemens Syngo Via); E) Z-score map generated from AI mapping ( $Z_{AI}$  map), which shows a clear glucose hypometabolic region (green circle) in the left temporal lobe, indicative of a potential EF; and F) hypometabolic PET ROI (yellow) from AI mapping overlaid onto structural MRI..... 58

Figure 3.3: PET-guided diffusion tractography in one MRE patient (patient #9) with a clinical hypothesis of left temporal lobe focal epilepsy. Ipsilateral (left) and contralateral (right) WM fibers (coloured lines) are shown for the three WM distances (3, 9, and 15 mm) away from the EF (yellow) identified by AI mapping of FDG-PET. Fewer WM fibers are observed on the ipsilateral side. Differences in WM fibers between ipsilateral and contralateral sides appear more prominent at closer distances (3 mm) to the EF. Abbreviations: L, left; R, right..... 61

Figure 3.4: Quantification of WM fibers around the hypometabolic PET ROI (suspected EF) in 14 MRE patients. Ipsilateral fiber measurements were normalized to contralateral fiber

measurements as a preliminary measure of WM tract asymmetry. Normalized values are plotted for the three distances away from the PET ROI. Wilcoxon signed-rank test was used to compare normalized fiber measurements across the three distances into surrounding WM ( $p < 0.05$  was considered significant). Fiber count, mean fiber length, and mean FA are decreased at closer distances to the PET ROI (3 mm) compared to 15 mm ( $p < 0.05$ ).

Abbreviations: \* $p \leq 0.05$ , \*\* $p \leq 0.01$ , \*\*\* $p \leq 0.001$ . ..... 62

## List of Abbreviations

<b>AED</b>	Anti-epileptic drug
<b>AI</b>	Asymmetry index
<b>ANTS</b>	Advanced normalization tools
<b>BW</b>	Body weight
<b>CS</b>	Cross-section
<b>CSF</b>	Cerebrospinal fluid
<b>CT</b>	Computed tomography
<b>CTAC</b>	CT-based attenuation correction
<b>df</b>	Degrees of freedom
<b>DRE</b>	Drug-resistant epilepsy
<b>DTI</b>	Diffusion tensor imaging
<b>DWI</b>	Diffusion-weighted imaging
<b>EEG</b>	Electroencephalography
<b>EF</b>	Epileptic focus
<b>EMU</b>	Epilepsy monitoring unit
<b>EPI</b>	Echo-planar imaging
<b>FA</b>	Fractional anisotropy
<b>FDG</b>	<sup>18</sup> F-fluorodeoxyglucose
<b>FLAIR</b>	Fluid-attenuated inversion recovery

<b>fMRI</b>	Functional MRI
<b>FOD</b>	Fiber orientation distribution
<b>FSL</b>	FMRIB's Software Library
<b>FWHM</b>	Full-width at half-maximum
<b>GM</b>	Gray matter
<b>IB</b>	Invalid bundles
<b>IC</b>	Invalid connections
<b>IC-EEG</b>	Intracranial EEG
<b>MNI</b>	Montreal Neurological Institute
<b>MPRAGE</b>	Magnetization-prepared rapid gradient-echo
<b>MRAC</b>	MRI-based attenuation correction
<b>MRE</b>	Medically refractory epilepsy
<b>MRI</b>	Magnetic resonance imaging
<b>PET</b>	Positron emission tomography
<b>PET/DTI</b>	PET-guided diffusion tractography
<b>RESOLUTE</b>	Region specific optimization of continuous linear attenuation coefficients based on UTE
<b>ROI</b>	Region of interest
<b>SEEG</b>	Stereo-EEG
<b>SOZ</b>	Seizure-onset zone

<b>SPACE</b>	Sampling perfection with application optimized contrasts using different flip angle evolution
<b>SPM</b>	Statistical parametric mapping
<b>SUV</b>	Standardized uptake value
<b>SUV<sub>r</sub></b>	Relative SUV
<b>VB</b>	Valid bundles
<b>VC</b>	Valid connections
<b>VEEG</b>	Video-EEG
<b>VOI</b>	Volume of interest
<b>WM</b>	White matter
<b>Z<sub>AI</sub></b>	Z-score AI
<b>Z<sub>db</sub></b>	Z-score SUV (compared to normal PET/CT database)

## Chapter 1

### 1 Introduction to Epilepsy Imaging

#### 1.1 Background and Motivation

Epilepsy affects approximately 50 million people worldwide and is a chronic neurological disorder characterized by seizures – spontaneous, synchronized neuronal activity – arising from pathological changes to brain networks.<sup>1,2</sup> Seizures typically originate in a brain region called the epileptic focus (EF) and then propagate throughout surrounding neural networks.<sup>3,4</sup> While the exact underlying physiological mechanisms responsible for seizure activity remain unknown<sup>5</sup>, one potential mechanism for seizure propagation may be due to removal of interneuronal inhibition by abnormally arranged neural networks around the EF.<sup>6</sup> Failure to control seizures in epilepsy has been associated with increased societal burden and in some patients, may lead to anxiety, depression, and chronic migraines.<sup>5</sup>

Epilepsy is usually treated in the clinical setting using either medication, dietary restrictions, surgery, or neurostimulation.<sup>5</sup> When a patient is first diagnosed with epilepsy, anti-epileptic drugs (AEDs) are often administered in an attempt to control seizures. Most epilepsy patients achieve full seizure control after being administered AEDs, however, approximately 30% of epilepsy patients have drug-resistant epilepsy (DRE).<sup>3,4,7</sup> DRE is a serious neurological condition that is clinically diagnosed when seizures persist after administering at least two adequate trials of AEDs.<sup>8</sup> If left untreated, DRE can lead to progressive memory decline, psychological impairment, social stigmatization, decreased quality of life, and increased risk of sudden death in epilepsy (SUDEP).<sup>2,5,8</sup>

DRE can be treated by surgically removing the EF which is a viable option for alleviating seizure occurrence and improving overall quality of life.<sup>9,10</sup> However, only about 50% of DRE patients achieve long-term seizure freedom after surgery.<sup>11,12</sup> Poor surgical outcomes can occur when the EF and its relationships with surrounding neural networks are poorly characterized prior to surgical resection.<sup>13</sup> Past studies have shown that

patients with multifocal epilepsy or epilepsy involving the eloquent cortex are at increased risk of post-surgical complications such as visual, speech, motor, or cognitive impairments.<sup>3,4,8,14</sup> Accurate localization of the EF and proper characterization of surrounding neural networks are therefore crucial to improving surgical outcomes and ensuring long-term seizure freedom in DRE.

Before surgery, DRE patients undergo presurgical evaluation to detect the EF and assess potential surgical candidacy. Presurgical evaluation protocols typically consist of patient history, neuropsychological assessment, and prolonged scalp video-electroencephalography (VEEG) to record seizure events in the brain.<sup>7</sup> The current gold standard for localizing the EF is intracranial EEG (IC-EEG), where surgeons place electrodes in or around the patient's scalp to record seizure events<sup>15,16</sup> (see **Figure 1.1**).



**Figure 1.1: IC-EEG brain monitoring.** Electrodes are placed on the surface of the patient's brain to record seizure events. Image courtesy of Dr. David Steven (Chief/Chair, Neurosurgery, Western University).

However, IC-EEG is an invasive procedure that is expensive, time-consuming and carries risk of side effects such as hemorrhage, edema, or infection.<sup>7,16</sup> Structural brain imaging

using magnetic resonance imaging (MRI) has been effective in reducing costs and improving patient quality of care by aiding or minimizing IC-EEG use. MRI can identify structural lesions (EF) that may be removed by surgical resection if MRI findings are concordant with VEEG and IC-EEG.<sup>7,9</sup> However, approximately one in four DRE patients have an EF that is not visible (non-lesional) and cannot be detected by MRI.<sup>17</sup> Consequently, past studies have shown that patients with no clear lesion on anatomical MRI (MRI-negative epilepsy) are likely to have recurrent seizures after surgery.<sup>11,12</sup> Thus, MRI-negative epilepsy has brought on an increasing demand for improved non-invasive methods for localizing the EF prior to surgical resection.

Recent advances in neuroimaging have provided alternative, non-invasive ways to visualize brain structures *in vivo* and may have promising applications in epilepsy surgical evaluation. In MRI-negative epilepsy, functional brain imaging using <sup>18</sup>F-fluorodeoxyglucose positron emission tomography (FDG-PET) can identify the EF as brain areas showing decreased FDG uptake, also known as glucose hypometabolism.<sup>7,10,13,18</sup> While FDG-PET is now well established in most epilepsy surgical centers, utility of PET in epilepsy surgery continues to evolve.<sup>7</sup> Recent studies have also shown that advanced MRI techniques such as diffusion tensor imaging (DTI) can map out white matter fiber pathways in the brain to investigate structural connections between the EF and surrounding neural networks.<sup>5,13</sup>

Although separate FDG-PET and MRI brain scanning remains the current clinical standard-of-care for epilepsy imaging, some DRE patients continue to have seizures after surgical treatment especially when MRI is negative or equivocal.<sup>10</sup> Separate acquisition of PET and MRI, which can be several months apart, can introduce registration bias and may lead to inaccurate EF localization responsible for surgical failure.<sup>19,20</sup> There is emerging evidence that multimodal brain imaging combining PET and MRI may further improve sensitivity of EF detection over standalone PET, MRI, or IC-EEG.<sup>7</sup> Indeed, simultaneous acquisition of PET and MRI using hybrid PET/MRI may shed new insight into DRE pathophysiology and could potentially improve surgical outcomes especially in MRI-negative epilepsy.<sup>20-24</sup> Furthermore, while clinical adoption of hybrid PET/MRI is



beginning to take place in some epilepsy surgical centers, the potential utility of combined PET and DTI in epilepsy surgical evaluation is still yet to be fully assessed.

## **1.2 Positron Emission Tomography**

### **1.2.1 Glucose Hypometabolism in Epilepsy**

Positron emission tomography (PET) is a functional imaging modality that is now widely accepted as clinical standard-of-care in most epilepsy surgical centers. Absence of a clear lesion on anatomical MRI is a common indication for PET in DRE.<sup>7</sup> While other PET tracers have been proposed for epilepsy brain imaging, <sup>18</sup>F-fluorodeoxyglucose PET (FDG-PET) has become well established as the most sensitive functional imaging approach for detecting the EF especially when MRI is negative or equivocal.<sup>7,18</sup> In MRI-negative DRE, interictal FDG-PET can detect the EF as brain regions showing decreased FDG uptake (glucose hypometabolism).<sup>7,10,13,18</sup> Glucose hypometabolism, which can be observed both within the EF and in surrounding neural networks<sup>13,18</sup>, has been associated with spread of epileptic activity<sup>25</sup> as well as cognitive impairment.<sup>26</sup> Furthermore, severity and location of FDG-PET hypometabolism in epilepsy may predict surgical outcome.<sup>18,27</sup> In temporal lobe epilepsy, extent of FDG-PET hypometabolism within the EF has been correlated with long-term seizure freedom after surgery.<sup>28,29</sup> Conversely, FDG-PET hypometabolism that extends beyond the EF, which can occur in bitemporal and extratemporal epilepsies, may lead to poor surgical outcome.<sup>27,30,31</sup> While the exact mechanisms underlying glucose hypometabolism in epilepsy remain unclear, some studies have suggested that decreased synaptic activity due to neuron loss from recurrent epileptic insults may be responsible for the metabolic alterations observed in DRE.<sup>25,32</sup> Neuronal damage has been previously observed using histopathological staining<sup>33</sup> and may be responsible for metabolic abnormalities in and around the EF.<sup>25</sup> Interestingly, suppression of glucose activity in DRE may also be due to inhibition of afferent signals between the EF and surrounding healthy brain tissue as a potential protective mechanism against further seizure-associated insult.<sup>25,34</sup> Nevertheless, utility of FDG-PET in epilepsy is evident and further investigation of metabolic dysfunction, as well as its association with neuronal damage, may shed new insight into DRE pathophysiology and could potentially improve surgical outcomes, especially in MRI-negative epilepsy.

### 1.2.2 Visual PET Assessment

Glucose hypometabolic regions of interest (ROIs) are typically identified by visual inspection of FDG-PET images. An example of visual PET assessment revealing a hypometabolic ROI (potential EF) in the right temporal lobe of an MRI-negative DRE patient is provided in **Figure 1.2**. During epilepsy surgical evaluation, visual FDG-PET assessment can guide electrode placement in the brain during IC-EEG as well as alter the decision to perform surgery if FDG-PET findings agree with EEG and electrophysiological reports.<sup>7,28,35</sup>

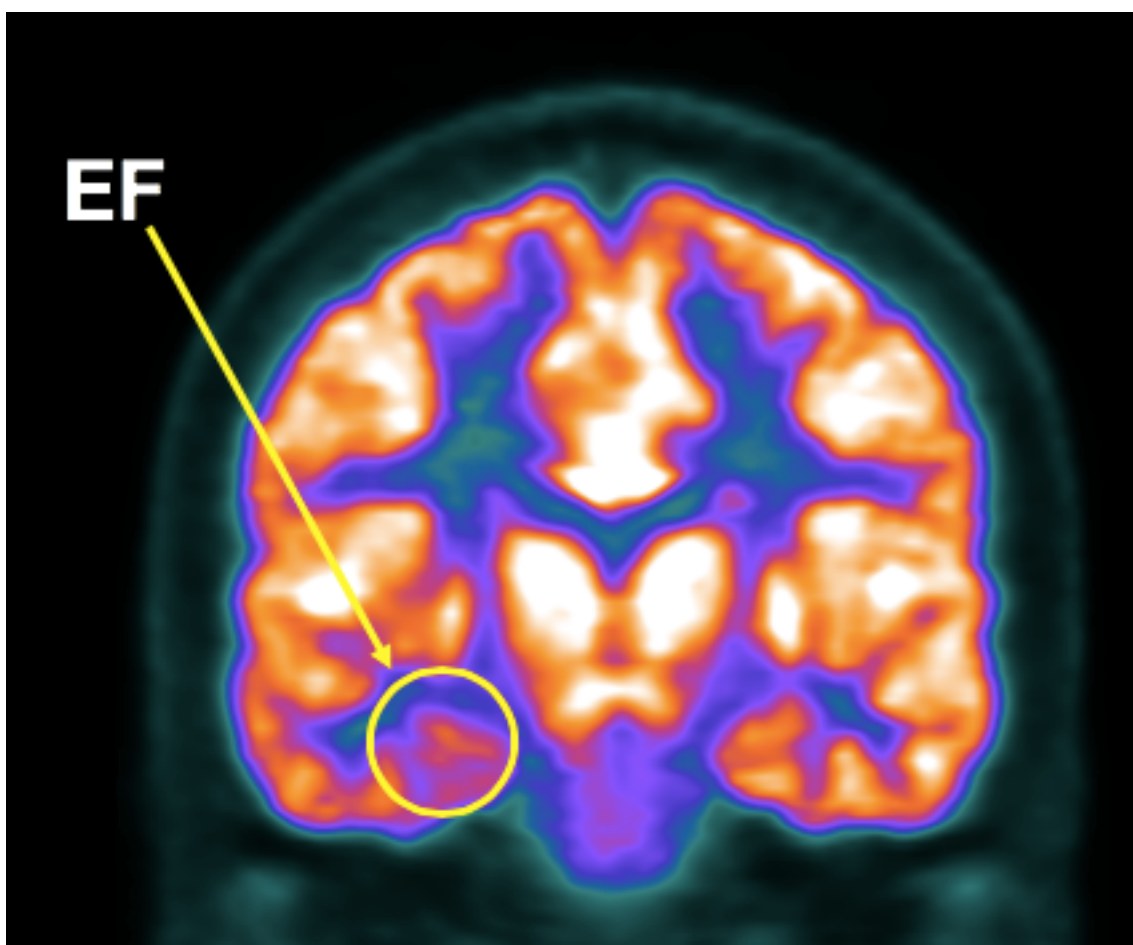


**Figure 1.2:** Visual FDG-PET assessment shows a clear hypometabolic PET ROI (yellow circle), indicative of a potential EF, in the right temporal lobe of an MRI-negative epilepsy patient. Image is displayed using the radiological convention. This patient was confirmed to have right temporal lobe focal epilepsy, determined based on all available diagnostic information.

### 1.2.3 Quantitative PET Analysis

Although visual FDG-PET assessment is well established as routine clinical practice in diagnosis of functional pathologies in epilepsy, visual reads are subject to inter-reader variability and some hypometabolic brain regions, especially when subtle, can be missed altogether.<sup>20,36,37</sup> As such, efforts have been made to develop more objective, quantitative approaches to aid visual detection of hypometabolic PET ROIs (potential EF). Early attempts to quantify FDG-PET in epilepsy measured metabolic asymmetries using manually defined *a priori* brain regions commonly interrogated in visual reads<sup>38,39</sup>, however, this approach was problematic as it still required manual implementation and results varied between studies due to different ROI-defining criteria.<sup>37</sup> Fortunately, this approach has been abandoned and FDG-PET quantification has migrated towards more advanced neuroimaging techniques that use semi-quantitative PET analyses, such as statistical parametric mapping (SPM) (Wellcome Department of Cognitive Neurology, Institute of Neurology, London) and asymmetry index (AI) mapping<sup>40</sup>, to automate detection of metabolic abnormalities on PET. Several studies have shown that semi-quantitative PET analysis can produce metabolic findings consistent with visual FDG-PET assessment and may be a reliable tool for aiding EF localization in DRE.<sup>20,36,37,40–43</sup> Consequently, visual FDG-PET readings are now typically augmented using statistical comparison of metabolic values between patients and a healthy control database for further improving detection of regional FDG-PET abnormalities in epilepsy.

#### 1.2.3.1 Statistical Parametric Mapping Analysis

Statistical parametric mapping (SPM) is a voxel-based analysis approach that statistically assesses differences in voxel intensities between two groups of interest (typically a patient group and a healthy control group).<sup>36,37,41</sup> In epilepsy patients, SPM analysis of FDG-PET can be used to detect metabolic brain abnormalities through statistical comparison of standardized uptake value (SUV) – activity concentration over time normalized by net injected dose of FDG and the patient’s body weight – between epilepsy patients and healthy controls, as is illustrated in **Figure 1.3**.<sup>20</sup> This group-wise SUV analysis is typically conducted using a user-defined statistical threshold after spatially normalizing the patient and control PET data to a standard space and correcting

for global metabolism effects in the brain using an appropriate proportional scaling technique.<sup>37</sup> However, a limitation is that SPM analysis of FDG-PET assesses group-level differences in SUV and thus can sometimes fail to detect metabolic abnormalities, especially interhemispheric asymmetries, in individual patients.<sup>37,43</sup>

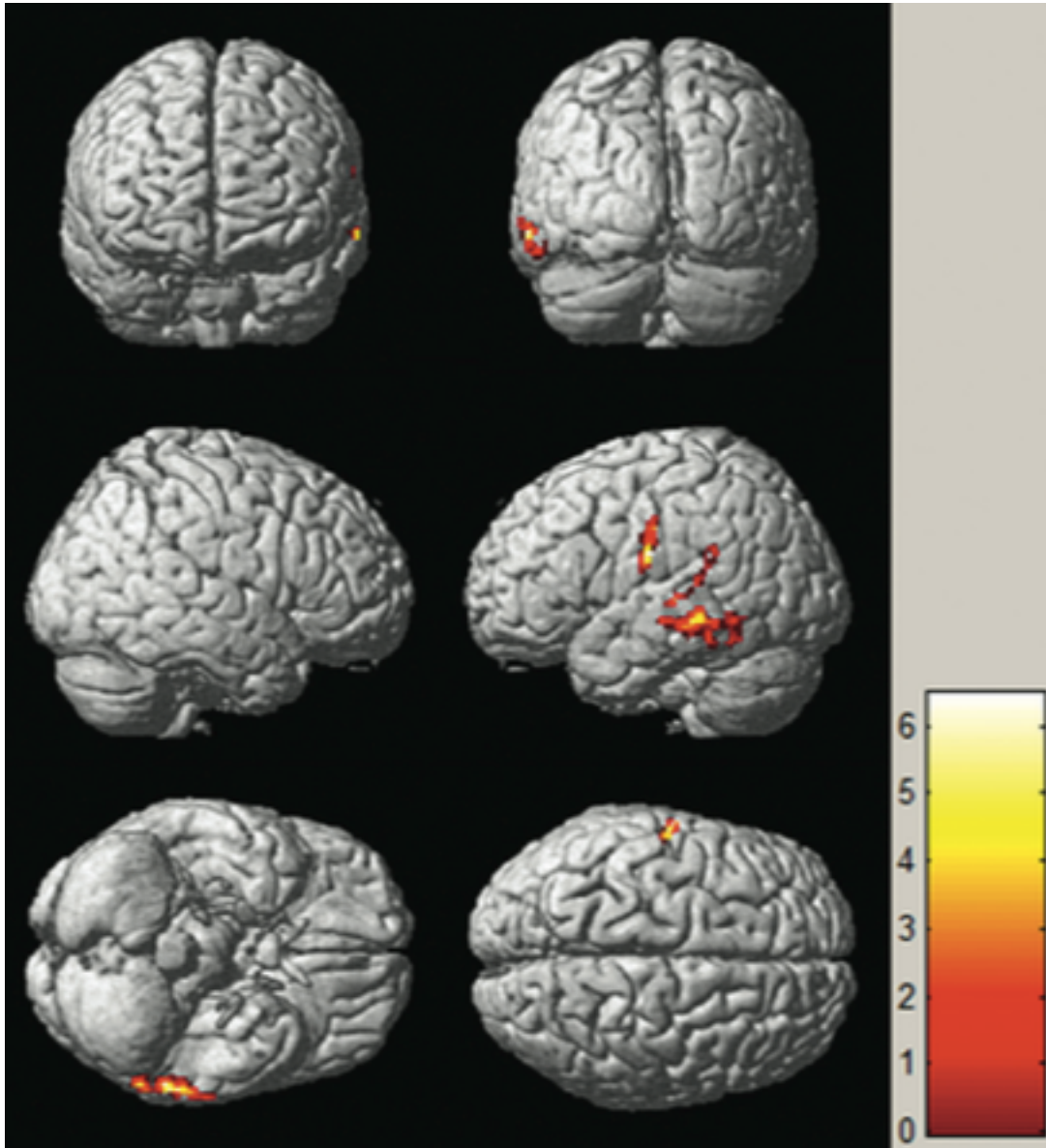


**Figure 1.3:** SPM analysis can reveal metabolic abnormalities in the brains of epilepsy patients through statistical comparison of FDG-PET images between patients and healthy controls. In this MRI-negative temporal lobe epilepsy cohort, FDG-PET hypometabolism (bright regions using patients < controls) is seen in the middle temporal gyrus. Colorbar represents t-values ( $p < 0.001$  was considered statistically significant). Adapted from Shang et al., *Am J Neuroradiol* (2018).<sup>20</sup> Image used with permission from the American Society of Neuroradiology.

### 1.2.3.2 Asymmetry Index Mapping

To overcome the group-wise limitation of SPM analysis, other semi-quantitative approaches such as asymmetry index (AI) mapping have been proposed to further improve specificity of FDG-PET in DRE localization. AI mapping of FDG-PET is an automated data-driven approach that calculates the voxel-wise difference in glucose metabolism between hemispheres and can be used to assess metabolic asymmetries in individual epilepsy patients by considering the contralateral hemisphere (with respect to EF) as an inherent control.<sup>20,40,43</sup> An example of the typical AI mapping analysis workflow is shown in **Figure 1.4**.<sup>40</sup> After spatially normalizing the patient's FDG-PET data to a standard space, the FDG-PET image is flipped about the sagittal plane and a voxel-wise AI map is calculated as the difference between the unflipped and flipped images. The AI map is then converted to a z-score AI ( $Z_{AI}$ ) map, where voxels with negative  $Z_{AI}$  represent FDG-PET hypometabolism (relative to the contralateral homologous brain region).<sup>43</sup> Lastly, the  $Z_{AI}$  map is thresholded by a user-defined negative  $Z_{AI}$  value to isolate significant metabolic asymmetries on FDG-PET (potential EF) as brain regions showing the largest decrease in  $Z_{AI}$ .<sup>40,43</sup> Past studies have demonstrated that AI mapping can successfully detect seizure-onset zones showing FDG-PET hypometabolism (sensitivity: 65-70%) in concordance with clinical reports and electrophysiological findings<sup>37,42,43</sup>, suggesting that AI mapping of FDG-PET could be a very sensitive biomarker for epileptogenicity and may be a promising tool for improving EF localization in DRE.

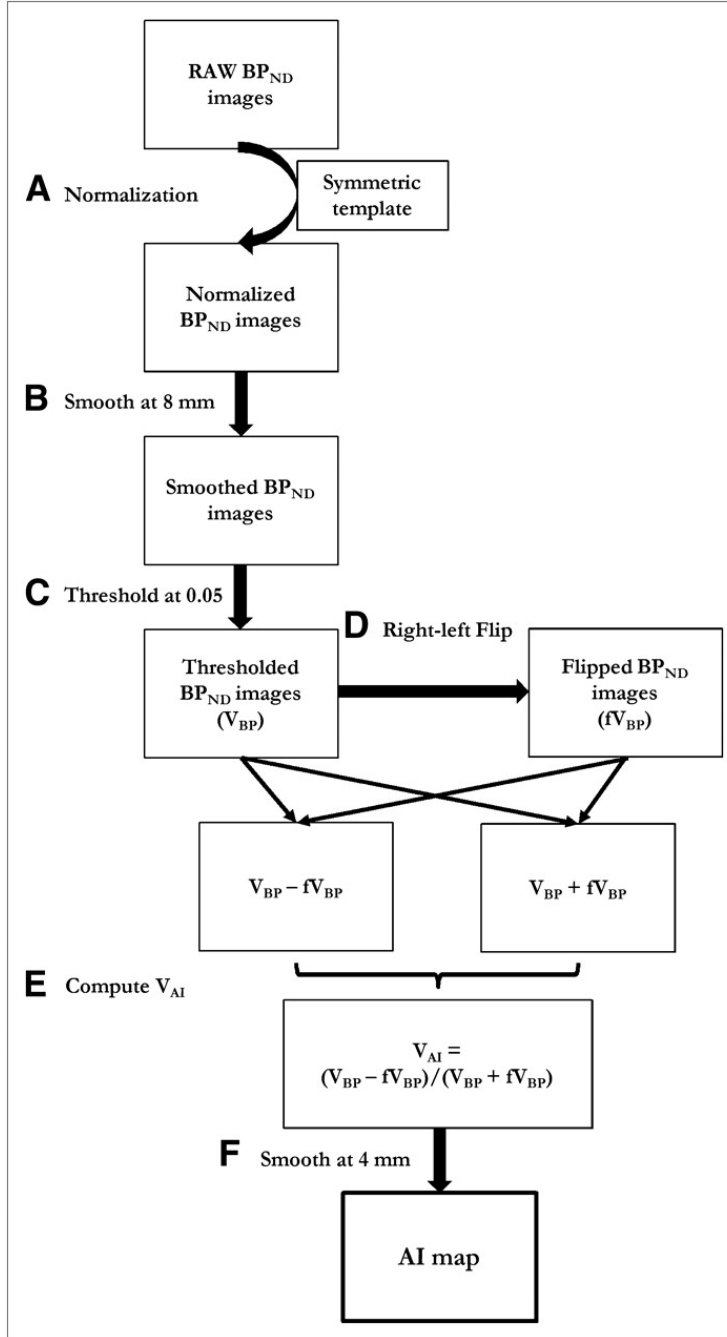


**Figure 1.4: Flowchart of a typical AI mapping analysis pipeline.** The PET image ( $BP_{ND}$ ) is spatially normalized, smoothed, and then thresholded to account for inter-subject variability in patient anatomy. The thresholded PET image ( $V_{BP}$ ) is flipped about the sagittal plane to generate an AI map ( $V_{AI}$ ). Adapted from Didelot et al., J Nucl Med (2010).<sup>40</sup>

## 1.3 Diffusion Tensor Imaging

### 1.3.1 Water Diffusion

In the human body, water diffuses in tissue at the microscopic level. This diffusion is commonly referred to as Brownian motion, which is defined as random molecular movement due to thermal motion.<sup>44</sup> Diffusion tensor imaging (DTI) is an advanced MRI method that models diffusion of water molecules in the brain and can be used to effectively characterize tissue microstructure *in vivo*.<sup>13,45,46</sup> By non-invasively probing tissue microstructure, DTI can infer information about tissue integrity and structural organization in the brain.<sup>44,47,48</sup>

Water diffusion is not the same in all tissue types. In gray matter (GM) and cerebral spinal fluid (CSF), water diffuses approximately the same in all directions (isotropic diffusion) at the spatial resolution of our DTI measurements (~2 mm), while in white matter (WM), water preferentially diffuses along the fiber bundle pathway (anisotropic diffusion).<sup>47,49</sup> The anisotropic water diffusion in WM is believed to be due to the physical arrangement of axons that permit water movement parallel to the fiber bundle, but hinder water movement in the perpendicular direction.<sup>49</sup> Loss of anisotropic water diffusion in WM can be associated with microstructural tissue breakdown and is implicated in many neurological and neurodegenerative disorders, such as epilepsy, stroke, multiple sclerosis, and Alzheimer's Disease.<sup>49</sup>

### 1.3.2 The Diffusion Tensor Model

DTI can non-invasively assess tissue microstructure in the brain using a diffusion tensor – a mathematical construct used to model water diffusion – which can be visualized as a 3D object and describes the movement of water diffusion at a particular voxel in the brain (see **Figure 1.5**).<sup>50</sup> Specifically, the shape of the diffusion tensor is characterized by three eigenvalues ( $\lambda_1, \lambda_2, \lambda_3$ ) and three eigenvectors ( $v_1, v_2, v_3$ ) representing the magnitude and direction of water diffusion along the major axes of the tensor, respectively.<sup>44,50</sup> Thus, the diffusion tensor can describe physical properties of biological tissue, especially in WM pathways in the brain where water diffusion is inherently anisotropic, by providing

information about the degree of diffusion anisotropy as well as structural orientation of neuronal fibers.<sup>49</sup>

Diffusion tensors have important applications in the assessment of WM pathways known to be implicated in a variety of neurological disorders, including epilepsy. WM pathways in the brain can be characterized using DTI-derived scalar values, which are generated by fitting diffusion tensors to the diffusion-weighted imaging (DWI) data.<sup>47,51,52</sup> A common tensor-derived parameter used to assess WM fiber pathways is fractional anisotropy (FA), which measures the degree to which water preferentially diffuses along the length of the fiber bundle.<sup>44,46,51</sup> Mathematically, FA is defined as:

$$FA = \sqrt{\frac{1}{2} \frac{\sqrt{(\lambda_1 - \lambda_2)^2 + (\lambda_1 - \lambda_3)^2 + (\lambda_2 - \lambda_3)^2}}{\sqrt{\lambda_1^2 + \lambda_2^2 + \lambda_3^2}}}, \quad (1.1)$$

where  $\lambda_1$ ,  $\lambda_2$ , and  $\lambda_3$  are the three eigenvalues in the diffusion tensor.<sup>50</sup> The three eigenvalues are calculated by measuring the apparent diffusion coefficient from the DWI signal along at least six non-collinear directions and then using these diffusion measurements to estimate the diffusion tensor ellipsoid.<sup>44,47</sup> Because  $\lambda_1$  represents maximal diffusion in anisotropic tissue, FA measures  $\lambda_1$  relative to  $\lambda_2$  and  $\lambda_3$ . Thus, FA is a measure of diffusion anisotropy and is the most common DTI measurement used to infer information about WM integrity in the brain.<sup>44,46,47,49,51,52</sup> Of note, the shape of the diffusion tensor indicates how anisotropic the tissue is and what FA value is assigned to that voxel. For example, a completely isotropic tensor will be a perfect spheroid with equal diffusion vectors pointing in all directions in 3D space ( $\lambda_1 = \lambda_2 = \lambda_3$ ) and has an FA value of 0 (no anisotropy). Conversely, in more anisotropic tissue such as WM, the tensor's shape will elongate in the direction of maximal diffusion and FA will approach 1 (complete anisotropy).<sup>44,50</sup> In epilepsy, FA reduction in WM can reveal widespread microstructural alterations associated with epileptic activity and may be an important biomarker in DRE.<sup>5,53,54</sup>



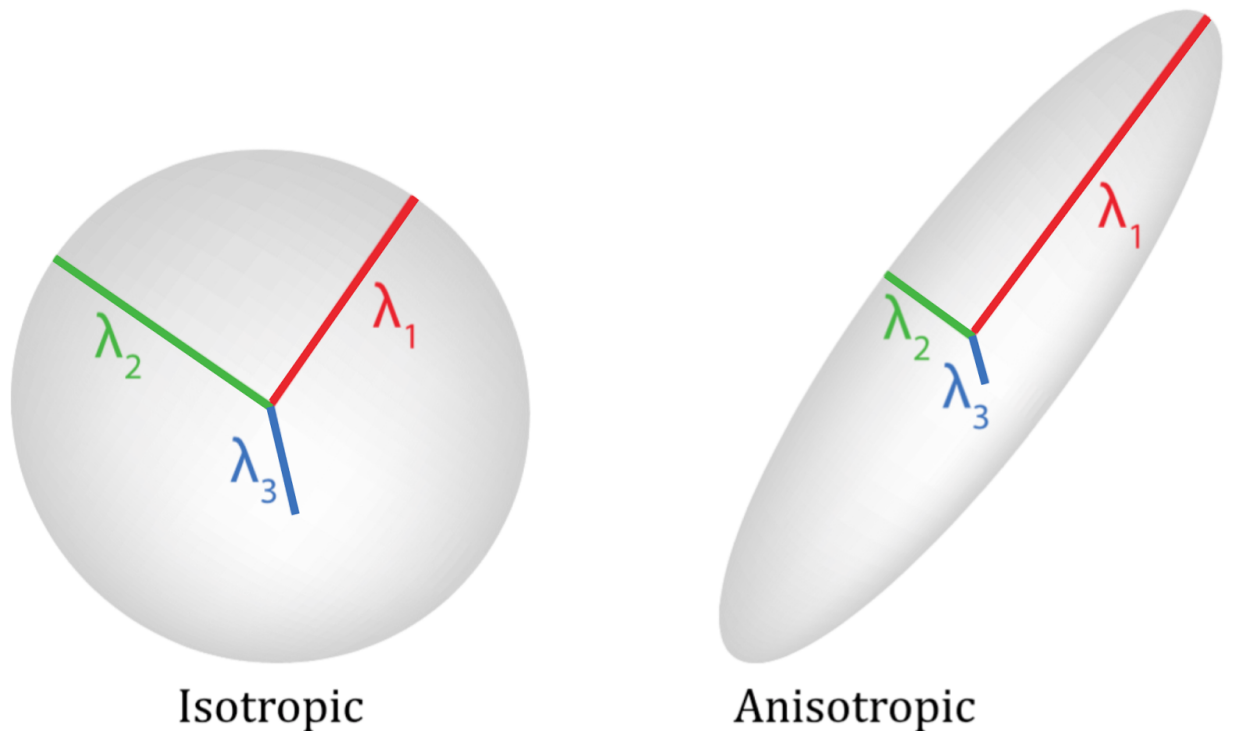


**Figure 1.5:** Isotropic and anisotropic diffusion tensor ellipsoids with the three eigenvalues labelled. Adapted from Tromp, *The Winnower* (2016).<sup>50</sup>

### 1.3.3 Diffusion Tractography

WM fiber pathways in the brain can be reconstructed and visualized using advanced diffusion MRI techniques such as diffusion tractography. Diffusion tractography can non-invasively probe tissue microstructure *in vivo* and may have promising applications in neurosurgical planning of epilepsy.<sup>49,55</sup> Previous epilepsy studies have shown that diffusion tractography can effectively reconstruct WM fiber pathways around seizure-onset zones as well as assess structural connectivity between EF and surrounding neural networks.<sup>56,57</sup> While diffusion tractography has not yet been adopted as a widespread clinical tool in epilepsy surgical evaluation, the potential clinical utility of diffusion tractography is evident and continues to be explored.

Diffusion tractography algorithms use information about diffusion orientation from each voxel in the DWI data to reconstruct WM fiber pathways in the brain. In general, WM fiber tracking typically involves three main steps: seeding, propagation, and

termination.<sup>49,58–60</sup> Seeding involves placement of seed points along voxels of interest with similar diffusion orientation (likely to be connected by a WM fiber pathway) and these seed points are then used to initiate neural fiber bundle tracking.<sup>49,58</sup> While tractography algorithms use different seeding point criteria and can generate varying results, some tractography methods have been shown to be superior than others. For example, streamlines tractography is a multi-directional 3D tractography approach that can reconstruct WM tracts by assigning each fiber orientation as a 3D vector, rather than a single seed point used in basic voxel-linking single-directional tractography methods, and uses that 3D vector to provide more accurate estimations of WM fiber trajectory.<sup>59,60</sup> An example of the streamlines tractography seeding approach is provided in **Figure 1.6**.<sup>59</sup>

After seeding, the streamlines are then propagated by taking small steps along the fiber orientation path using a user-defined stepping distance known as the step size.<sup>55,61</sup> As demonstrated in **Figure 1.6**, choice of step size is critical to ensuring accurate tractography results.<sup>59</sup> Too large of a step size can cause streamlines to deviate and go into an adjacent WM region, leading to erroneous reconstruction. Conversely, too small of a step size can be computationally inefficient.<sup>58–60</sup> Previous diffusion tractography studies comparing different fiber tracking parameters in WM fiber pathway reconstruction have shown that a step size of 0.5–2 mm is a reasonable choice for ensuring accurate streamline propagation.<sup>55,62</sup>

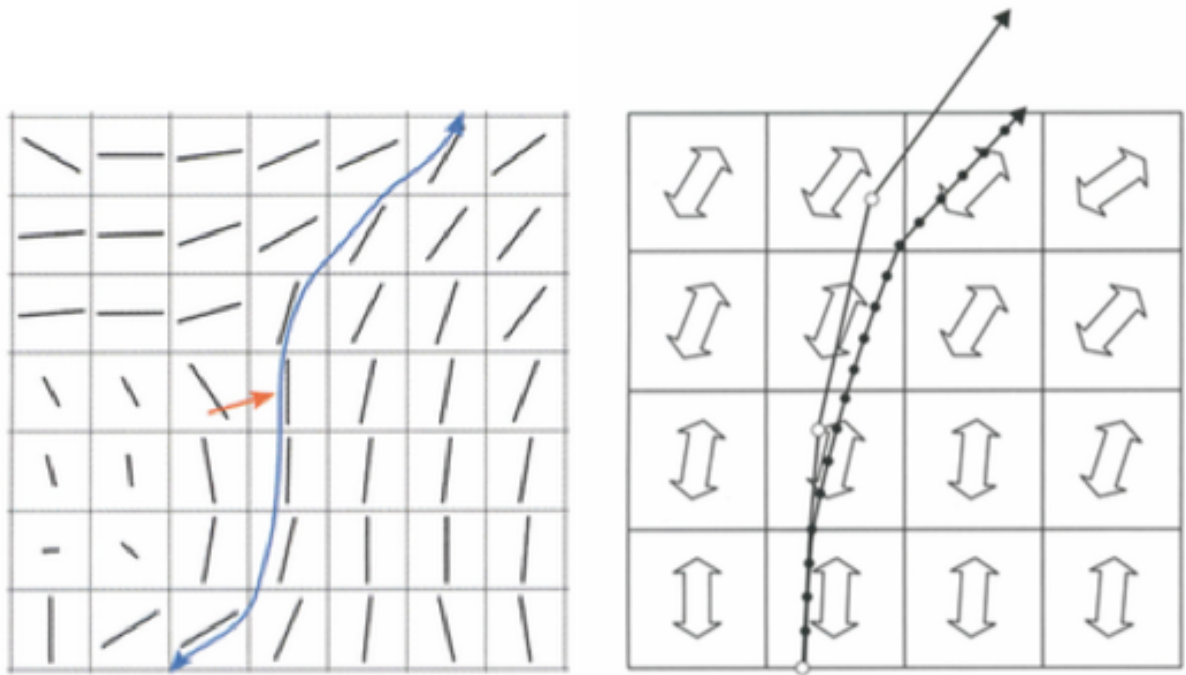


**Figure 1.6: Schematic representation of streamlines tractography.** *Left:* Fiber tractography is initiated using a user-defined seed point (red arrow) and this seed point is used to link voxels with similar diffusion orientation (likely to be connected by a WM fiber pathway). *Right:* Streamlines are propagated along the fiber orientation path at an incremental distance called the step size (mm). Too large of a step size (white dots) can cause the streamline to deviate off-course, leading to inaccurate fiber reconstruction. Adapted from Mori & Tournier (2013).<sup>59</sup> Image used with permission from Elsevier.

The last step in WM fiber reconstruction is to terminate the streamlines. Most tractography algorithms use a termination criterion to stop streamline propagation such as a whole brain WM mask from a co-registered anatomical T1-weighted image, an FA threshold (usually  $FA = 0.1-0.2$ ), or a curvature threshold.<sup>55,58</sup> Of note, errors in WM tractography can still occur due to a variety of other factors such as noise, partial volume effects, and crossing fibers.<sup>49,59,60</sup> To mitigate these errors, accuracy of WM fiber reconstruction can be further improved by supplying the tractography algorithm with *a priori* brain tissue masks – whole-brain WM, GM, and CSF masks – to minimize false positive and false negative tracts.<sup>59</sup>

### 1.3.4 Diffusion MRI Image Analysis Pipeline

After DWI are acquired, the data must be preprocessed to correct for noise, motion, and other image artifacts that can cause biases in DTI scalar maps and WM fiber tractography.<sup>48,52,58,63</sup> However, multiple approaches exist for preprocessing DWI data and performing diffusion tractography. Indeed, there are numerous DWI preprocessing pipelines available that offer different methods of data correction and can lead to varying FA and tractography results.<sup>64–66</sup> It is therefore crucial to select appropriate preprocessing steps to ensure accurate and reliable results. We have put together a robust diffusion MRI image analysis pipeline, illustrated in **Figure 1.7**, that can handle clinical data that are susceptible to noise, subject motion, as well as GM and WM pathologies. Our pipeline uses a variety of different diffusion MRI software packages<sup>64–70</sup> to preprocess the DWI data and output an FA map as well as images that can be used to perform WM fiber tractography (see **section 3.2.3** for further details).

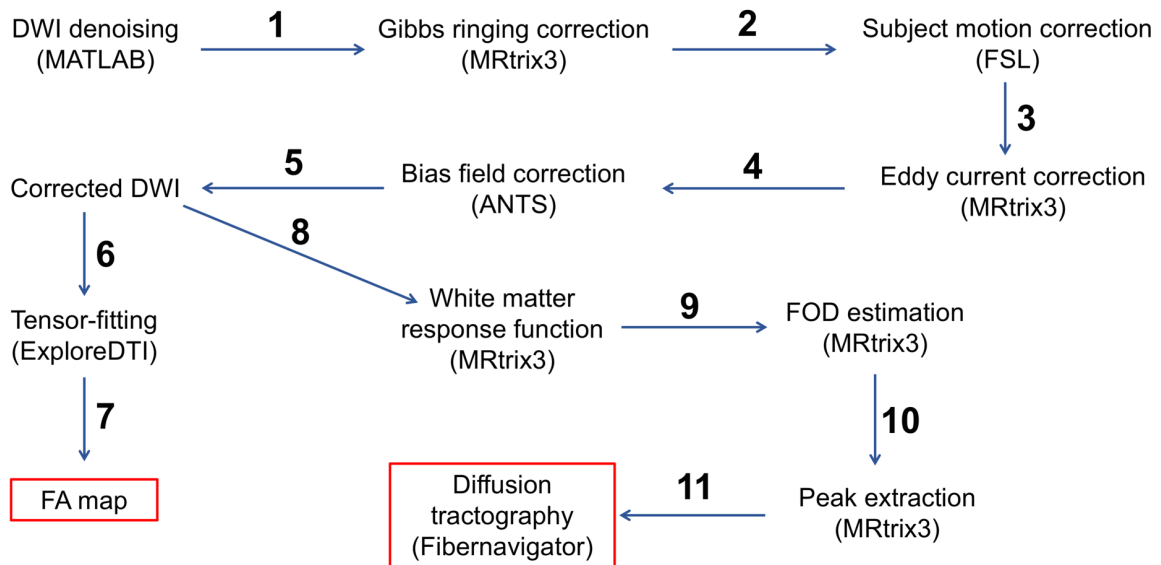


**Figure 1.7: Diffusion MRI image analysis pipeline.** DWI data were preprocessed using a variety of different image processing software packages to generate an FA map and images that can be used to visualize WM fiber pathways in the brain using diffusion tractography.

To validate the accuracy of this pipeline in reconstructing WM fiber pathways in the brain, we empirically evaluated the pipeline using a ground-truth WM phantom from the

ISMRM 2015 Tractography Challenge<sup>71,72</sup> (see **Appendix A**). Using the raw DWI as input, our pipeline can generate a whole-brain tractogram showing all the WM fiber pathways in the brain, as illustrated in a representative epilepsy patient in **Figure 1.8**.

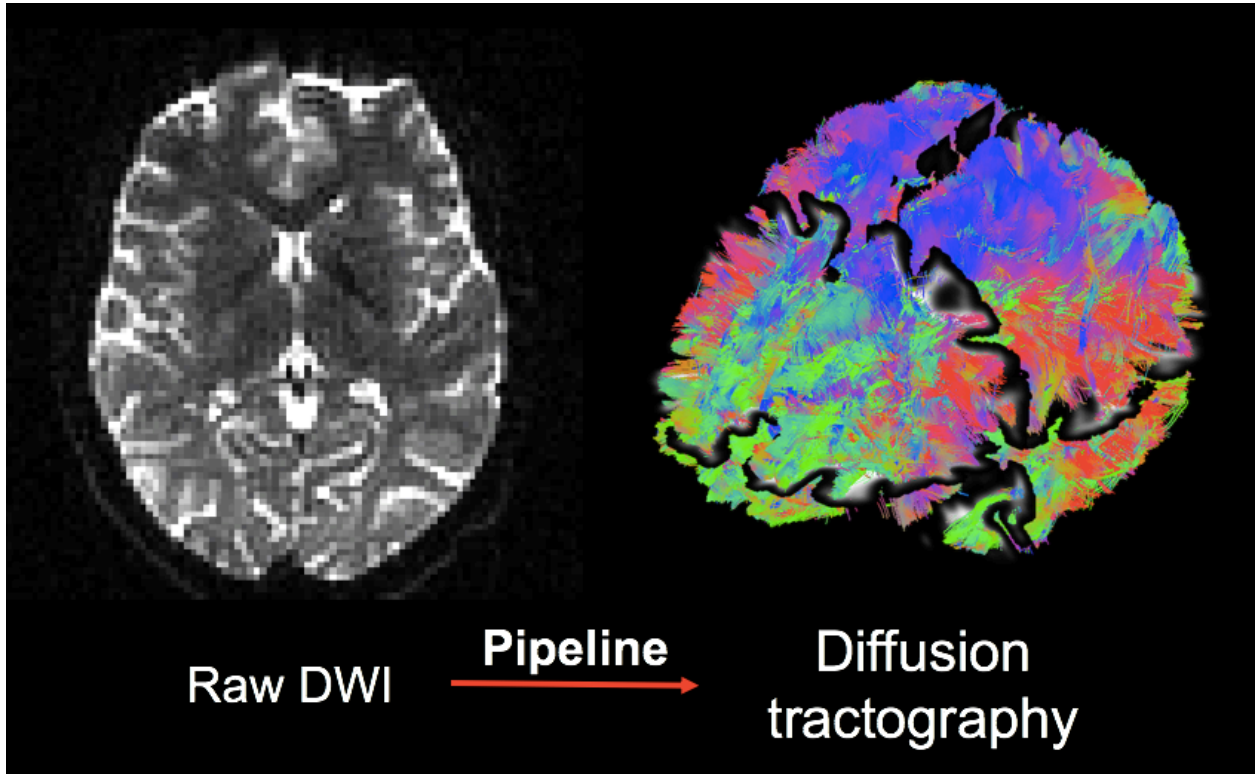


**Figure 1.8:** Raw DWI data from an epilepsy patient preprocessed using our in-house diffusion MRI image analysis pipeline to generate WM fiber pathways in the brain via diffusion tractography.

## 1.4 Hybrid PET/MRI in Epilepsy Imaging

The current clinical standard-of-care epilepsy imaging protocol for assessing structural and functional abnormalities in the brain, indicative of potential EF, is 1.5T/3T MRI followed by PET and computed tomography (PET/CT).<sup>22</sup> Separate acquisition of PET and MRI, which in some cases may be several months apart, can be problematic and may result in misalignment and motion biases, making it difficult to accurately detect the seizure-onset zone in the brain.<sup>19</sup> These co-registration errors can be obviated using hybrid PET/MRI scanners, which allow simultaneous acquisition of PET and MRI, and may have promising applications in the clinical management of epilepsy. Furthermore,

hybrid PET/MRI may be especially useful in improving EF detection through further advancements in PET quantification.<sup>73–76</sup> However, concerns over PET bias from MRI-based attenuation correction approaches have limited clinical adoption of hybrid PET/MRI.<sup>77,78</sup> A few epilepsy studies have attempted to investigate whether these PET biases impact clinical diagnosis<sup>20–22,43,79</sup>, however, these studies did not compare FDG-PET/MRI findings against the current clinical standard FDG-PET/CT, IC-EEG, surgical outcome and gold-standard histopathology. Thus, the diagnostic equivalency of PET/MRI against PET/CT in DRE needs to be further assessed, especially when improved brain MRI-based attenuation correction approaches (for example RESOLUTE)<sup>80</sup> are used for PET reconstruction.

Another promise PET/MRI holds in clinical management of epilepsy is the co-localization of PET with advanced functional and structural MRI for brain connectivity mapping.<sup>56</sup> Specifically, the potential clinical utility of combining PET and DTI for epilepsy surgical evaluation is yet to be fully investigated. The integration of FDG-PET and diffusion tractography may shed new insight into seizure-related structural abnormalities in and around the EF, which could minimize potential risks associated with surgical resection and improve patient outcomes, especially in MRI-negative epilepsy or non-localizing epilepsy where IC-EEG and MRI findings lack concordance.<sup>15,56</sup>

## 1.5 Thesis Objectives

The overall goal of this thesis is to develop a non-invasive approach using hybrid PET/MRI to improve EF localization, especially in MRI-negative epilepsy, as well as assess structural integrity around EF, for improving DRE surgical evaluation. However, the effect of quantitative PET biases from MRI-based attenuation correction on clinical diagnosis of DRE was first assessed. Thus, our specific research objectives were to:

- 1) Assess the diagnostic equivalency and clinical value of PET/MRI against PET/CT (current clinical standard for FDG-PET imaging) in DRE. This objective is the focus of **Chapter 2**, which has been adapted from the following manuscript draft:

**Poirier SE**, Kwan BYM, Jurkiewicz MT, Samargandy L, Iacobelli M, Steven DA, Lam Shin Cheung V, Moran G, Prato FS, Thompson RT, Burneo JG, Anazodo UC, Thiessen JD. An evaluation of the diagnostic competence of hybrid PET/MRI in clinical management of drug-resistant epilepsy. Submitted to *Am J Neuroradiol* in June 2020. Under Review. Manuscript ID: AJNR-20-00760

2) Develop a non-invasive approach combining FDG-PET and diffusion tractography (PET/DTI) for assessing WM integrity around EF in the brains of MRI-negative DRE patients. The potential clinical utility of our PET/DTI approach in epilepsy surgical evaluation was also assessed. This objective is the focus of **Chapter 3**, which has been adapted from the following manuscript publication:

**Poirier SE**, Kwan BYM, Jurkiewicz MT, Samargandy L, Steven DA, Suller-Marti A, Lam Shin Cheung V, Khan AR, Prato FS, Burneo JG, Thiessen JD, Anazodo UC. <sup>18</sup>F-FDG PET-guided diffusion tractography reveals white matter abnormalities around the epileptic focus in medically refractory epilepsy: implications for epilepsy surgical evaluation. *European J Hybrid Imaging*. 2020;4:10. DOI: <https://doi.org/10.1186/s41824-020-00079-7>

Finally, **Chapter 4** provides a summary of the work presented in Chapters 2 and 3, and also discusses some future directions for this research.

## 1.6 References

1. Kwan P, Schachter SC, Brodie MJ. Drug-Resistant Epilepsy. *New England Journal of Medicine* 2011;365:919–26.
2. Caciagli L, Bernhardt BC, Hong SJ, et al. Functional network alterations and their structural substrate in drug-resistant epilepsy. *Front Neurosci* 2014;8:411.
3. Helmstaedter C, Kurthen M, Lux S, et al. Chronic epilepsy and cognition: A longitudinal study in temporal lobe epilepsy. *Ann Neurol* 2003;54:425–32.
4. Richardson MP, Strange BA, Thompson PJ, et al. Pre-operative verbal memory fMRI predicts post-operative memory decline after left temporal lobe resection. *Brain* 2004;127:2419–26.
5. Jiang Y, Mao L, Yan X, et al. Investigation of altered microstructure in patients with drug refractory epilepsy using diffusion tensor imaging. *Neuroradiology* 2017;59:597–608.
6. Munsell BC, Wee C-Y, Keller SS, et al. Evaluation of machine learning algorithms for treatment outcome prediction in patients with epilepsy based on structural connectome data. *Neuroimage* 2015;118:219–30.
7. Burneo JG, Poon R, Kellett S, et al. The Utility of Positron Emission Tomography in Epilepsy. *Canadian Journal of Neurological Sciences* 2015;42:360–71.
8. Dalkilic EB. Neurostimulation Devices Used in Treatment of Epilepsy. *Curr Treat Options Neurol* 2017;19:7.
9. Bettus G, Guedj E, Joyeux F, et al. Decreased basal fMRI functional connectivity in epileptogenic networks and contralateral compensatory mechanisms. *Human Brain Mapping* 2009;30:1580–91.
10. Cahill V, Sinclair B, Malpas CB, et al. Metabolic patterns and seizure outcomes following anterior temporal lobectomy. *Annals of Neurology* 2019;85:241–50.
11. Téllez-Zenteno JF, Dhar R, Wiebe S. Long-term seizure outcomes following epilepsy surgery: a systematic review and meta-analysis. *Brain* 2005;128:1188–98.
12. de Tisi J, Bell GS, Peacock JL, et al. The long-term outcome of adult epilepsy surgery, patterns of seizure remission, and relapse: a cohort study. *The Lancet* 2011;378:1388–95.
13. Aparicio J, Carreño M, Bargalló N, et al. Combined 18F-FDG-PET and diffusion tensor imaging in mesial temporal lobe epilepsy with hippocampal sclerosis. *NeuroImage: Clinical* 2016;12:976–89.



14. Khalil AF, Iwasaki M, Nishio Y, et al. Verbal Dominant Memory Impairment and Low Risk for Post-operative Memory Worsening in Both Left and Right Temporal Lobe Epilepsy Associated with Hippocampal Sclerosis. *Neurol Med Chir(Tokyo)* 2016;56:716–23.
15. Knowlton RC. The role of FDG-PET, ictal SPECT, and MEG in the epilepsy surgery evaluation. *Epilepsy Behav* 2006;8:91–101.
16. Blount JP, Cormier J, Kim H, et al. Advances in intracranial monitoring. *FOC* 2008;25:E18.
17. Rathore C, Dickson JC, Teotónio R, et al. The utility of 18F-fluorodeoxyglucose PET (FDG PET) in epilepsy surgery. *Epilepsy Research* 2014;108:1306–14.
18. Sarikaya I. PET studies in epilepsy. *Am J Nucl Med Mol Imaging* 2015;5:416–30.
19. Wang YH, An Y, Fan XT, et al. Comparison between simultaneously acquired arterial spin labeling and 18F-FDG PET in mesial temporal lobe epilepsy assisted by a PET/MR system and SEEG. *NeuroImage: Clinical* 2018;19:824–30.
20. Shang K, Wang J, Fan X, et al. Clinical Value of Hybrid TOF-PET/MR Imaging–Based Multiparametric Imaging in Localizing Seizure Focus in Patients with MRI-Negative Temporal Lobe Epilepsy. *American Journal of Neuroradiology* 2018;39:1791–8.
21. Ding YS, Chen BB, Glielmi C, et al. A pilot study in epilepsy patients using simultaneous PET/MR. *Am J Nucl Med Mol Imaging* 2014;4:459–70.
22. Paldino MJ, Yang E, Jones JY, et al. Comparison of the diagnostic accuracy of PET/MRI to PET/CT-acquired FDG brain exams for seizure focus detection: a prospective study. *Pediatr Radiol* 2017;47:1500–7.
23. Oldan JD, Shin HW, Khandani AH, et al. Subsequent experience in hybrid PET-MRI for evaluation of refractory focal onset epilepsy. *Seizure* 2018;61:128–34.
24. Salamon N, Kung J, Shaw SJ, et al. FDG-PET/MRI coregistration improves detection of cortical dysplasia in patients with epilepsy. *Neurology* 2008;71:1594–601.
25. Engel JJr, Brown WJ, Kuhl DE, et al. Pathological findings underlying focal temporal lobe hypometabolism in partial epilepsy. *Annals of Neurology* 1982;12:518–28.
26. Jokeit H. Prefrontal asymmetric interictal glucose hypometabolism and cognitive impairment in patients with temporal lobe epilepsy. *Brain* 1997;120:2283–94.
27. Choi JY, Kim SJ, Hong SB, et al. Extratemporal hypometabolism on FDG PET in temporal lobe epilepsy as a predictor of seizure outcome after temporal lobectomy. *Eur J Nucl Med Mol Imaging* 2003;30:581–7.

28. Theodore WH, Sato S, Kufta C, et al. Temporal lobectomy for uncontrolled seizures: The role of positron emission tomography. *Annals of Neurology* 1992;32:789–94.
29. Dupont S, Semah F, Clémenceau S, et al. Accurate Prediction of Postoperative Outcome in Mesial Temporal Lobe Epilepsy: A Study Using Positron Emission Tomography With 18Fluorodeoxyglucose. *Arch Neurol* 2000;57:1331–6.
30. Lee KK, Salamon N. [18F] Fluorodeoxyglucose–Positron-Emission Tomography and MR Imaging Coregistration for Presurgical Evaluation of Medically Refractory Epilepsy. *American Journal of Neuroradiology* 2009;30:1811–6.
31. Koutroumanidis M, Hennessy MJ, Seed PT, et al. Significance of interictal bilateral temporal hypometabolism in temporal lobe epilepsy. *Neurology* 2000;54:1811–21.
32. Henry TR, Babb TL, Engel J, et al. Hippocampal neuronal loss and regional hypometabolism in temporal lobe epilepsy. *Annals of Neurology* 1994;36:925–7.
33. Scheibel ME, Crandall PH, Scheibel AB. The hippocampal-dentate complex in temporal lobe epilepsy. A Golgi study. *Epilepsia* 1974;15:55–80.
34. Collins RC, Kennedy C, Sokoloff L, et al. Metabolic Anatomy of Focal Motor Seizures. *Arch Neurol* 1976;33:536–42.
35. Traub-Weidinger T, Muzik O, Sundar LKS, et al. Utility of Absolute Quantification in Non-lesional Extratemporal Lobe Epilepsy Using FDG PET/MR Imaging. *Front Neurol* 2020;11:54.
36. Kim YK, Lee DS, Lee SK, et al. 18F-FDG PET in Localization of Frontal Lobe Epilepsy: Comparison of Visual and SPM Analysis. *J Nucl Med* 2002;43:1167–74.
37. Van Bogaert P, Massager N, Tugendhaft P, et al. Statistical Parametric Mapping of Regional Glucose Metabolism in Mesial Temporal Lobe Epilepsy. *NeuroImage* 2000;12:129–38.
38. Henry TR, Mazziotta JC, Engel J. Interictal Metabolic Anatomy of Mesial Temporal Lobe Epilepsy. *Archives of Neurology* 1993;50:582–9.
39. Henry TR, Mazziotta JC, Engel J, et al. Quantifying Interictal Metabolic Activity in Human Temporal Lobe Epilepsy. *Journal of Cerebral Blood Flow & Metabolism* 1990;10:748–57.
40. Didelot A, Mauguier F, Redoute J, et al. Voxel-Based Analysis of Asymmetry Index Maps Increases the Specificity of 18F-MPPF PET Abnormalities for Localizing the Epileptogenic Zone in Temporal Lobe Epilepsies. *Journal of Nuclear Medicine* 2010;51:1732–9.

41. Kim YK, Lee DS, Lee SK, et al. Differential Features of Metabolic Abnormalities Between Medial and Lateral Temporal Lobe Epilepsy: Quantitative Analysis of 18F-FDG PET Using SPM. *J Nucl Med* 2003;44:1006–12.
42. Zhu Y, Feng J, Wu S, et al. Glucose Metabolic Profile by Visual Assessment Combined with Statistical Parametric Mapping Analysis in Pediatric Patients with Epilepsy. *Journal of Nuclear Medicine* 2017;58:1293–9.
43. Boscolo Galazzo I, Mattoli MV, Pizzini FB, et al. Cerebral metabolism and perfusion in MR-negative individuals with refractory focal epilepsy assessed by simultaneous acquisition of 18 F-FDG PET and arterial spin labeling. *NeuroImage: Clinical* 2016;11:648–57.
44. Mori S, Zhang J. Principles of Diffusion Tensor Imaging and Its Applications to Basic Neuroscience Research. *Neuron* 2006;51:527–39.
45. Le Bihan D, Breton E, Lallemand D, et al. MR imaging of intravoxel incoherent motions: application to diffusion and perfusion in neurologic disorders. *Radiology* 1986;161:401–7.
46. Le Bihan D. Looking into the functional architecture of the brain with diffusion MRI. *International Congress Series* 2006;1290:1–24.
47. Basser PJ, Jones DK. Diffusion-tensor MRI: theory, experimental design and data analysis – a technical review. *NMR Biomed* 2002;15:456–67.
48. Jones DK, Cercignani M. Twenty-five pitfalls in the analysis of diffusion MRI data. *NMR Biomed* 2010;23:803–20.
49. Ciccarelli O, Catani M, Johansen-Berg H, et al. Diffusion-based tractography in neurological disorders: concepts, applications, and future developments. *Lancet Neurology* 2008;7:715–27.
50. Tromp D. The diffusion tensor, and its relation to FA, MD, AD and RD. *The Winnower* <https://doi.org/10.15200/winn.146119.94804>.
51. Soares J, Marques P, Alves V, et al. A hitchhiker’s guide to diffusion tensor imaging. *Front Neurosci* 2013;7:31.
52. Tournier J-D, Mori S, Leemans A. Diffusion tensor imaging and beyond. *Magn Reson Med* 2011;65:1532–56.
53. Labate A, Cherubini A, Tripepi G, et al. White matter abnormalities differentiate severe from benign temporal lobe epilepsy. *Epilepsia* 2015;56:1109–16.
54. Focke NK, Yogarajah M, Bonelli SB, et al. Voxel-based diffusion tensor imaging in patients with mesial temporal lobe epilepsy and hippocampal sclerosis. *NeuroImage* 2008;40:728–37.

55. Chamberland M, Whittingstall K, Fortin D, et al. Real-time multi-peak tractography for instantaneous connectivity display. *Front Neuroinform* 2014;8:59.
56. Sivakanthan S, Neal E, Murtagh R, et al. The evolving utility of diffusion tensor tractography in the surgical management of temporal lobe epilepsy: a review. *Acta Neurochirurgica* 2016;158:2185–93.
57. Ahmadi ME, Hagler DJ, McDonald CR, et al. Side Matters: Diffusion Tensor Imaging Tractography in Left and Right Temporal Lobe Epilepsy. *American Journal of Neuroradiology* 2009;30:1740–7.
58. Johansen-Berg H, Behrens TEJ. *Diffusion MRI: From Quantitative Measurement to In vivo Neuroanatomy*. Academic Press; 2013.
59. Mori S, Tournier JD. *Introduction to Diffusion Tensor Imaging: And Higher Order Models*. Academic Press; 2013.
60. Hecke WV, Emsell L, Sunaert S. *Diffusion Tensor Imaging: A Practical Handbook*. Springer; 2015.
61. Calamante F. The Seven Deadly Sins of Measuring Brain Structural Connectivity Using Diffusion MRI Streamlines Fibre-Tracking. *Diagnostics* 2019;9:115.
62. Chamberland M, Bernier M, Fortin D, et al. 3D interactive tractography-informed resting-state fMRI connectivity. *Front Neurosci* 2015;9:275.
63. Perrone D, Aelterman J, Pižurica A, et al. The effect of Gibbs ringing artifacts on measures derived from diffusion MRI. *NeuroImage* 2015;120:441–55.
64. Woolrich MW, Jbabdi S, Patenaude B, et al. Bayesian analysis of neuroimaging data in FSL. *NeuroImage* 2009;45:S173–86.
65. Tournier JD, Smith R, Raffelt D, et al. MRtrix3: A fast, flexible and open software framework for medical image processing and visualisation. *NeuroImage* 2019;202:116137.
66. Leemans A, Jeurissen B, Sijbers J, et al. ExploreDTI: a graphical toolbox for processing, analyzing, and visualizing diffusion MR data. *Proc Intl Soc Mag Reson Med* 2009;17:3537.
67. Wiest-Daesslé N, Prima S, Coupé P, et al. Rician Noise Removal by Non-Local Means Filtering for Low Signal-to-Noise Ratio MRI: Applications to DT-MRI. In: Metaxas D, Axel L, Fichtinger G, et al., eds. *Medical Image Computing and Computer-Assisted Intervention – MICCAI 2008*. Vol 5242. Berlin, Heidelberg: Springer Berlin Heidelberg; 2008:171–9.
68. Coupé P, Yger P, Prima S, et al. An optimized blockwise nonlocal means denoising filter for 3-D magnetic resonance images. *IEEE Trans Med Imaging* 2008;27:425–41.

69. Coupé P, Manjón JV, Gedamu E, et al. Robust Rician noise estimation for MR images. *Medical Image Analysis* 2010;14:483–93.
70. Avants BB, Tustison NJ, Song G, et al. A reproducible evaluation of ANTs similarity metric performance in brain image registration. *NeuroImage* 2011;54:2033–44.
71. Maier-Hein KH, Neher PF, Houde JC, et al. The challenge of mapping the human connectome based on diffusion tractography. *Nature Communications* 2017;8:1349.
72. Neher PF, Laun FB, Stieltjes B, et al. Fiberfox: Facilitating the creation of realistic white matter software phantoms: Realistic White Matter Software Phantoms. *Magnetic Resonance in Medicine* 2014;72:1460–70.
73. Johnson PM, Taylor R, Whelan T, et al. Rigid-body motion correction in hybrid PET/MRI using spherical navigator echoes. *Phys Med Biol* 2019;64:08NT03.
74. Mehranian A, Belzunce MA, Niccolini F, et al. PET image reconstruction using multi-parametric anato-functional priors. *Phys Med Biol* 2017;62:5975–6007.
75. Anazodo U, Kewin M, Finger E, et al. Preliminary evaluation of MRI-derived input function for quantitative measurement of glucose metabolism in an integrated PET-MRI. *EJNMMI Phys* 2015;2:A80.
76. Shiyam Sundar LK, Muzik O, Rischka L, et al. Promise of Fully Integrated PET/MRI: Noninvasive Clinical Quantification of Cerebral Glucose Metabolism. *J Nucl Med* 2020;61:276–84.
77. Andersen FL, Ladefoged CN, Beyer T, et al. Combined PET/MR imaging in neurology: MR-based attenuation correction implies a strong spatial bias when ignoring bone. *NeuroImage* 2014;84:206–16.
78. Larsson A, Johansson A, Axelsson J, et al. Evaluation of an attenuation correction method for PET/MR imaging of the head based on substitute CT images. *Magn Reson Mater Phy* 2013;26:127–36.
79. Shin HW, Jewells V, Sheikh A, et al. Initial experience in hybrid PET-MRI for evaluation of refractory focal onset epilepsy. *Seizure* 2015;31:1–4.
80. Ladefoged CN, Benoit D, Law I, et al. Region specific optimization of continuous linear attenuation coefficients based on UTE (RESOLUTE): application to PET/MR brain imaging. *Phys Med Biol* 2015;60:8047–65.

## Chapter 2

### 2 An evaluation of the diagnostic competence of hybrid PET/MRI in clinical management of drug-resistant epilepsy

This chapter has been adapted from the following manuscript draft:

**Poirier SE**, Kwan BYM, Jurkiewicz MT, Samargandy L, Iacobelli M, Steven DA, Lam Shin Cheung V, Moran G, Prato FS, Thompson RT, Burneo JG, Anazodo UC, Thiessen JD. An evaluation of the diagnostic competence of hybrid PET/MRI in clinical management of drug-resistant epilepsy. Submitted to *Am J Neuroradiol* in June 2020. Under Review. Manuscript ID: AJNR-20-00760

#### 2.1 Introduction

Approximately one in three epilepsy patients are diagnosed with drug-resistant epilepsy (DRE) – seizures uncontrolled with anti-epileptic drugs – and may be considered for surgical resection using an extensive surgical evaluation protocol, which includes prolonged video-electroencephalography (VEEG) and MRI, to localize the seizure-onset zone (SOZ).<sup>1,2</sup> Absence of a clear lesion on MRI in about 25% of DRE patients is common.<sup>3,4</sup> The lack of a structural lesion significantly lowers a patient's chances of achieving long-term seizure freedom after surgery.<sup>5,6</sup> In such cases, functional imaging such as FDG-PET can be used to improve SOZ detection. Specifically, interictal FDG-PET can indirectly locate the SOZ as brain regions showing decreased FDG uptake and has been shown to aid detection of SOZ when MRI is negative or equivocal.<sup>1,7-9</sup> FDG-PET can resolve causative epileptic foci when multiple structural lesions are seen on MRI<sup>10</sup>, as well as guide electrode placement in the brain during intracranial EEG (IC-EEG) monitoring.<sup>7</sup>

Hybrid PET/MRI, the simultaneous acquisition of PET and MRI, has promising applications in the clinical management of epilepsy.<sup>11,12</sup> When PET is simultaneously combined with MRI, the accuracy of localizing the SOZ is significantly improved<sup>7,10,13-15</sup> and positive surgical outcomes can increase by up to 23%.<sup>7</sup> Salamon et al. (2008)

reported that in patients with focal cortical dysplasias, a common cause for apparently MRI-negative epilepsy, co-registration of PET and MRI enhances lesion detection and reduces the use of IC-EEG.<sup>13</sup> What is more important is the promise PET/MRI holds in further enhancement of PET quantification. MRI approaches for motion<sup>16</sup> and partial volume correction of PET<sup>17</sup> show significant PET contrast enhancements which translate to improvements in lesion localization and lateralization. Anatomical MRI-guided approaches for non-invasive PET quantification may negate the need for standardized uptake value (SUV) and move clinical PET towards parametric lesion characterization and kinetic analysis of features hidden in SUV.<sup>18,19</sup> These improvements in PET combined with advanced multi-parametric MRI can revolutionize clinical management of epilepsy.<sup>20</sup>

Despite the potential of hybrid PET/MRI, there have been concerns about its reliance on MRI-based attenuation correction (MRAC) approaches, which have been shown to produce biases in quantitative PET compared to traditional CT-based attenuation correction (CTAC), particularly in the temporal and posterior aspects of the brain – areas of the brain commonly implicated in DRE – prone to tissue misclassifications and high inter-subject variability in bone density.<sup>21,22</sup> However, few epilepsy studies have investigated whether these biases have any effect on the diagnostic information provided by PET/MRI relative to PET/CT. Previous reports have provided some preliminary evidence that MRAC biases do not seem to affect the diagnostic accuracy of hybrid PET/MRI in epilepsy<sup>23,24</sup>, but these studies lacked validation of PET/MRI and PET/CT findings against gold standard post-surgical outcomes, such as histopathology. Furthermore, new segmentation-based MRAC methods (such as RESOLUTE<sup>25</sup>) that aim to improve bone tissue modelling especially around the base of the skull – a major challenge of MRAC – have been shown to reduce MRAC PET biases in the human brain.<sup>26</sup> In this study, we evaluated the diagnostic equivalency and clinical value of PET/MRI for epilepsy imaging against PET/CT, the current clinical standard for FDG-PET imaging. SUVs and z-scores (number of standard deviations from the population mean) were compared between PET/MRI and PET/CT to estimate regional MRAC bias, particularly in brain regions often implicated in DRE. Diagnostic accuracy and sensitivity of PET/MRI and PET/CT for SOZ detection were also compared using established

reference standards (clinical hypothesis and histopathology, respectively) to assess the potential clinical utility of hybrid PET/MRI in epilepsy surgical evaluation.

## **2.2 Materials and Methods**

### **2.2.1 Patients**

This retrospective study initially consisted of 23 DRE patients recruited from the London Health Sciences Centre epilepsy monitoring unit. Data from two patients were excluded because of retrospective reconstruction failure of the FDG-PET data. Data from three additional patients acquired after the scanner software upgrade were also excluded because of MRAC compatibility issues. Thus, this study had a final sample size of 18 DRE patients (9 females, mean age =  $37 \pm 13$  years). Presurgical evaluation included patient history, physical examination, neuropsychological assessment, scalp VEEG, 1.5T MRI, and PET/CT of the brain to localize the SOZ. A subset of the patients (n=10) underwent surgical resection to remove the SOZ based on the clinical hypothesis, determined through multi-disciplinary meetings at epilepsy surgical rounds. Surgical outcome was assessed by evaluating degree of seizure freedom using the Engel classification<sup>27</sup> after a postoperative follow-up period of at least one-year. Patient demographics, clinical profile, and surgical outcome are provided in **Table 2.1**. All patients provided written informed consent and the study was approved by the University Research Ethics Board.



**Table 2.1: Study patient demographics and surgical outcomes**

Patient #	Sex	Age (yr)	Epilepsy Duration (yr)	Seizure Frequency	Clinical Hypothesis	Surgery Performed [Engel <sup>25</sup> ]	Histopathology
1	M	32	2	1–2/day	R temp	Y [IIIA]	Gliososis
2	M	52	48	–	L temp-front	N	NA
3	M	29	13	4/week	L front	N	NA
4	F	18	4	1/month	R front	Y [IA]	GGM WHO I
5	M	60	19	6/year	L temp-front	N	NA
6	F	28	1	Unpredictable	R temp	Y [IIIA]	Gliososis
7	M	53	39	Unpredictable	L temp	N	NA
8	M	29	6	2–3/month	L temp-front	Y [IA]	Gliososis
9	F	32	7	–	L temp	N	NA
10	F	36	21	1/week	R front	Y [IIIA]	FCD Ib
11	F	45	10	5–7/month	L temp	Y [IA]	HS
12	M	23	2	1–2/month	R temp	Y [IV]	Gliososis
13	F	26	9	2–3/month	R temp-front	Y [IA]	Gliososis
14	M	23	17	3/month	L temp	Y [IA]	Gliososis
15	F	58	37	–	L temp	N	NA
16	F	38	31	–	R temp	N	NA
17	M	55	1	–	R temp	Y [IA]	Unremarkable <sup>a</sup>
18	F	33	12	1/week	L temp	N	NA

Note. Modified from a prior study<sup>33</sup>, where the sample size has now been increased from n=14 to n=18.

Abbreviations: –, missing data; F, female; FCD, focal cortical dysplasia; front, frontal lobe; GGM, ganglioglioma; HS, hippocampal sclerosis; L, left; M, male; N, no; NA, not applicable; R, right; temp, temporal lobe; temp-front, temporal-frontal lobe; WHO, World Health Organization grade; Y, yes.

\*Surgical outcome was assessed one-year following surgery.

<sup>a</sup>No specific structural changes that could explain the etiopathogenesis of patient's epilepsy.

## 2.2.2 Data Acquisition

The 18 DRE patients, who had a prior clinical 1.5T brain MRI scan using an epilepsy protocol and had been referred for PET/CT, were scanned in a 3T hybrid PET/MRI (Biograph mMR, Siemens Healthineers, Erlangen, Germany) immediately after clinical PET/CT (Discovery VCT, GE Healthcare, Waukesha, WI) imaging. PET/MRI was acquired ~40 min after intravenous bolus injection of  $190 \pm 16$  MBq of <sup>18</sup>F-FDG and patients had a fasting blood glucose of  $4.3 \pm 0.6$  mmol/L. Structural MRI was acquired during a 45 min list-mode PET imaging session and included; high resolution T1-weighted MRI (1 mm<sup>3</sup> isotropic voxels) acquired using a 3D magnetization-prepared rapid gradient-echo sequence (MPRAGE), 3D T2-weighted FLAIR (1 mm<sup>3</sup> isotropic voxels) and the vendor-provided ultrashort echo time sequence for MRAC.

In order to compare PET images between PET/MRI and PET/CT negating potential scanner biases, we reconstructed only PET images from the PET/MRI. PET images from PET/MRI were corrected for scatter and decay while attenuation corrections were performed using the RESOLUTE approach<sup>25</sup> to generate PET<sub>MRAC</sub> images and using

CTAC to generate  $PET_{CTAC}$  images. Each patient's CT images were first aligned and transformed to the RESOLUTE MRAC maps using the expert automated registration module in 3D Slicer<sup>28</sup> (<https://www.slicer.org/>; Version 4.8), with custom combination of 6-parameter rigid and 12-parameter affine registration and normalized mutual information as objective function. The patient bed and head holder were removed from the CT images using a head mask generated from the RESOLUTE MRAC map. Volume compensation was added from the RESOLUTE MRAC images to the CT slices in the neck to account for the smaller CT field-of-view. CTAC maps were generated by converting from CT Hounsfield units to linear attenuation coefficients for 511 keV positron annihilation photons using the bilinear scaling approach.<sup>29</sup> The 45-minute list-mode PET data were reconstructed to one image volume (344 x 344 x 127 matrix) for each attenuation correction type using Siemens e7 tools and an iterative algorithm (ordered subset expectation maximization with point-spread function model; 3 iterations, 21 subsets, 3D Gaussian filter with a full-width at half-maximum of 2 mm, 2.09 x 2.09 x 2.03 mm<sup>3</sup> voxel size, and zoom factor of 2.5).

### **2.2.3 Qualitative Image Analysis**

In order to assess the diagnostic competence of PET/MRI compared to PET/CT (current clinical standard),  $PET_{MRAC}$ ,  $PET_{CTAC}$ , 3T T1-weighted, and 3T T2-weighted images of the 18 DRE patients were read by two neuroradiologists with over five and eight years of clinical imaging experience, respectively.  $PET_{MRAC}$  and  $PET_{CTAC}$  were also read by a nuclear medicine physician with over five years of clinical PET reading experience. The three readers were aware of all clinical information while visually assessing patient FDG-PET and MRI images. Images were visually inspected for quality and assessed for evidence of brain abnormalities using syngo.via MI Neurology (Siemens Healthcare, Erlangen, Germany). Rating scales were used to compare image quality, presence of image artifacts, and extent of regional FDG-PET abnormalities on  $PET_{MRAC}$  and  $PET_{CTAC}$  images. Image quality was assessed based on image smoothness, noise, resolution, sharpness of contours and contrast-to-noise using the following rating scheme: 4 = excellent; 3 = good; 2 = acceptable; and 1 = poor. Similarly, presence of image artifacts was assigned to one of three categories: 3 = none; 2 = slight; or 1 = considerable. Lastly,

extent of regional abnormalities on PET<sub>MRAC</sub> and PET<sub>CTAC</sub> was categorized using a standard 4-point rating scale: 4 = normal; 3 = mildly decreased; 2 = moderately decreased; and 1 = severely decreased.<sup>30</sup> Diagnostic accuracy of PET<sub>MRAC</sub> and PET<sub>CTAC</sub> for detecting the SOZ in the brain was qualitatively evaluated through comparison to a reference standard. For this study, the reference standard was the clinical hypothesis which was determined based on all available diagnostic information through multidisciplinary meetings at epilepsy surgical rounds. Additionally, sensitivity of PET<sub>MRAC</sub> and PET<sub>CTAC</sub> for SOZ localization was also assessed based on ground-truth histopathological findings in DRE patients who underwent surgery (n=10).

#### **2.2.4 Region-Based Quantitative Assessment of PET<sub>MRAC</sub> and PET<sub>CTAC</sub>**

We assessed quantitative PET<sub>MRAC</sub> bias and its potential impact on epilepsy diagnosis by comparing regional SUVs and z-scores between PET<sub>MRAC</sub> and PET<sub>CTAC</sub> using syngo.via MI Neurology software with cerebellar normalization. MI Neurology is used in routine clinical assessment to augment visual PET readings and quantify brain pathologies by comparing individual patient PET scans against an age-appropriate normal database (Scenium VD20).<sup>31</sup> Mean SUVs and z-scores ( $Z_{db}$ ) were compared between PET<sub>MRAC</sub> and PET<sub>CTAC</sub> in thirty-six specific *a priori* brain regions often implicated in DRE.

To further quantify the agreement between PET/MRI and PET/CT, we used asymmetry index (AI) mapping<sup>32</sup>, an automated data-driven approach, to non-invasively detect hypometabolic brain regions (potential SOZ) and compared AI maps between PET<sub>MRAC</sub> and PET<sub>CTAC</sub>. AI maps were generated as previously described.<sup>33</sup> Mean and minimum z-score AI ( $Z_{AI}$ ) values were calculated in hypometabolic PET ROIs and compared between PET<sub>MRAC</sub> and PET<sub>CTAC</sub>. The degree of overlap between PET<sub>MRAC</sub> and PET<sub>CTAC</sub>  $Z_{AI}$  ROIs was also assessed using the Dice similarity coefficient. Diagnostic accuracy and sensitivity of PET<sub>MRAC</sub> and PET<sub>CTAC</sub> using AI mapping for SOZ detection were determined based on the reference standard (clinical hypothesis) and histopathological findings, respectively. All data analyses were conducted with knowledge of patient clinical reports, diagnostic information, and post-surgical outcomes.

### 2.2.5 Statistical Analysis

For qualitative evaluation of PET<sub>MRAC</sub> and PET<sub>CTAC</sub> images, we assessed inter-reader agreement between the three clinical readers using Randolph's free-marginal multirater kappa test (<http://justusrandolph.net/kappa/>), where a value  $\geq 0.70$  indicates adequate agreement. For quantitative FDG-PET assessment, we used Pearson product-moment analysis to determine the correlation in SUV as well as  $Z_{db}$  across all brain regions between PET<sub>MRAC</sub> and PET<sub>CTAC</sub>. We used Bland-Altman analysis to assess brain SUV and  $Z_{db}$  bias between modalities. Additionally, we used the two-sample t-test to compare regional mean SUV between PET<sub>MRAC</sub> and PET<sub>CTAC</sub>. For all analyses,  $p < 0.05$  (uncorrected) was considered statistically significant.

## 2.3 Results

Visual assessment of PET<sub>MRAC</sub> and PET<sub>CTAC</sub> revealed similar SUV<sub>MRAC</sub> and SUV<sub>CTAC</sub> images in all 18 DRE patients, as illustrated in a representative patient (patient #2) in **Figure 2.1**. Interestingly, in this patient, although visual readings were comparable between modalities, the PET<sub>MRAC</sub>  $Z_{db}$  images were slightly exaggerated relative to the PET<sub>CTAC</sub> (**Figure 2.1B**). However, all three readers reached the same clinical outcome on PET<sub>MRAC</sub> and PET<sub>CTAC</sub>. In all 18 patients, inter-reader agreement for visual assessment was similar between PET<sub>MRAC</sub> and PET<sub>CTAC</sub> (overall agreement = 78% and 81%, respectively; kappa = 0.70 and 0.75, respectively). Compared to 1.5T MRI, 3T MRI revealed 50% more structural lesions. Positive lesions were identified in 5/18 (28%) patients on 1.5T MRI and 12/18 (67%) patients on 3T MRI.

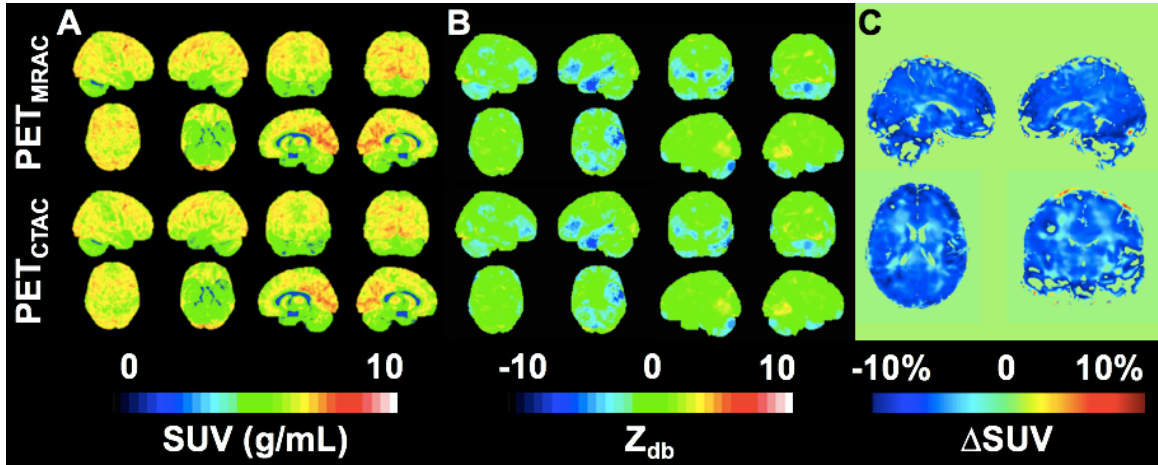


**Figure 2.1:** Comparison of visual PET assessment between PET<sub>MRAC</sub> and PET<sub>CTAC</sub> in an MRI-negative epilepsy patient (patient #2). **A)** SUV images are well matched between PET<sub>MRAC</sub> and PET<sub>CTAC</sub>. **B)** Z-score maps show exaggerated regional hypometabolism (especially in the left temporal lobe) in PET<sub>MRAC</sub>. **C)** Slices of percent difference SUV ( $\Delta$ SUV) map show low quantitative bias between PET<sub>MRAC</sub> and PET<sub>CTAC</sub>.

Quantitative PET analysis revealed a strong correlation in mean SUV ( $r = 0.99$ ,  $p < 0.001$ ) and mean  $Z_{db}$  ( $r = 0.92$ ,  $p < 0.001$ ) between modalities across all brain regions in the 18 DRE patients with low SUV and  $Z_{db}$  biases ( $0.35 \pm 0.30$  and  $-0.05 \pm 0.64$  respectively), suggesting PET<sub>MRAC</sub> provided similar metabolic information as PET<sub>CTAC</sub> (**Figure 2.2**). Regional mean SUV was well matched between PET<sub>MRAC</sub> and PET<sub>CTAC</sub> ( $p > 0.05$ ). Similarly, strong correlations in mean SUV and  $Z_{db}$  were also observed in specific brain regions included in visual clinical readings (**Table 2.2**). In these brain regions, overall inter-reader agreement, kappa values, mean SUV and mean  $Z_{db}$  were all comparable between PET<sub>MRAC</sub> and PET<sub>CTAC</sub>.

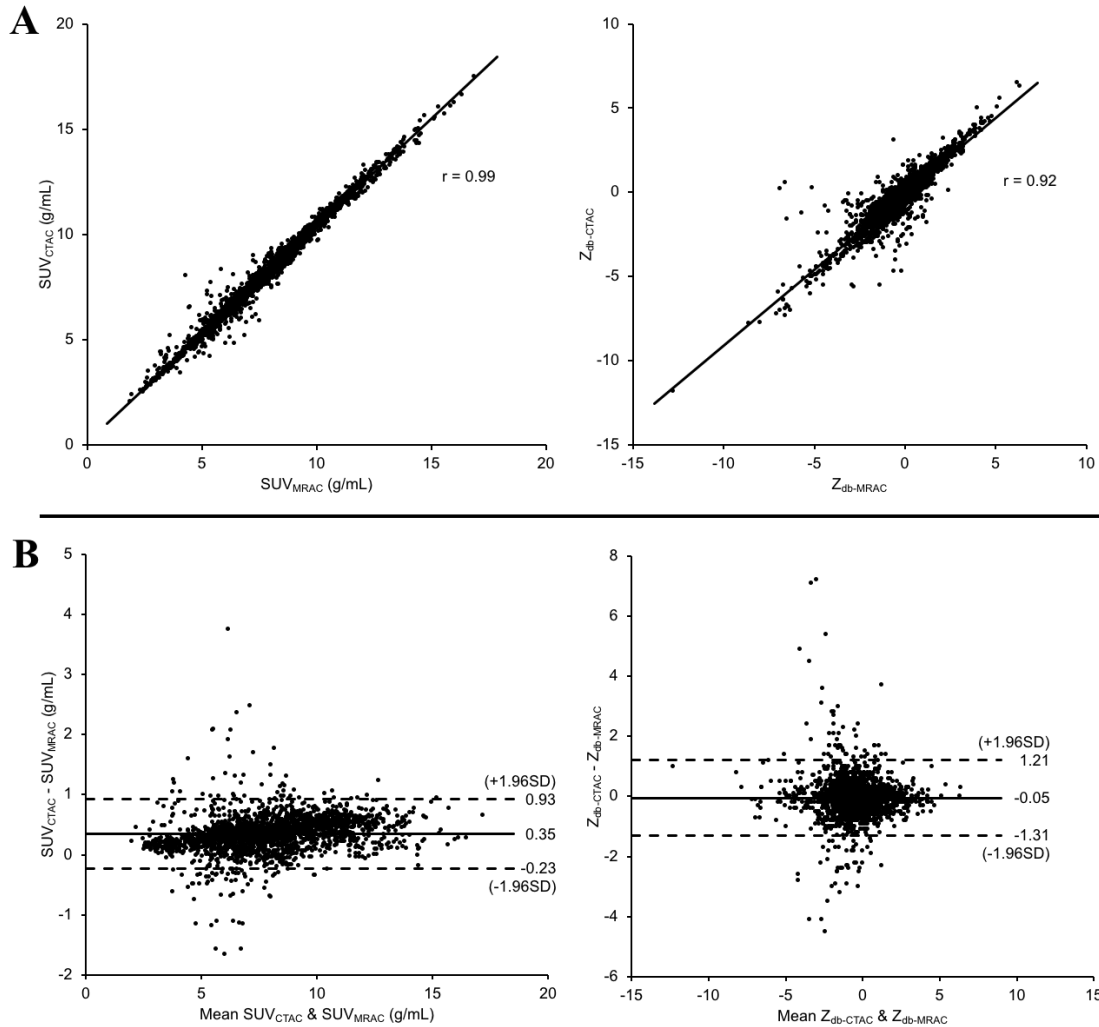


**Figure 2.2:** Association between  $PET_{MRAC}$  and  $PET_{CTAC}$  across all brain regions in 18 DRE patients. **A)** Regression plots show a tight correlation in mean SUV ( $r = 0.99$ ,  $p < 0.001$ ) and mean  $Z_{db}$  ( $r = 0.92$ ,  $p < 0.001$ ) between modalities. **B)** Bland-Altman plots reveal close agreement in SUV (bias: -0.23 to 0.93) and  $Z_{db}$  (bias: -1.31 to 1.21) between  $PET_{MRAC}$  and  $PET_{CTAC}$ .

**Table 2.2: Qualitative and quantitative regional assessments of diagnostic competency between PET<sub>MRAC</sub> and PET<sub>CTAC</sub>**

Region	PET AC	Pearson r (SUV)	Pearson r (Z <sub>db</sub> )	Mean SUV (g/mL)	Mean Z <sub>db</sub>	Inter-reader agreement (%)	Kappa
Frontal	MRAC	0.99	0.91	8.08 ± 2.17	-1.10 ± 1.08	81	0.75
	CTAC			8.43 ± 2.23	-1.20 ± 1.12	85	0.80
Temporal	MRAC	0.99	0.96	7.95 ± 2.08	-0.85 ± 1.49	56	0.41
	CTAC			8.34 ± 2.15	-0.83 ± 1.53	56	0.41
Parietal	MRAC	0.99	0.97	8.33 ± 2.25	-0.55 ± 1.33	88	0.84
	CTAC			8.69 ± 2.32	-0.68 ± 1.28	92	0.90
Hippocampus	MRAC	0.99	0.95	5.67 ± 1.57	-0.59 ± 1.67	64	0.52
	CTAC			5.85 ± 1.60	-0.83 ± 1.76	69	0.58
Occipital	MRAC	0.99	0.97	8.71 ± 2.32	0.96 ± 1.59	94	0.92
	CTAC			9.09 ± 2.40	0.83 ± 1.52	98	0.97
Cerebellum	MRAC	0.99	0.84	6.52 ± 1.75	-2.18 ± 1.91	82	0.76
	CTAC			6.96 ± 1.86	-1.60 ± 1.95	86	0.82

Note. SUV and Z-score values are reported as mean ± standard deviation.

In thirty-six *a priori* brain regions commonly implicated in DRE, mean SUV and Z<sub>db</sub> values were similar between PET<sub>MRAC</sub> and PET<sub>CTAC</sub> (**Figure 2.3**). Most notably, regional MRAC SUV and Z<sub>db</sub> biases were low (<5% and <0.5, respectively) in all *a priori* brain regions, except for inferior aspects of the brain (**Figure 2.4**).

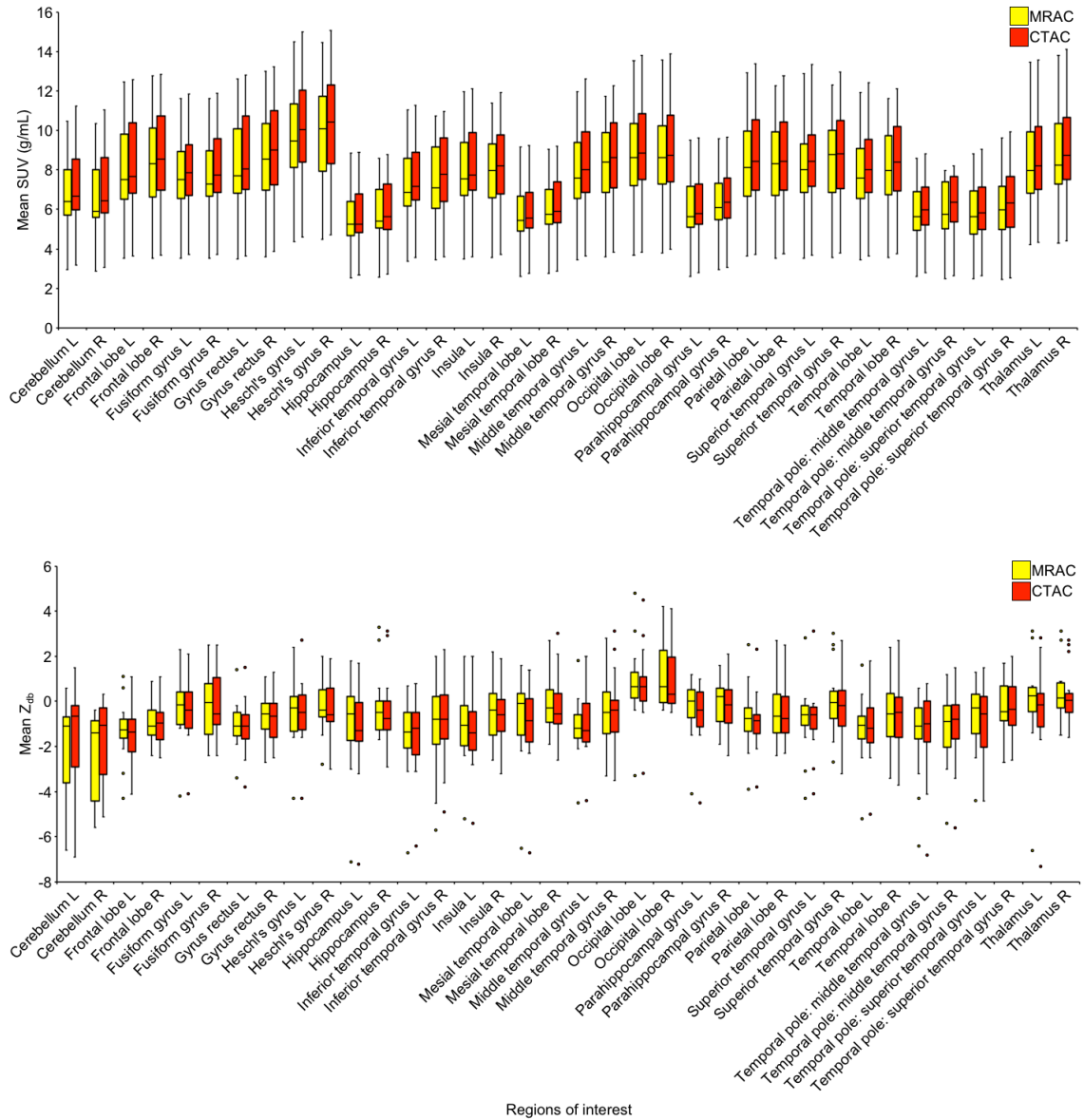


**Figure 2.3:** Mean SUV and  $Z_{db}$  values ( $n=18$ ) in thirty-six *a priori* brain regions often interrogated in DRE. MRAC and CTAC produce similar mean SUV,  $Z_{db}$  and in most cases matched outliers (black dots) across all brain regions ( $p > 0.05$ ).



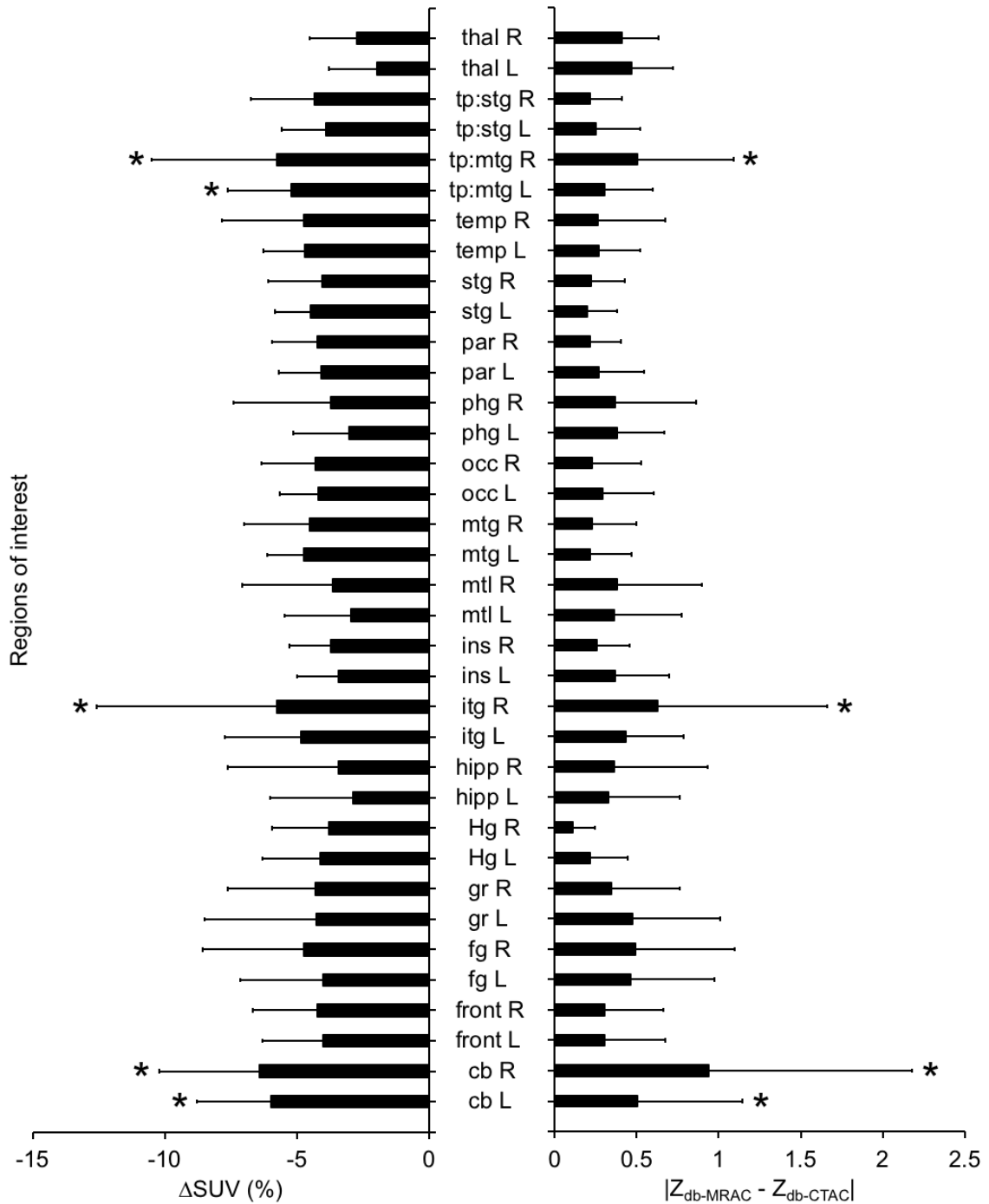


**Figure 2.4:** Group percent difference in SUV (*left*) and absolute difference in  $Z_{db}$  (*right*) between  $\text{PET}_{\text{MRAC}}$  and  $\text{PET}_{\text{CTAC}}$  in thirty-six *a priori* brain regions often interrogated in DRE. Error bars indicate standard deviation. Mean MRAC SUV and  $Z_{db}$  biases across all thirty-six *a priori* brain regions were  $-4.02 \pm 2.03\%$  and  $0.35 \pm 0.27$ , respectively. Most brain regions have  $<5\%$   $\text{SUV}_{\text{MRAC}}$  bias or  $<0.5$   $Z_{db-MRAC}$  bias except regions in lateral aspects at the base of the skull (denoted with an \*). Abbreviations: cb, cerebellum; front, frontal lobe; fg, fusiform gyrus; gr, gyrus rectus; Hg, Heschl's gyrus; hipp, hippocampus; itg, inferior temporal gyrus; ins, insula; mtl, mesial temporal lobe; mtg, middle temporal

gyrus; occ, occipital lobe; phg, parahippocampal gyrus; par, parietal lobe; stg, superior temporal gyrus; temp, temporal lobe; tp:mtg, temporal pole: middle temporal gyrus; tp:stg, temporal pole: superior temporal gyrus; thal, thalamus.

A summary of the qualitative and quantitative findings comparing the diagnostic competency of PET<sub>MRAC</sub> and PET<sub>CTAC</sub> are provided in **Table 2.3**. Image quality, presence of image artifacts, visual PET assessment, and diagnostic accuracy all showed good agreement and were comparable between modalities. In the ten patients who underwent surgery, sensitivity of both PET<sub>MRAC</sub> and PET<sub>CTAC</sub> in detecting the SOZ was 83% (visual) and 70% (AI). In all 18 patients, Z<sub>AI</sub> maps had high similarity between modalities (mean Dice coefficient =  $0.88 \pm 0.08$ ), as illustrated in a representative patient (patient #11) in **Figure 2.5**.

**Table 2.3: Qualitative and quantitative assessments of diagnostic competency between modalities**

	PET <sub>MRAC</sub>	PET <sub>CTAC</sub>
Diagnostic accuracy (visual)	87%	85%
Diagnostic accuracy (AI)	78%	78%
Sensitivity (visual; n=10)	83%	83%
Sensitivity (AI; n=10)	70%	70%
Image quality agreement (kappa)	92% (0.89)	92% (0.90)
Image artifact agreement (kappa)	83% (0.75)	88% (0.82)
Visual PET agreement (kappa)	78% (0.70)	81% (0.75)
Mean $Z_{AI}$	$-2.54 \pm 0.41$	$-2.56 \pm 0.42$
Minimum $Z_{AI}$	$-4.40 \pm 1.22$	$-4.38 \pm 1.21$
Dice coefficient (AI) = $0.88 \pm 0.08$		

Note. Visual PET agreement is the average concordance in visual PET readings across all brain regions between the three clinical readers. Visual PET readings were augmented with quantitative PET ( $Z_{db}$ ). Mean and minimum  $Z_{AI}$  values are reported as mean  $\pm$  standard deviation.

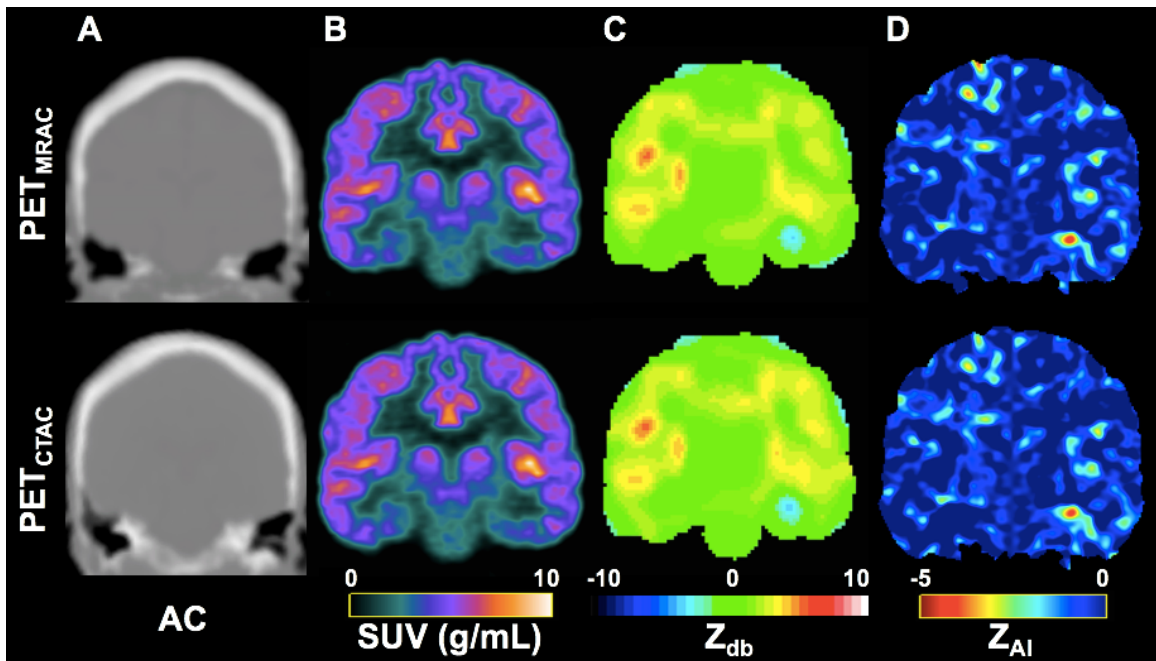


**Figure 2.5:** Visual assessment reveals similar A) attenuation correction, B) SUV, C)  $Z_{db}$  and D)  $Z_{AI}$  maps (L < R) between PET<sub>MRAC</sub> and PET<sub>CTAC</sub> in one DRE patient (patient #11).

## 2.4 Discussion

This study assessed the potential clinical value of hybrid PET/MRI in epilepsy imaging for DRE surgical evaluation by first evaluating the diagnostic equivalency of qualitative and quantitative PET/MRI against the clinical standard PET/CT and post-surgical outcomes. Visual assessments of PET/MRI and PET/CT were similar and yielded comparable diagnostic outcome in our DRE patient cohort. Likewise, the quantitative bias between  $PET_{MRAC}$  and  $PET_{CTAC}$  was low and of no practical significance.

Other studies have attempted to evaluate the clinical value of hybrid PET/MRI in DRE.<sup>11,12,23,34,35</sup> For example, Shang et al. (2018) assessed concordance between ASL-MRI and FDG-PET in MRI-negative epilepsy, but did not compare metabolic findings to the clinical standard PET/CT.<sup>12</sup> Shin et al. (2015) aimed to evaluate the potential added value of 3T hybrid PET/MRI in localizing the epileptic focus in DRE compared to standalone 1.5T MRI and PET/CT, however, PET/CT was acquired in only 40% of patients and use of PET/MRI was not evaluated against IC-EEG and post-surgical outcomes.<sup>35</sup> Similarly, other studies such as Boscolo-Galazzo et al. (2016), Ding et al. (2014) and Paldino et al. (2017) that attempted to assess concordance between PET/MRI and PET/CT findings in DRE also lacked validation against post-surgical outcomes, most notably gold-standard histopathology.<sup>11,23,34</sup> Thus, our study, by comparing PET findings to post-surgical and histopathology outcomes, appears to be the first to comprehensively demonstrate the potential clinical utility of hybrid PET/MRI in epilepsy imaging using a recently optimized MRAC approach.

The advantages of hybrid PET/MRI in epilepsy extend beyond co-registration and co-interpretation of PET and structural MRI to co-localization of PET with advanced functional MRI and structural connectivity techniques such as diffusion tractography imaging.<sup>33</sup> Recently, several groups have already shown promising first results when assessing patients with epilepsy using simultaneous PET/MRI.<sup>11,34,35</sup> These studies focused on localization of SOZ using conventional structural MRI and qualitative visual FDG-PET assessments. While it is not yet fully known if combined quantitative PET and MRI can provide higher rates of SOZ localization compared to qualitative co-interpretation of PET and MRI, one study has shown that quantitative PET can improve

confidence of a clinical reader's visual assessment of PET.<sup>11</sup> As demonstrated here, although quantitative PET/MRI using an existing normal PET/CT database to augment visual assessments can be limited, these limitations may be compensated for using other semi-quantitative approaches, such as AI mapping when a normal database is not available or suitable, for example in pediatrics.<sup>11,32</sup> Because AI mapping compares glucose metabolism between hemispheres within individual patients, it may be less sensitive to the attenuation correction approach and could be a promising tool for assessing PET/MRI abnormalities in epilepsy, especially if comparison of AI values between patients and healthy controls are used.

Although we found that regional mean SUVs were well matched across brain regions, biases in mean SUV from PET/MRI of up to 10% can occur in brain regions at the base of the skull where there is greater variability in bone densities and higher proportion of mixed tissue signals such as the inferior temporal gyrus, temporal pole, and cerebellum. This SUV underestimation is most likely related to inadequate tissue classification in MRAC approaches, a challenge for MRI, given that bone and air in sinuses both appear black on MRI and can be challenging to distinguish. While these MRAC errors further bias quantitative PET and could limit the clinical adoption of hybrid PET/MRI for epilepsy imaging, we have demonstrated in our study the diagnostic equivalency of PET/MRI to PET/CT, suggesting that these MRAC biases do not seem to affect the overall clinical impression provided by PET/MRI, a finding that is consistent with past studies.<sup>23,24</sup> Nevertheless, if PET/MRI in conjunction with quantitative PET evaluation (such as syngo.via MI Neurology) is to be used for improving SOZ localization, then further improvements in MRAC as well as consideration of practical issues related to PET/MRI scanning such as inaccurate compensation for head pads and the use of headphones<sup>36</sup>, are still required before the use of these novel technologies can be recommended as clinical standard of care. It is expected that improvements in brain tissue classification and bone modelling from novel machine learning approaches<sup>37</sup> will further improve PET/MRI performance at the base of the skull, potentially reducing the MRAC biases observed in this study.

Although we have demonstrated the diagnostic equivalency of PET/MRI to PET/CT in this study, the potential added value of hybrid PET/MRI in epilepsy imaging above and beyond the current clinical standard – PET/CT and 1.5T/3T MRI – is still yet to be fully investigated. It is apparent that 3T MRI provides a clear advantage over 1.5T MRI for anatomical localization of DRE as demonstrated here and reported elsewhere.<sup>35</sup> However, the added value of simultaneous acquisition of PET/3T MRI in providing pharmacokinetic modeling of PET<sup>38</sup>, as well as novel iterative partial volume and motion correction algorithms that use MRI to improve PET resolution<sup>39</sup> have not been explored in DRE, particularly in MRI-negative epilepsy. Recently, Poirier et al. (2020) used AI mapping of FDG-PET to guide diffusion tractography of white matter fiber pathways around hypometabolic brain regions, revealing macrostructural breakdown around SOZ in MRI-negative DRE.<sup>33</sup> While the clinical significance of hybrid PET/MRI in epilepsy surgical evaluation is still yet to be fully characterized, the potential for hybrid PET/MRI is evident.

## **2.5 Conclusions**

Although PET/MRI has been advocated as standard of care for epilepsy imaging, the performance of PET/MRI compared to PET/CT or its clinical value for epilepsy imaging has not been fully established. This study demonstrated the diagnostic equivalency and clinical value of hybrid PET/MRI in epilepsy imaging against the current clinical standard of care. In general, PET/MRI with optimal MRAC can yield similar diagnostic performance as PET/CT. Further improvements in MRAC as well as novel approaches using fully quantitative PET analysis are likely necessary to evaluate the potential added value of hybrid PET/MRI in epilepsy before widespread clinical adoption of hybrid PET/MRI in DRE surgical evaluation can take place.

## **2.6 Acknowledgements**

The authors would like to thank John Butler and Heather Biernaski (PET/MRI Technologists) for assistance in data acquisition, Krista Doyle, the Nurse Navigator at the

London Health Sciences Centre Epilepsy Program and Don Khul, Chief Nuclear Medicine Technologist at St. Joseph's HealthCare London, for assistance with patient recruitment, and Marilyn Bignall and Autif Muhammad of Siemens Healthineers for assistance in using MI Neurology.

## 2.7 References

1. Cahill V, Sinclair B, Malpas CB, et al. Metabolic patterns and seizure outcomes following anterior temporal lobectomy. *Annals of Neurology* 2019;85:241–50.
2. Pustina D, Avants B, Sperling M, et al. Predicting the laterality of temporal lobe epilepsy from PET, MRI, and DTI: A multimodal study. *NeuroImage: Clinical* 2015;9:20–31.
3. Rathore C, Dickson JC, Teotónio R, et al. The utility of 18F-fluorodeoxyglucose PET (FDG PET) in epilepsy surgery. *Epilepsy Research* 2014;108:1306–14.
4. Duncan JS. Imaging in the surgical treatment of epilepsy. *Nature Reviews Neurology* 2010;6:537–50.
5. Téllez-Zenteno JF, Dhar R, Wiebe S. Long-term seizure outcomes following epilepsy surgery: a systematic review and meta-analysis. *Brain* 2005;128:1188–98.
6. de Tisi J, Bell GS, Peacock JL, et al. The long-term outcome of adult epilepsy surgery, patterns of seizure remission, and relapse: a cohort study. *The Lancet* 2011;378:1388–95.
7. Burneo JG, Poon R, Kellett S, et al. The Utility of Positron Emission Tomography in Epilepsy. *Canadian Journal of Neurological Sciences* 2015;42:360–71.
8. Sarikaya I. PET studies in epilepsy. *Am J Nucl Med Mol Imaging* 2015;5:416–30.
9. Aparicio J, Carreño M, Bargalló N, et al. Combined 18F-FDG-PET and diffusion tensor imaging in mesial temporal lobe epilepsy with hippocampal sclerosis. *NeuroImage: Clinical* 2016;12:976–89.
10. Gok B, Jallo G, Hayeri R, et al. The evaluation of FDG-PET imaging for epileptogenic focus localization in patients with MRI positive and MRI negative temporal lobe epilepsy. *Neuroradiology* 2013;55:541–50.
11. Boscolo Galazzo I, Mattoli MV, Pizzini FB, et al. Cerebral metabolism and perfusion in MR-negative individuals with refractory focal epilepsy assessed by simultaneous acquisition of 18 F-FDG PET and arterial spin labeling. *NeuroImage: Clinical* 2016;11:648–57.
12. Shang K, Wang J, Fan X, et al. Clinical Value of Hybrid TOF-PET/MR Imaging–Based Multiparametric Imaging in Localizing Seizure Focus in Patients with MRI–Negative Temporal Lobe Epilepsy. *American Journal of Neuroradiology* 2018;39:1791–8.



13. Salamon N, Kung J, Shaw SJ, et al. FDG-PET/MRI coregistration improves detection of cortical dysplasia in patients with epilepsy. *Neurology* 2008;71:1594–601.
14. Lee KK, Salamon N. [18F] Fluorodeoxyglucose–Positron-Emission Tomography and MR Imaging Coregistration for Presurgical Evaluation of Medically Refractory Epilepsy. *American Journal of Neuroradiology* 2009;30:1811–6.
15. Rubi S, Setoain X, Donaire A, et al. Validation of FDG-PET/MRI coregistration in nonlesional refractory childhood epilepsy. *Epilepsia* 2011;52:2216–24.
16. Johnson PM, Taylor R, Whelan T, et al. Rigid-body motion correction in hybrid PET/MRI using spherical navigator echoes. *Phys Med Biol* 2019;64:08NT03.
17. Mehranian A, Belzunce MA, Niccolini F, et al. PET image reconstruction using multi-parametric anatofunctional priors. *Phys Med Biol* 2017;62:5975–6007.
18. Anazodo U, Kewin M, Finger E, et al. Preliminary evaluation of MRI-derived input function for quantitative measurement of glucose metabolism in an integrated PET-MRI. *EJNMMI Phys* 2015;2:A80.
19. Shiyam Sundar LK, Muzik O, Rischka L, et al. Promise of Fully Integrated PET/MRI: Noninvasive Clinical Quantification of Cerebral Glucose Metabolism. *J Nucl Med* 2020;61:276–84.
20. Tan YL, Kim H, Lee S, et al. Quantitative surface analysis of combined MRI and PET enhances detection of focal cortical dysplasias. *NeuroImage* 2018;166:10–8.
21. Andersen FL, Ladefoged CN, Beyer T, et al. Combined PET/MR imaging in neurology: MR-based attenuation correction implies a strong spatial bias when ignoring bone. *NeuroImage* 2014;84:206–16.
22. Larsson A, Johansson A, Axelsson J, et al. Evaluation of an attenuation correction method for PET/MR imaging of the head based on substitute CT images. *Magn Reson Mater Phys* 2013;26:127–36.
23. Paldino MJ, Yang E, Jones JY, et al. Comparison of the diagnostic accuracy of PET/MRI to PET/CT-acquired FDG brain exams for seizure focus detection: a prospective study. *Pediatr Radiol* 2017;47:1500–7.
24. Oldan JD, Shin HW, Khandani AH, et al. Subsequent experience in hybrid PET-MRI for evaluation of refractory focal onset epilepsy. *Seizure* 2018;61:128–34.
25. Ladefoged CN, Benoit D, Law I, et al. Region specific optimization of continuous linear attenuation coefficients based on UTE (RESOLUTE): application to PET/MR brain imaging. *Phys Med Biol* 2015;60:8047–65.

26. Ladefoged CN, Law I, Anazodo U, et al. A multi-centre evaluation of eleven clinically feasible brain PET/MRI attenuation correction techniques using a large cohort of patients. *NeuroImage* 2017;147:346–59.
27. Engel JJr, Van Ness PC, Rasmussen TB, et al. Outcome with respect to epileptic seizures. Engel JJr, ed. *Surgical Treatment of the Epilepsies* 1993. [Epub ahead of print].
28. Fedorov A, Beichel R, Kalpathy-Cramer J, et al. 3D Slicer as an Image Computing Platform for the Quantitative Imaging Network. *Magn Reson Imaging* 2012;30:1323–41.
29. Carney JPJ, Townsend DW, Rappoport V, et al. Method for transforming CT images for attenuation correction in PET/CT imaging. *Medical Physics* 2006;33:976–83.
30. Musiek ES, Chen Y, Korczykowski M, et al. Direct comparison of fluorodeoxyglucose positron emission tomography and arterial spin labeling magnetic resonance imaging in Alzheimer’s disease. *Alzheimer’s & Dementia* 2012;8:51–9.
31. Siemens Medical. syngo.via Operator Manual - syngo.MI Neurology, VB10A.
32. Didelot A, Mauguiere F, Redoute J, et al. Voxel-Based Analysis of Asymmetry Index Maps Increases the Specificity of 18F-MPPF PET Abnormalities for Localizing the Epileptogenic Zone in Temporal Lobe Epilepsies. *Journal of Nuclear Medicine* 2010;51:1732–9.
33. Poirier SE, Kwan BYM, Jurkiewicz MT, et al. 18F-FDG PET-guided diffusion tractography reveals white matter abnormalities around the epileptic focus in medically refractory epilepsy: implications for epilepsy surgical evaluation. *European Journal of Hybrid Imaging* 2020;4:10.
34. Ding YS, Chen BB, Glielmi C, et al. A pilot study in epilepsy patients using simultaneous PET/MR. *Am J Nucl Med Mol Imaging* 2014;4:459–70.
35. Shin HW, Jewells V, Sheikh A, et al. Initial experience in hybrid PET-MRI for evaluation of refractory focal onset epilepsy. *Seizure* 2015;31:1–4.
36. Mackewn JE, Stirling J, Jeljeli S, et al. Practical issues and limitations of brain attenuation correction on a simultaneous PET-MR scanner. *EJNMMI Phys* 2020;7:24.
37. Liu F, Jang H, Kijowski R, et al. Deep Learning MR Imaging–based Attenuation Correction for PET/MR Imaging. *Radiology* 2017;286:676–84.
38. Traub-Weidinger T, Muzik O, Sundar LKS, et al. Utility of Absolute Quantification in Non-lesional Extratemporal Lobe Epilepsy Using FDG PET/MR Imaging. *Front Neurol* 2020;11:54.

39. Silva-Rodríguez J, Cortés J, Rodríguez-Osorio X, et al. Iterative Structural and Functional Synergistic Resolution Recovery (iSFS-RR) Applied to PET-MR Images in Epilepsy. *IEEE Transactions on Nuclear Science* 2016;63:2434–42.

## Chapter 3

### **3 <sup>18</sup>F-FDG PET-guided diffusion tractography reveals white matter abnormalities around the epileptic focus: implications for epilepsy surgical evaluation**

This chapter has been adapted from the following manuscript publication:

**Poirier SE**, Kwan BYM, Jurkiewicz MT, Samargandy L, Steven DA, Suller-Marti A, Lam Shin Cheung V, Khan AR, Prato FS, Burneo JG, Thiessen JD, Anazodo UC. <sup>18</sup>F-FDG PET-guided diffusion tractography reveals white matter abnormalities around the epileptic focus in medically refractory epilepsy: implications for epilepsy surgical evaluation. *European J Hybrid Imaging*. 2020;4:10. DOI: <https://doi.org/10.1186/s41824-020-00079-7>

#### **3.1 Introduction**

Medically refractory epilepsy (MRE) affects approximately 30% of epilepsy patients and is defined as a chronic neurological disorder where seizures persist despite administration of anti-epileptic drugs (AEDs) (Helmstaedter et al. 2003; Richardson et al. 2004; Jiang et al. 2017). In some MRE patients, surgical resection of the epileptic focus (EF) – the brain region responsible for seizures – can alleviate seizure occurrence and improve overall quality of life (Richardson et al. 2004; Caciagli et al. 2014; Cahill et al. 2019). Positive surgical outcomes are highly dependent on accurate identification of the EF to ensure the epileptic region is safely removed without harming surrounding healthy brain tissue (Bettus et al. 2009). The current gold standard for identifying the EF is intracranial electroencephalography (IC-EEG), where either subdural or depth electrodes are used to directly locate abnormal brain activity (suspected EF) before surgical resection is performed (Knowlton 2006; Blount et al. 2008). However, about 50% of MRE patients continue to have seizures after surgery (Téllez-Zenteno et al. 2005; de Tisi et al. 2011). Surgery can fail to prevent seizures when the EF is not properly delineated or detected prior to resection. Additionally, poor surgical outcomes can occur due to unknown interactions between the EF and surrounding neural networks (Aparicio et al. 2016).

Recent advances in medical imaging have seen the increased clinical use of magnetic resonance imaging (MRI) and positron emission tomography (PET) to non-invasively locate the EF and map out the structure and function of surrounding brain regions. Anatomical MRI can detect structural lesions responsible for seizures in about 60% of MRE patients (Burneo et al. 2015), while other advanced MRI techniques, such as diffusion tensor imaging (DTI), can be used to effectively characterize the EF and its relationships with surrounding brain regions (Aparicio et al. 2016; Jiang et al. 2017). DTI non-invasively characterizes tissue microstructure by providing a three-dimensional model of water diffusion in the brain (Basser and Jones 2002; Jones and Cercignani 2010). In addition, DTI can be used to investigate the structural connectivity of neural networks through mapping out diffusion along white matter (WM) fiber pathways (Le Bihan et al. 1986; Le Bihan 2006; Aparicio et al. 2016; Sivakanthan et al. 2016). WM pathways can be characterized using DTI-derived parameters, which are extracted from the diffusion tensor used to model water diffusion at each voxel in the brain. The most commonly used tensor-derived scalar is fractional anisotropy (FA), which is a measure of WM integrity and describes the tendency of water to preferentially diffuse along the length of the fiber bundle (Le Bihan 2006; Mori and Zhang 2006; Soares et al. 2013). Recent DTI studies have revealed that severe FA reduction in WM may correspond to widespread microstructural abnormalities in MRE (Labate et al. 2015; Jiang et al. 2017). To further assess tissue microstructure breakdown, WM pathways can be visualized by reconstructing WM fibers using diffusion tractography. Diffusion tractography techniques continue to be refined and adapted for neurosurgical planning and these techniques have been shown to accurately track WM fibers in temporal lobe regions essential for surgical success (Sivakanthan et al. 2016).

PET, on the other hand, is the most sensitive non-invasive clinical tool for identifying the EF especially in cases where MRI is negative or equivocal (Burneo et al. 2015).  $^{18}\text{F}$ -Fluorodeoxyglucose PET (FDG-PET) can be used to detect the EF as brain areas showing decreased glucose uptake (glucose hypometabolism) (Sarıkaya 2015; Burneo et al. 2015; Aparicio et al. 2016; Cahill et al. 2019). Glucose hypometabolic regions of interest (ROIs) are often identified by visual assessment of FDG-PET images, however, some abnormalities may be missed during this process. Therefore, semi-quantitative

approaches such as asymmetry index (AI) mapping have been proposed to aid visual detection of hypometabolic PET ROIs (Henry et al. 1990; Rausch et al. 1994; Van Bogaert et al. 2000; Didelot et al. 2010; Boscolo Galazzo et al. 2016; Anazodo et al. 2018; Kamm et al. 2018; Shang et al. 2018). AI mapping investigates metabolic abnormalities by measuring the voxel-wise difference in cerebral glucose metabolism between hemispheres and has been shown to be a very sensitive biomarker for epileptogenicity (Didelot et al. 2010; Boscolo Galazzo et al. 2016). Using AI to investigate metabolic asymmetries can be useful because the process may be done on individual patients and does not require comparison to a healthy control database.

Recently, it has been shown that multimodal brain imaging combining PET and MRI information may improve seizure site characterization compared to standalone IC-EEG, PET, or MRI (Burneo et al. 2015). Opportunely, this finding coincides with increased availability of advanced imaging systems that combine PET/MRI into an integrated system. Although researchers are starting to implement simultaneous PET/MRI in the clinical setting, the combined use of PET and DTI for presurgical evaluation of epilepsy is yet to be fully investigated. To our knowledge, only two studies to date have assessed whether cortical glucose hypometabolism seen on FDG-PET is related to WM alterations identified by DTI in the brains of MRE patients (Lippé et al. 2012; Aparicio et al. 2016). However, these studies acquired PET and MRI scans at separate timepoints which can introduce registration errors between modalities, making it difficult to accurately detect the seizure onset zone in the brain and assess relationships between PET and MRI findings. Simultaneous acquisition of PET and MRI data using a hybrid PET/MRI scanner acquires both datasets in the same imaging session with intrinsic spatial and temporal registration, potentially improving the accuracy of detecting the EF and may shed new insight into the pathophysiology of MRE. In this hybrid PET/MRI study, we developed a PET-guided diffusion tractography (PET/DTI) approach combining FDG-PET and diffusion MRI to investigate WM integrity in the brains of MRE patients. AI mapping of FDG-PET was used to guide diffusion tractography of WM tracts in MRE patients to better understand structural connectivity of WM fibers affected by glucose hypometabolic regions (suspected EF). WM fibers were also visually inspected by a

neurologist to assess potential clinical impact of PET/DTI on decision-making in epilepsy surgery.

## **3.2 Materials and Methods**

### **3.2.1 Patients**

The study included 14 MRE patients (6 males and 8 females; mean age =  $38 \pm 14$  years) from the London Health Sciences Centre epilepsy monitoring unit (EMU), diagnosed after failing two or more adequate trials of AEDs. Clinical assessment in the EMU included neuropsychological evaluation, prolonged scalp video-EEG, and 1.5T MRI to localize the EF. Patient demographics and clinical profile are provided in **Table 3.1**. Mean epilepsy onset and duration was  $23 \pm 13$  and  $15 \pm 15$  years, respectively. The cohort consisted of 10 MRI-negative and 4 MRI-equivocal MRE patients, determined based on all available diagnostic information (clinical hypothesis, semiology, and 1.5T MRI reports). All patients provided written informed consent. The study was approved by the University Research Ethics Board and conducted in accordance with the Declaration of Helsinki ethical standards.

**Table 3.1: Patient demographics and clinical profile**

Patient No.	Sex	Age (yr)	Onset/Duration (yr)	Seizure Frequency	1.5T MRI	Clinical Hypothesis
1	M	52	4/48	–	Left MTS*	Left temporal-frontal lobe
2	M	29	16/13	4/wk	Left temporal FCD*	Left frontal lobe
3	F	18	14/4	1/mo	Unremarkable	Right frontal lobe
4	M	60	41/19	6/yr	Unremarkable	Left temporal-frontal lobe
5	F	28	27/1	Unpredictable	Unremarkable	Right temporal lobe
6	M	29	23/6	2–3/mo	Unremarkable	Left temporal-frontal lobe
7	F	32	25/7	–	Unremarkable	Left temporal lobe
8	F	36	15/21	1/wk	Bitemporal SH*	Right frontal lobe
9	F	45	35/10	5–7/mo	Left MTS*	Left temporal lobe
10	M	23	21/2	1–2/mo	Unremarkable	Right temporal lobe
11	F	26	17/9	2–3/mo	Unremarkable	Right temporal-frontal lobe
12	F	58	21/37	–	Unremarkable	Left temporal lobe
13	F	38	7/31	–	Unremarkable	Right temporal lobe
14	M	55	54/1	–	Unremarkable	Right temporal lobe

Abbreviations: \*, equivocal finding; –, missing data; F, female; FCD, focal cortical dysplasia; M, male; MTS, mesial temporal sclerosis; SH, subcortical heterotopia.

### 3.2.2 Data Acquisition

Data were acquired using a 3T hybrid PET/MRI scanner (Biograph mMR, Siemens Healthineers, Erlangen, Germany) located at the Lawson Health Research Institute. Patients fasted for at least 6 h prior to the study (fasting blood glucose =  $4.3 \pm 0.6$  mmol/L). PET/MRI were acquired immediately after clinical PET/CT scans (net injected dose of FDG =  $190 \pm 17$  MBq, PET/MRI post-injection time =  $72 \pm 5$  minutes) and the PET/MRI data were used in this study. Serial MRI scans were performed during a 30-min list-mode PET imaging session. An isotropic ( $1 \text{ mm}^3$ ) high resolution T1-weighted MRI and T2-weighted FLAIR MRI were acquired covering the whole brain using a three-dimensional magnetization-prepared rapid gradient-echo sequence (MPRAGE) and fast-spin echo sequence (SPACE) respectively to assess evidence of structural abnormalities (Brant-Zawadzki et al. 1992). Diffusion-weighted imaging (DWI) was acquired using a single shot echo-planar imaging (EPI) sequence with the following parameters: 2 mm



isotropic resolution, 64 contiguous slices, b-values = 0, 1000 s/mm<sup>2</sup> and 64 diffusion encoding directions. Two spin-echo images were acquired in opposite phase-encoding directions with b-values = 0 s/mm<sup>2</sup> and 6 directions to correct for inherent susceptibility-induced distortions in DWI. The PET data were reconstructed to one image volume (ordered subset expectation maximization algorithm; 3 iterations, 21 subsets, 2 mm full-width at half-maximum (FWHM) Gaussian filter, 2.5 zoom factor, 344 × 344 × 127 matrix and 2.09 × 2.09 × 2.03 mm<sup>3</sup> voxels). Attenuation correction was performed using an ultrashort echo time MRI sequence and an offline MRI-based attenuation correction approach (RESOLUTE) (Ladefoged et al. 2015).

### 3.2.3 DWI Preprocessing

Before image preprocessing, all DWI volumes were visually inspected for artifacts to ensure only good quality data were used. DWI data were preprocessed using an in-house image analysis pipeline that incorporated steps from a variety of different image processing software packages (see **Figure 1.7**). Each patient's DWI images were first denoised using an optimized non-local means filter (Wiest-Daesslé et al. 2008; Coupé et al. 2008, 2010) in MATLAB (MathWorks®, Natick, MA) followed by subject motion, eddy current, and bias field corrections using FMRIB's Software Library (FSL) (Woolrich et al. 2009), MRtrix3 (Tournier et al. 2019) and ANTS (Avants et al. 2011), respectively. Tensors were fit to the data using non-linear least-squares estimation in ExploreDTI (Leemans et al. 2009) to generate an FA map. For WM fiber reconstruction, all diffusion tractography steps were performed using MRtrix3. A single fiber WM response function was estimated from the preprocessed DWI data using a spherical harmonics order of 8. The DWI data were upsampled to 1x1x1 mm<sup>3</sup> isotropic voxels, and the fiber orientation distribution function was calculated by constrained spherical deconvolution with a spherical harmonics order of 8 and a whole-brain mask to constrain calculations to voxels within the brain. The maximas of the fiber orientation distribution function were then extracted and used to visualize the WM fibers.

### 3.2.4 PET Data Analysis

PET preprocessing steps were completed using FSL, ANTS and SPM12 (Wellcome Department of Cognitive Neurology, Institute of Neurology, London). For AI mapping, we used the MNI T1 1 mm isotropic image provided by FSL as a template for spatial alignment of patient FDG-PET images. To account for geometric distortions in patient anatomy between hemispheres, this template was made symmetric by flipping it about the sagittal plane and then calculating the mean image of the flipped and unflipped images. Each patient's FDG-PET data were spatially normalized to the symmetric template using a three-step registration method in ANTS that consisted of linear and non-linear warping transformations that aligned brain structures in the PET image as closely as possible to the template.

A voxel-wise standardized uptake value (SUV) map was calculated using:

$$\text{SUV} = \frac{C_{\text{PET}}(t) \times \text{BW}}{\text{Dose}}$$

where  $C_{\text{PET}}(t)$  is the activity concentration in each voxel of the spatially normalized PET image, BW is the patient's body weight, and Dose is the net injected dose of FDG. The SUV map was smoothed using a FWHM of 2 mm to account for differences in patient anatomy. Each patient's T1-weighted image was spatially normalized to the symmetric MNI template and then segmented into gray matter (GM), WM, and cerebrospinal fluid tissue probability maps. Because the EF is typically in GM focal regions, we only considered SUV values in voxels with at least 30% GM (based on segmentation of the aligned T1-weighted MRI). The GM SUV maps were then scaled by the individual mean GM SUV in the cerebellum to account for global metabolism effects in the brain (Anazodo et al. 2018). The relative GM SUV ( $\text{SUV}_r$ ) map was spatially flipped about the sagittal plane and a voxel-wise AI map was calculated using:

$$\text{AI} = \frac{I - fI}{2(I + fI)} \times 100$$

where  $I$  and  $fl$  are the unflipped and flipped SUVr images, respectively. To determine significant hypometabolic areas on PET, a Z-score AI ( $Z_{AI}$ ) map was calculated using:

$$Z_{AI} = \frac{X - \mu}{\sigma}$$

where  $X$  is the voxel intensity in the AI map,  $\mu$  is the mean AI of all GM voxels in the brain, and  $\sigma$  is the standard deviation AI of all GM voxels. Because we did not know the exact distribution of AI values in our sample of patients, we scaled  $Z_{AI}$  by the degrees of freedom (df) in our sample (Crawford and Garthwaite 2012). For our sample of 14 MRE patients, df was 13 therefore we considered  $Z_{AI} < -1.77$  to represent significant hypometabolism compared to the contralateral brain region. In each  $Z_{AI}$  map, the largest focal GM area containing voxels with  $Z_{AI} < -1.77$  was extracted as the hypometabolic PET ROI (suspected EF). To validate our AI mapping approach, these PET ROIs were compared against clinical findings on seizure onset area, including clinical hypothesis, scalp video-EEG, clinical reader assessment of PET SUV images, stereo-EEG (SEEG), and surgical outcome (Engel classification and ground-truth histopathology).

### **3.2.5 PET/MR Image Reading**

All FDG-PET and MR images were visually inspected by two Neuroradiologists (B.Y.M.K. and M.J.). FDG-PET was also inspected by a third reader, a Nuclear Medicine Physician (L.S.). FDG-PET was co-registered and overlaid onto MRI. T1-weighted, T2-weighted, and SUV images were visually assessed using a standard clinical imaging software (MI Neurology, SyngoVia, Siemens Healthcare, Erlangen, Germany). To aid visual assessment of PET, semi-quantitative analysis was also included in the image reading through statistical comparison of SUV values with cerebellar normalization to an age-matched healthy control database provided by the software.

### **3.2.6 PET-Guided Diffusion Tractography (PET/DTI)**

We developed a PET/DTI approach by using seed-based diffusion tractography to investigate structural integrity of WM regions around the hypometabolic PET ROI (suspected EF) identified by AI mapping. The PET ROI, which was initially defined in

MNI space, was inverse mapped back to the subject's diffusion space and used as a seed to initiate fiber tracking. WM fiber tracts were visualized and quantified using Fibernavigator, a novel diffusion tractography tool (Chamberland et al. 2015). In Fibernavigator, a  $3 \times 3 \times 3 \text{ mm}^3$  volume of interest (VOI) was placed in the GM PET ROI that was directly adjacent to the closest WM area. This VOI was dilated at incremental distances of 3, 9, and 15 mm into surrounding WM (**Figure 3.1**). Each dilated VOI was used as a seed region to generate WM tracts at each distance from the PET ROI. Another  $3 \times 3 \times 3 \text{ mm}^3$  VOI was manually defined in the contralateral brain region and dilated to generate fibers for the same three distances into surrounding WM. To assess WM tract asymmetry between ipsilateral and contralateral WM fiber tracts, WM fiber quantification was performed by extracting measurements readily available in Fibernavigator, such as fiber count (number of fibers within the bundle), mean fiber length (mm), and mean fiber cross-section (CS) ( $\text{mm}^2$ ). In addition, the mean FA was calculated as the weighted average of all FA values along the length of the tracts. Normalized (ipsilateral / contralateral) fiber count, mean FA, mean fiber length, and mean CS measurements served as preliminary assessments of WM tract asymmetry and the Wilcoxon signed-rank test was then used to compare fiber measurements across the three WM distances from the PET ROI ( $p < 0.05$  was considered significant).

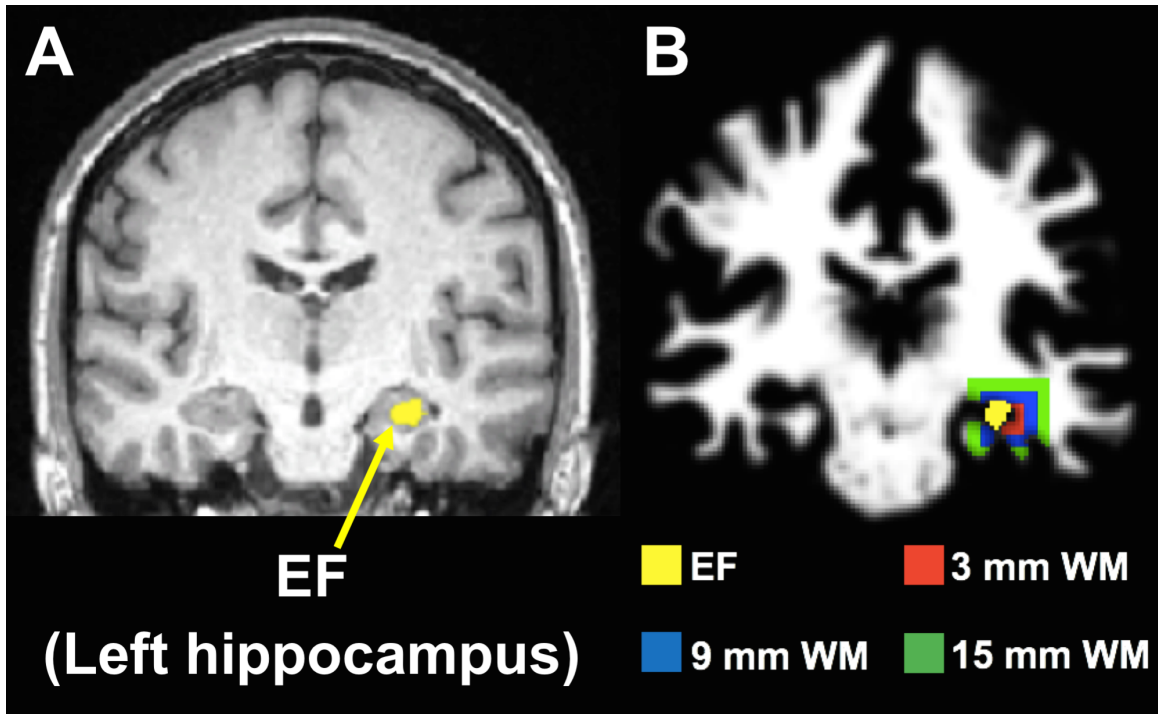


**Figure 3.1:** 2D representation of the 3D procedure for tracking WM regions around the EF in one MRE patient (patient #9). A) EF (detected by AI mapping of FDG-PET) overlaid onto structural MRI. B) EF overlaid onto a WM probability map. Because the EF is located in a cortical area (left hippocampus), WM tracking was performed at three distances away from the EF: 3 mm, 9 mm, and 15 mm. The coloured regions around the EF represent WM areas covering the three distances. These WM regions were used as seed ROIs to initiate neural fiber bundle tracking in Fibernavigator.

### 3.2.7 Clinical Assessment of PET/DTI Findings

WM fibers around the hypometabolic PET ROI for each patient were visualized by a senior Neurologist with over 15 years of practice experience (J.G.B.) in order to assess the potential clinical impact of the PET/DTI approach in guiding epilepsy surgical evaluation. For each patient, the neurologist first viewed the summary of presurgical evaluation findings (clinical hypothesis, scalp video-EEG, 1.5T MRI, PET report from PET/CT, SEEG) and then using Fibernavigator, interactively viewed the ipsilateral and contralateral WM fibers 3 mm away from the hypometabolic PET ROI identified by AI mapping. A distance of 3 mm away from the PET ROI was chosen for this assessment, as WM fibers generated from this distance pass directly adjacent to the GM PET ROI and are likely to give the best indicator of structural integrity around the epileptic zone. For

the clinical assessment of the PET/DTI approach, the neurologist determined whether the differences between ipsilateral and contralateral WM fibers around the hypometabolic PET ROI (suspected EF) were concordant with the clinical hypothesis. In order to assess potential clinical impact of PET/DTI, the neurologist's confidence after viewing the WM fibers was assigned to one of the following categories: unchanged or improved. If confidence was improved, the neurologist also reported if reassessment of surgical candidacy would be beneficial in patients who had not undergone surgery.

### **3.3 Results**

#### **3.3.1 AI Mapping of FDG-PET for EF Localization and Lateralization in MRE**

AI mapping was used to detect the EF based on regions showing significant metabolic asymmetry between hemispheres in the brain. A visual example of the AI mapping results for one MRE patient (patient #9) is shown in **Figure 3.2**. In this patient, AI mapping was able to detect a clear hypometabolic region (suspected EF) in the left temporal lobe, which matched the overall clinical hypothesis.

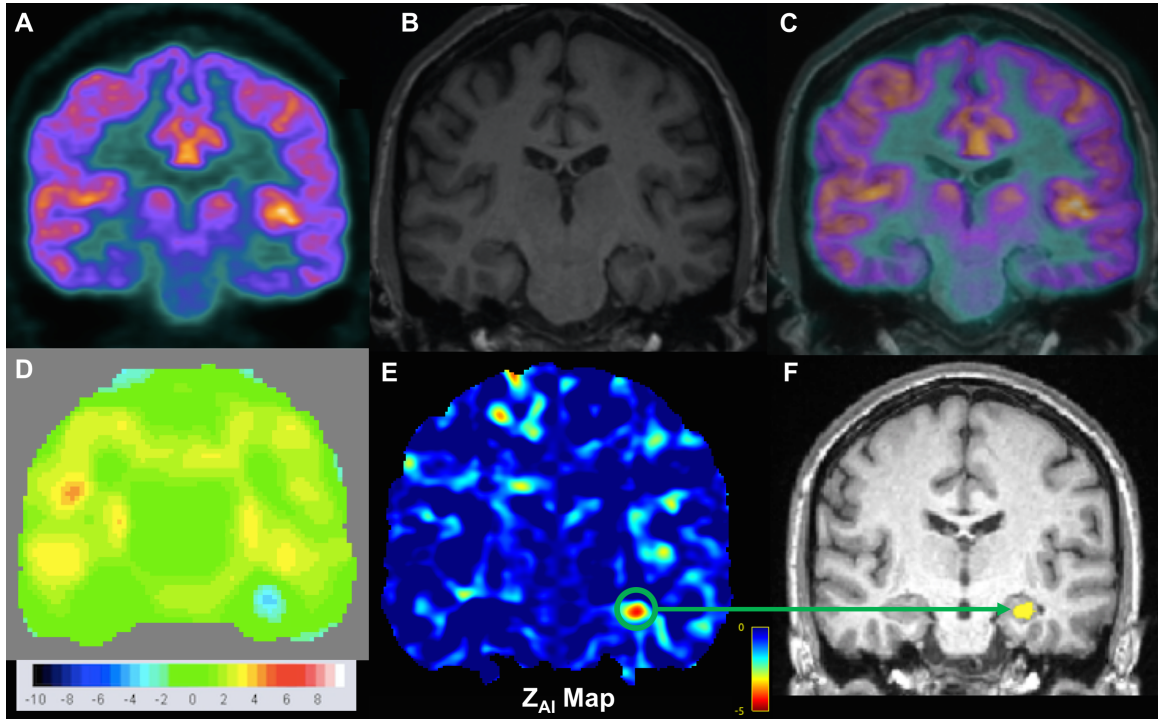


**Figure 3.2:** Images from a 45 year old female MRE patient (patient #9) with a clinical hypothesis of left temporal lobe focal epilepsy: A) PET SUV map; B) Anatomical MRI; C) PET fused with MRI; D) Z-score map from computer-assisted diagnosis of PET data (Siemens Syngo Via); E) Z-score map generated from AI mapping ( $Z_{AI}$  map), which shows a clear glucose hypometabolic region (green circle) in the left temporal lobe, indicative of a potential EF; and F) hypometabolic PET ROI (yellow) from AI mapping overlaid onto structural MRI.

Clinical hypothesis, scalp video-EEG findings from the EMU, FDG-PET hypometabolism reports from the three clinical readers (3T MRI visual assessment reported in **Table S1**), AI mapping, SEEG, and surgical findings for our cohort of 14 MRE patients are summarized in **Table 3.2**. AI mapping findings were concordant with the clinical hypothesis in localizing and lateralizing the epileptic region in 12/14 (86%) and 9/14 (64%) patients, respectively. AI mapping agreed with scalp video-EEG in 13/14 (93%) patients for both EF localization and lateralization. Concordance between AI mapping and clinical PET readings was 64%/69% (average EF localization/lateralization from the three clinical readers). Five patients underwent SEEG prior to surgical resection, and EF localization/lateralization concordance with AI mapping was observed in four patients. Mean SUV, max SUV, and mean  $Z_{AI}$  were decreased in hypometabolic PET

ROIs identified by AI mapping (see **Table S2**). Eight patients underwent surgical resection to remove the EF on the suspected epileptogenic side based on all clinical information and diagnoses available. After a one-year follow-up, 5/8 (62.5%) patients achieved Engel class IA (long-term seizure freedom), 2/8 (25%) patients achieved Engel class IIIA (significant improvement, but not completely seizure free), and 1/8 (12.5%) patients had Engel class IV (no improvement). AI mapping was concordant with surgical findings, where histopathology was performed to determine the ground-truth EF classification, in localizing and lateralizing the EF in six and four patients, respectively.



**Table 3.2: EEG, PET, and surgical findings**

Pt.	Clinical Hypothesis	Scalp EEG	PET R1	PET R2	PET R3	AI Mapping	PET/DTI	SEEG	Surgery	Engel Class	Histopathology
1	L temp/ L front	L temp/ L front	Bitemporal (L>R)	L temp	L temp	L temp	L temp	None	None	None	None
2	L front	Bifrontal	L temp/ L front/L par	L temp/ L front/L par	L front/ L par	L front	L front	None	None	None	None
3	R front	Bifrontal	Unremarkable	Unremarkable	Unremarkable	L front	R front	R front	R front lobectomy	IA	GGM WHO I
4	L temp/ L front	L temp	Unremarkable	L temp	Bitemporal	L temp	L temp	None	None	None	None
5	R temp	Bitemporal	R temp	R temp	Bitemporal	R temp	R temp	R temp	R temp lobectomy	IIIA	Gliososis
6	L temp/ L front	L temp/ L front	Bitemporal	L temp/ R front	L temp	L front	Unremarkable	L temp	L temp lobectomy	IA	Gliososis
7	L temp	L temp/ L front	Bitemporal	Bitemporal	L temp	L front	Unremarkable	None	None	None	None
8	R front	Bitemporal + extratemporal	R temp	R temp/ L front	Bitemporal/ Bifrontal	L front	Unremarkable	Bifrontal	R front lobectomy	IIIA	FCD Ib
9	L temp	L temp	Bitemporal	Bitemporal	Bitemporal	L temp	L temp	None	L temp lobectomy	IA	HS
10	R temp	R temp	R temp	R temp	R temp	L front	Unremarkable	None	R temp lobectomy	IV	Gliososis
11	R temp/ R front	R temp	R temp	R temp/ R par/L front	R temp	R temp	R temp	R temp	R temp lobectomy	IA	Gliososis
12	L temp	Bitemporal	L temp	L temp	L temp	L temp	L temp	None	None	None	None
13	R temp	Bitemporal + extratemporal	Bitemporal	Unremarkable	R temp	L temp/ L front	R temp	None	None	None	None
14	R temp	Bitemporal	Unremarkable	R temp	R temp	L temp	R temp	None	R temp lobectomy	IA	Unremarkable <sup>a</sup>

Note. FDG-PET hypometabolism reports from three clinical readers are summarized under the headings PET R1, PET R2, and PET R3.

Abbreviations: FCD, focal cortical dysplasia; front, frontal lobe; GGM, ganglioglioma; L, left; par, parietal lobe; R, right; temp, temporal lobe; WHO, World Health Organization grade.

<sup>a</sup>No specific structural changes that could explain the etopathogenesis of patient's epilepsy.

### 3.3.2 PET/DTI – Tracking WM Around Glucose Hypometabolic Regions (Suspected EF)

An example of the WM fiber visualization at each distance away from the hypometabolic PET ROI (suspected EF) for one MRE patient (patient #9) is shown in **Figure 3.3**. In this patient, visual assessment revealed noticeable differences between ipsilateral (left) and contralateral (right) fiber bundles in WM 3 mm away from the EF. No notable differences between ipsilateral and contralateral WM fibers were observed in WM 15 mm away from the EF.

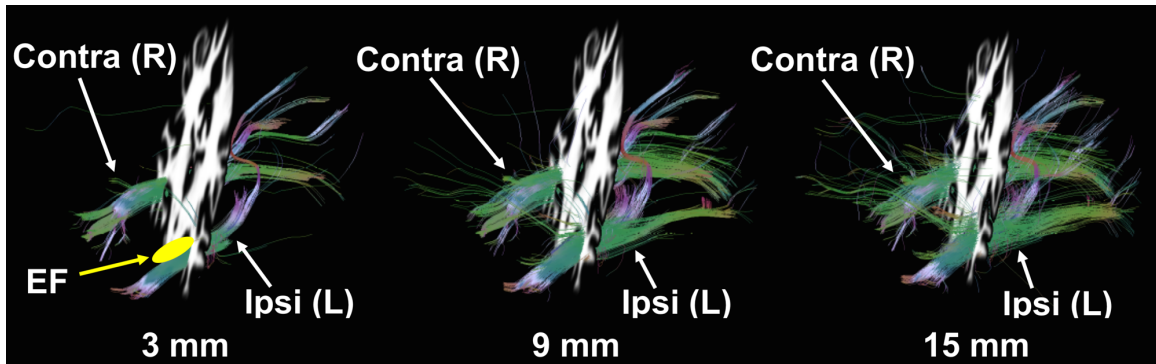


**Figure 3.3:** PET-guided diffusion tractography in one MRE patient (patient #9) with a clinical hypothesis of left temporal lobe focal epilepsy. Ipsilateral (left) and contralateral (right) WM fibers (coloured lines) are shown for the three WM distances (3, 9, and 15 mm) away from the EF (yellow) identified by AI mapping of FDG-PET. Fewer WM fibers are observed on the ipsilateral side. Differences in WM fibers between ipsilateral and contralateral sides appear more prominent at closer distances (3 mm) to the EF. Abbreviations: L, left; R, right.

When comparing fiber values across the three distances (3, 9, and 15 mm) into surrounding WM, normalized fiber count, mean FA, and mean fiber length were the lowest at a distance of 3 mm (**Figure 3.4**). At 3 mm, normalized mean FA, fiber count, and mean fiber length were decreased in 14/14 (100%), 13/14 (93%), and 12/14 (86%) patients, respectively. Normalized mean CS was decreased in 7/14 (50%) patients at this same distance. Analysis using the Wilcoxon signed-rank test revealed that mean FA was

significantly decreased at 3 mm compared to 9 mm ( $p = 0.0031$ ) and 15 mm ( $p = 0.0004$ ). Fiber count was the lowest at 3 mm and 9 mm, compared to 15 mm ( $p < 0.01$ ). Mean fiber length was significantly reduced across all three distances ( $p < 0.05$ ). The same trend was also observed when DTI scalar measurements were made in the WM seed regions used for tracking around the hypometabolic PET ROI, where mean FA was decreased at distance 3 mm compared to 9 mm and 15 mm (see **Table S3**).

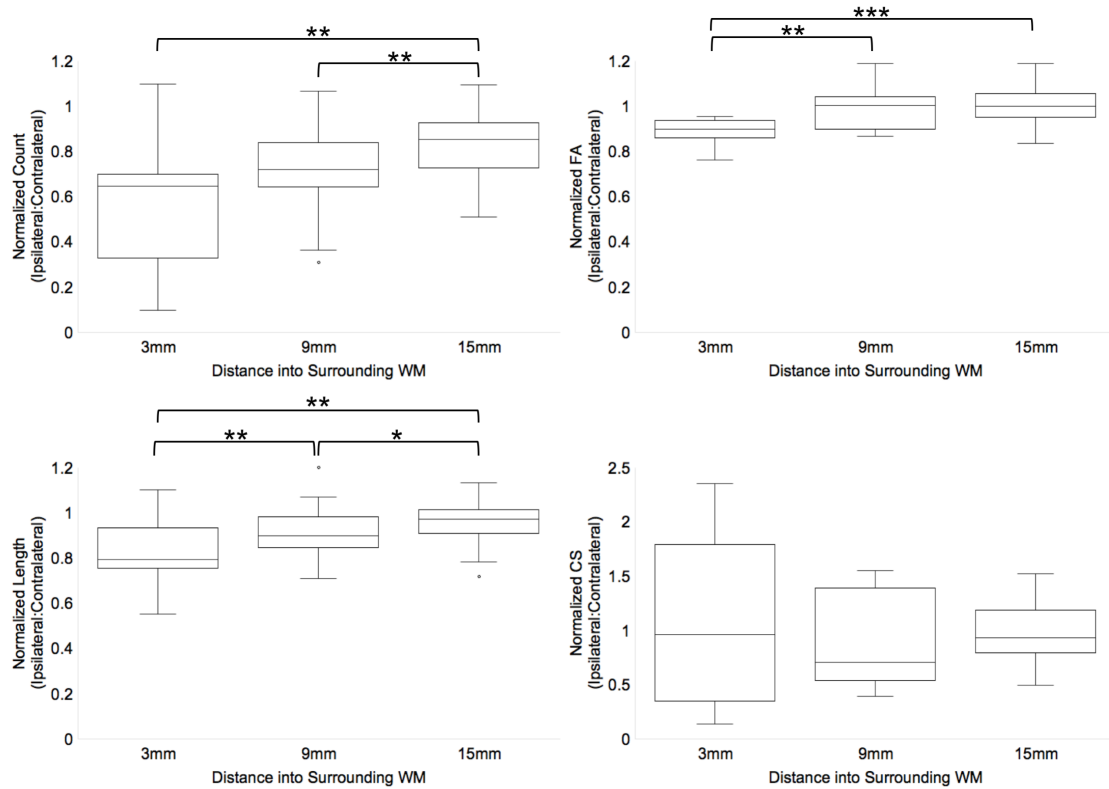


**Figure 3.4:** Quantification of WM fibers around the hypometabolic PET ROI (suspected EF) in 14 MRE patients. Ipsilateral fiber measurements were normalized to contralateral fiber measurements as a preliminary measure of WM tract asymmetry. Normalized values are plotted for the three distances away from the PET ROI. Wilcoxon signed-rank test was used to compare normalized fiber measurements across the three distances into surrounding WM ( $p < 0.05$  was considered significant). Fiber count, mean fiber length, and mean FA are decreased at closer distances to the PET ROI (3 mm) compared to 15 mm ( $p < 0.05$ ). Abbreviations: \* $p \leq 0.05$ , \*\* $p \leq 0.01$ , \*\*\* $p \leq 0.001$ .

### 3.3.3 Clinical Assessment of PET/DTI Findings

**Table 3.3** summarizes findings from the neurologist's clinical assessment of the PET/DTI approach. Eight patients had already undergone surgery. Based on clinical hypotheses, the MRE cohort consisted of seven temporal lobe, four extratemporal lobe, and three frontal lobe epilepsy patients. Upon inspection of PET/DTI, WM fiber abnormalities in the epileptic lobe were observed in 10/14 (71%) patients and these findings were concordant with the clinical hypothesis. In all 10 patients, diagnostic confidence improved after presentation of PET/DTI. Specifically, PET/DTI was contributive in five temporal lobe, three extratemporal lobe, and two frontal lobe epilepsy patients. Most importantly, PET/DTI indicated that surgical resection could be beneficial in 3/6 (50%) patients who had not undergone surgery.

**Table 3.3: Clinical assessment of PET/DTI findings**

Patient	AI Mapping	PET/DTI	Confidence after PET/DTI
1	+	+	++
2	+	+	++
3	+	+	+
4	+	+	++
5	+	+	+
6	+	-	-
7	-	-	-
8	+	-	-
9	+	+	+
10	-	-	-
11	+	+	+
12	+	+	+
13	+	+	+
14	+	+	+

Note: EF localization concordance between AI mapping and the clinical hypothesis is reported in the second column.

Abbreviations: +, concordant with clinical hypothesis or improved confidence after PET/DTI; ++, PET/DTI improved confidence and indicated that the patient may benefit from an anterior temporal lobectomy; -, discordant with clinical hypothesis or unchanged confidence after PET/DTI.

### 3.4 Discussion and Conclusions

To our knowledge, this is the first study to simultaneously combine FDG-PET and diffusion MRI to investigate WM integrity in the brains of MRE patients. We showed that AI mapping of FDG-PET can successfully detect hypometabolic brain regions (suspected EF) that are concordant with conventional epilepsy surgical evaluation techniques (1.5T MRI, EEG, visual PET assessment). We used AI mapping and diffusion tractography to develop a non-invasive approach that combines PET and MRI information into one integrated tool (PET/DTI). We demonstrated that our PET/DTI approach is feasible and can detect epileptic zones in the brains of MRI-negative epilepsy patients. We localized seizure-onset sites using AI mapping of FDG-PET and tracked WM fibers from these sites to the rest of the brain using diffusion tractography. This was achieved by implementing a robust image analysis process standardized for use in each

patient and adapting readily available imaging analysis tools for ROI mask generation and subsequent fiber tracking.

The potential clinical impact of PET/DTI in epilepsy surgical evaluation was also demonstrated in this study. Specifically, we showed that investigation of WM abnormalities adjacent to seizure-onset zones in the brain can improve diagnostic confidence in MRE. Furthermore, we found PET/DTI can even indicate that surgical resection may be beneficial in some MRE patients who have not undergone surgery. Of course, surgical candidacy of these patients would first need to be reassessed through future interdisciplinary meetings before concrete decisions to proceed with the resection can be made. Nevertheless, our findings suggest that PET/DTI can potentially impact clinical decision-making in epilepsy surgery and is a promising tool for advancing epilepsy treatment and management.

Numerous standalone PET and diffusion MRI studies have reported functional and structural alterations in MRE (Henry and Pennell 1998; Knowlton 2006; Focke et al. 2008; Lin et al. 2008; Thivard et al. 2011; James et al. 2015; Labate et al. 2015; Burneo et al. 2015; Sivakanthan et al. 2016; Jiang et al. 2017; Güvenç et al. 2018; Cahill et al. 2019), however, very few studies have assessed relationships between FDG-PET and diffusion MRI findings in epilepsy. Similar to our study, one previous report also found microstructural alterations (decreased FA and increased apparent diffusion coefficient) in WM adjacent to the epileptic zone identified by FDG-PET hypometabolism (Lippé et al. 2012), while another study revealed that metabolic and structural alterations seen using FDG-PET and DTI involve similar brain regions in mesial temporal lobe epilepsy (Aparicio et al. 2016). In contrast to (Lippé et al. 2012) and (Aparicio et al. 2016) who acquired PET and DTI separately, we used a hybrid PET/MRI scanner to simultaneously acquire PET and MRI in our study. While this may appear as a trivial difference, this has profound implications. Patients typically undergo PET and MRI scans on different days, up to a few months apart. In our cohort, the initial 1.5T MRI evaluation was on average eight months prior to the clinically indicated PET/CT. Acquiring PET and diffusion MRI scans separately can create spatial and temporal registration problems, making it difficult to accurately identify the seizure-onset zone and map its effects on brain structure and

function undergoing disease-related changes (Wang et al. 2018; Shang et al. 2018). Misalignment errors are usually due to the subject's head position being different in image space between scans which are significantly minimized by hybrid PET/MRI. Co-registration of PET with MRI through multimodal imaging therefore may allow for improved diagnostic accuracy and more precise EF detection than standalone PET or MRI, especially in MRI-negative epilepsy (Boscolo Galazzo et al. 2016; Shang et al. 2018).

The majority of the patients with temporal lobe epilepsy in our cohort had apparent PET/DTI WM abnormalities. This result is consistent with past studies that have illustrated the utility of diffusion tractography in revealing microstructural breakdown of WM pathways implicated in drug-resistant temporal lobe epilepsy (Ahmadi et al. 2009; Sivakanthan et al. 2016), as well as other studies reporting FDG-PET to have higher sensitivity for detecting the EF in temporal lobe epilepsy patients (70-90%) who had good surgical outcomes compared to those with other types of epilepsy, especially extratemporal lobe epilepsy (30-60%) (Sarıkaya 2015; Burneo et al. 2015; Aparicio et al. 2016). The surgical success rates in extratemporal lobe epilepsy are much lower than temporal lobe epilepsy (30-40% vs. 60-70%) with likelihood of achieving long-term seizure freedom further decreasing in the MRI-negative cases (Télez-Zenteno et al. 2005; de Tisi et al. 2011), suggesting the possible involvement of intricate neural networks extending beyond the EF in extratemporal lobe epilepsy that may be responsible for surgical failure. Interestingly, PET/DTI identified WM abnormalities around the EF in 3/4 patients with extratemporal lobe epilepsy in our MRE cohort (patients #1, #4, and #11 in **Table 3.3**) with improved diagnostic confidence observed in all three patients. While this is a very small number of patients, we argue this might provide some preliminary evidence that PET/DTI may potentially shed new insight into neural networks altered in extratemporal lobe epilepsy and is thus a promising tool for improving surgical outcomes, even in patients where the EF and its interactions with surrounding brain tissue extend beyond the temporal lobe.

In our study, PET/DTI was unremarkable in four patients (see patients #6, #7, #8, and #10 in **Table 3.3**). Specifically, in patients #6, #7, and #8, all clinical findings lacked

concordance, with only patient #6 becoming seizure-free after surgery (see **Table 3.2**). In patient #10, AI mapping was not concordant with visual PET assessment from the three clinical readers and the patient showed no improvement after surgery (Engel class IV). These findings suggest that the four PET/DTI-negative patients in our study may have had a seizure focus with underlying physiological abnormalities that were too subtle to confidently detect using neuroimaging. Further research needs to be conducted on why functional and structural properties measured using PET and MRI are impaired in some epilepsy patients while in others, they appear intact.

It is well established that FDG-PET is the most sensitive functional imaging tool for indirectly identifying epileptic regions based on glucose hypometabolism (Knowlton 2006; Burneo et al. 2015; Aparicio et al. 2016). However, glucose hypometabolic regions identified by PET could extend beyond the true EF especially in extratemporal lobe epilepsy and may reflect pathophysiology of seizure propagation from the epileptic zone to surrounding neural networks (Sarıkaya 2015; Aparicio et al. 2016). Recent studies have found that using semi-quantitative approaches, such as AI mapping that extend beyond visual reads, can not only detect hypometabolic regions in high agreement with other clinical and electrophysiological findings, but can also increase a reader's confidence in their visual assessment of PET (Didelot et al. 2010; Boscolo Galazzo et al. 2016; Shang et al. 2018). Here, we demonstrated – albeit retrospectively – the utility of AI mapping in epilepsy surgical evaluation, where AI mapping was able to successfully localize and lateralize the epileptogenic focus in most MRE patients. While it is possible that some of the metabolic asymmetries observed could simply reflect normal physiological asymmetries in the brain, especially in patients with multi-focal hypometabolism, we used a standard AI mapping thresholding approach to isolate significant hypometabolic brain regions that has been validated by past studies (Boscolo Galazzo et al. 2016; Shang et al. 2018), which gives us confidence that the metabolic asymmetries detected in our study are more likely associated with epileptic regions rather than normal healthy brain tissue. AI mapping is thus a promising tool for guiding assessment of surgical candidacy in epilepsy, especially in MRI-negative cases. Furthermore, similar to our findings, past studies have reported FDG-PET hypometabolism in contralateral brain regions in some epilepsy patients (Aparicio et al.



2016; Cahill et al. 2019), presumably due to spread of epileptic activity across hemispheres. Despite these challenges with FDG-PET specificity, we were still able to show that FDG-PET can aid detection of the epileptogenic zone and assessment of surgical candidacy in epilepsy, especially when combined with DTI. Perhaps the use of novel PET tracers targeted to pathogenesis of epilepsy such as imaging reduced synaptic density using PET-ligands targeting the synaptic vesicle protein 2A (Finnema et al. 2016) as well as receptor imaging using PET tracers targeting serotonin and gamma-aminobutyric acid (Sarikaya 2015; Galovic and Koepp 2016), could increase the specificity of PET in detecting the true EF.

In this study, we used diffusion tractography to assess structural integrity around MRI-negative epileptic zones identified by FDG-PET. Although there is no current gold standard for validation of WM fibers generated using diffusion tractography techniques, there are a number of phantom models adapted to simulate WM pathways in healthy human brains and provide some evaluation of tractography approaches. We empirically evaluated our diffusion MRI preprocessing and tractography approach to a computer-simulated WM phantom (Neher et al. 2014). However, this and other phantom models do not take into account any GM or WM pathologies present in epilepsy patients (Neher et al. 2014; Maier-Hein et al. 2017). As such, we opted not to compare WM fibers between epilepsy patients and a healthy control group, and instead assessed structural integrity by comparing WM fibers between hemispheres within individual patients. This individual assessment is more likely to be of clinical utility in epilepsy surgical centers where epilepsy patients are typically evaluated on a case-by-case basis. Nevertheless, we were able to show that WM fibers appear to be affected at multiple distances away from the epileptic tissue. Interestingly, these abnormalities were most apparent in WM directly surrounding the epileptic zone. While no other studies to date have assessed WM fiber integrity at different distances from MRI-negative EF sites using WM fiber quantification, some studies have shown that diffusion tractography can reveal widespread microstructural changes in drug-resistant epilepsy that could be responsible for surgical failure (Sivakanthan et al. 2016; Jiang et al. 2017). Our results suggest that WM directly adjacent to the epileptic zone is most prone to structural alterations. More specifically, we found that out of the three WM distances investigated, WM anomalies

were most prominent at an average distance of approximately 3 mm away from the epileptic zone. This finding suggests that investigation of WM at this distance from epileptic tissue may better inform clinicians about whether surgery is an option, and if so, how to properly resect the EF without damaging surrounding healthy brain tissue. This is especially important to assess in WM affecting memory, language, and visual pathways in the brain, which are of prime importance in perioperative planning (Lin et al. 2008; James et al. 2015; Sivakanthan et al. 2016; Li et al. 2019).

Because our AI mapping procedure detected hypometabolism (suspected EF) in cortical brain areas, we were left with the task of developing a method to track surrounding WM regions closest to the EF. We sampled WM regions at three incremental distances away from the epileptic zone using a VOI placed manually in the part of the EF directly adjacent to surrounding WM. This manual implementation poses a few issues. First, because we manually defined VOIs in GM regions contralateral to the EF, there is the possibility of spatial error between ipsilateral and contralateral VOIs. Second, focal cortical dysplasias and other GM/WM pathologies may result in different amounts of WM being sampled between ipsilateral and contralateral regions. However, it is conceivable that any differences in WM size between ipsilateral and contralateral regions are presumably small and are likely offset by the noticeable WM fiber abnormalities observed around the EF in the majority of our MRE patient cohort.

The clinical potential of the proposed PET/DTI approach could be impacted by the relatively small size of our heterogeneous MRE patient cohort, making it difficult to draw any conclusions regarding what epilepsy patient groups are most likely to benefit from PET/DTI. However, the purpose of this hybrid PET/MRI study was to demonstrate the feasibility of PET/DTI and provide some preliminary assessment on whether PET/DTI could potentially impact clinical decision-making in epilepsy surgery, particularly in MRI-negative epilepsy where FDG-PET could instead be used to non-invasively locate the EF. Of note, hybrid PET/MRI relies on MR-based attenuation correction (MRAC) for PET reconstruction instead of CT-based AC used in PET/CT, which is the current clinical standard for FDG-PET imaging in epilepsy. While some studies show that traditional MRAC approaches can produce small bias in quantitative PET due to inadequate

modelling of bone (Larsson et al. 2013; Andersen et al. 2014), recent reports have revealed that these MRAC biases do not significantly impact clinical diagnosis of FDG-PET readings in epilepsy (Paldino et al. 2017; Oldan et al. 2018). Nevertheless, alternative MRAC methods have been proposed to reduce potential bias in reconstructed PET (Ladefoged et al., 2017). In our study, we used an improved robust MRAC method (Ladefoged et al. 2015) that adequately models bone tissue information to produce PET/MR images that provide comparable diagnostic information to PET/CT.

Because clinical assessment of our PET/DTI approach was retrospectively completed by one neurologist, potential interobserver variability could not be determined from this study. A potential future direction of this research is to pilot a prospective study to assess the clinical utility of combined PET/DTI through interdisciplinary meetings that would evaluate MRE patients both with and without including our PET/DTI approach to determine whether this approach will have any impact on the final surgical decision in these patients.

In general, this retrospective study demonstrated the feasibility of combining PET and DTI to investigate WM integrity in the brains of MRE patients to further enhance clinical decision-making in epilepsy surgery. An extension of this study could combine functional MRI (fMRI) with DTI and PET to map out the structure and function of brain networks in the presence of seizure-related brain abnormalities. fMRI is another non-invasive imaging modality that may have promising applications in neurosurgical planning. While DTI investigates structural connections, fMRI measures functional correlates between brain regions based on differences in blood flow and can be used to effectively map neural connections in the brain (Bettus et al. 2009, 2010; Fox and Greicius 2010; Moeller et al. 2011; Pittau et al. 2012). By combining structural and functional connectivity analysis, we would be able to even better characterize seizure sites in MRE surgical candidates. We plan to incorporate PET, DTI, and fMRI modalities into an integrated software platform that would allow clinicians to non-invasively probe healthy brain tissue and areas around the epileptic zone to further improve neurosurgical planning, especially in challenging epilepsy cases where MRI and IC-EEG findings lack concordance. The integration and proper use of these non-invasive imaging modalities will help advance the

field of epilepsy treatment and management and may lead to completely non-invasive epilepsy surgical planning (Knowlton 2006; Sivakanthan et al. 2016).

### 3.5 Supplementary Tables

Table S1. EEG and MRI findings from clinical reports and visual assessment

Patient No.	Clinical Hypothesis	Scalp EEG	1.5T MRI	3T MRI R1	3T MRI R2	AI Mapping
1	L temp/front	L temp/front	L MTS*	L MTS	L MTS	L temp
2	L front	Bifrontal	L temp FCD*	L front/par FCD	L front/par FCD	L front
3	R front	Bifrontal	Unremarkable	Unremarkable	Unremarkable	L front
4	L temp/front	L temp	Unremarkable	Unremarkable	Unremarkable	L temp
5	R temp	Bitemporal	Unremarkable	Unremarkable	Unremarkable	R temp
6	L temp/front	L temp/front	Unremarkable	Unremarkable	Unremarkable	L front
7	L temp	L temp/front	Unremarkable	Unremarkable	Unremarkable	L front
8	R front	Bitemporal + extratemporal	Bitemporal SH*	R MTS	Unremarkable	L front
9	L temp	L temp	L MTS*	Signal (L>R)	Unremarkable	L temp
10	R temp	R temp	Unremarkable	Unremarkable	Unremarkable	L front
11	R temp/front	R temp	Unremarkable	Unremarkable	Unremarkable	R temp
12	L temp	Bitemporal	Unremarkable	Unremarkable	Unremarkable	L temp
13	R temp	Bitemporal + extratemporal	Unremarkable	Unremarkable	Unremarkable	L temp/front
14	R temp	Bitemporal	Unremarkable	Unremarkable	Unremarkable	L temp

Note. Findings from visual assessment of T1-weighted images from PET/MRI by two Neuroradiologists are summarized under the headings 3T MRI R1 and 3T MRI R2, while 1.5T MRI findings are from reports of clinically indicated MRI scans acquired prior to PET.

Abbreviations: \*, equivocal finding; FCD, focal cortical dysplasia; front, frontal lobe; L, left; MTS, mesial temporal sclerosis; par, parietal lobe; R, right; SH, subcortical heterotopia; temp, temporal lobe.

**Table S2. SUV analysis in hypometabolic PET ROIs and contralateral ROIs from AI mapping in 14 MRE patients**

Patient No.	Mean SUV			Max SUV			Mean $Z_{AI}$		
	Hypometabolic ROI	Contralateral ROI	Contralateral ROI	Hypometabolic ROI	Contralateral ROI	Contralateral ROI	Hypometabolic ROI	Contralateral ROI	Contralateral ROI
1	2.24	3.16	3.16	3.11	4.10	4.10	-2.30		2.02
2	4.90	8.00	8.00	5.89	9.45	9.45	-2.10		1.93
3	4.81	6.82	6.82	6.41	7.86	7.86	-2.70		2.40
4	1.63	2.16	2.16	2.06	2.69	2.69	-2.20		1.83
5	3.03	3.94	3.94	4.17	5.46	5.46	-2.07		1.69
6	5.35	7.48	7.48	6.68	8.75	8.75	-2.34		1.96
7	2.01	2.70	2.70	4.05	4.78	4.78	-3.21		2.85
8	4.66	8.14	8.14	8.29	10.85	10.85	-3.42		3.09
9	2.83	4.04	4.04	3.89	5.08	5.08	-2.66		2.31
10	3.87	5.43	5.43	5.10	6.60	6.60	-2.73		2.37
11	5.87	8.09	8.09	7.67	11.16	11.16	-2.12		1.87
12	4.95	6.73	6.73	7.25	9.69	9.69	-2.53		2.19
13	6.16	7.98	7.98	8.58	10.68	10.68	-2.33		1.95
14	4.34	5.78	5.78	5.00	6.46	6.46	-2.71		2.35
Group	4.04 ± 1.47	5.75 ± 2.18	5.75 ± 2.18	5.58 ± 2.00	7.40 ± 2.76	7.40 ± 2.76	-2.53 ± 0.41		2.20 ± 0.40

Note: For mean SUV and mean  $Z_{AI}$ , group values are reported as mean ± standard deviation.

**Table S3. Regional FA analysis in WM surrounding hypometabolic PET ROIs and contralateral ROIs detected by AI mapping of FDG-PET**

Patient No.	3 mm into WM		9 mm into WM		15 mm into WM	
	Hypometabolic ROI	Contralateral ROI	Hypometabolic ROI	Contralateral ROI	Hypometabolic ROI	Contralateral ROI
1	0.08	0.18	0.15	0.12	0.16	0.13
2	0.07	0.17	0.11	0.19	0.12	0.16
3	0.14	0.13	0.26	0.22	0.28	0.24
4	0.08	0.14	0.12	0.14	0.13	0.16
5	0.06	0.05	0.08	0.06	0.08	0.07
6	0.10	0.15	0.15	0.26	0.19	0.27
7	0.01	0.02	0.03	0.04	0.06	0.05
8	0.08	0.17	0.11	0.16	0.13	0.20
9	0.12	0.19	0.22	0.26	0.24	0.25
10	0.12	0.18	0.21	0.21	0.22	0.20
11	0.07	0.14	0.16	0.22	0.15	0.19
12	0.05	0.10	0.12	0.09	0.10	0.09
13	0.13	0.13	0.19	0.18	0.18	0.18
14	0.13	0.16	0.24	0.29	0.26	0.31
Group	0.09 ± 0.04	0.13 ± 0.05	0.15 ± 0.06	0.17 ± 0.08	0.16 ± 0.07	0.18 ± 0.08

Note: Group values are reported as mean ± standard deviation.

### 3.6 Acknowledgements

The authors would like to thank John Butler and Heather Biernaski (PET/MRI Technologists) for their assistance in data acquisition and Krista Doyle, the Nurse Navigator at the London Health Sciences Centre Epilepsy Program, for her assistance with patient recruitment.

### 3.7 References

- Ahmadi ME, Hagler DJ, McDonald CR, et al (2009) Side Matters: Diffusion Tensor Imaging Tractography in Left and Right Temporal Lobe Epilepsy. *American Journal of Neuroradiology* 30:1740–1747. <https://doi.org/10.3174/ajnr.A1650>
- Anazodo UC, Finger E, Kwan BYM, et al (2018) Using simultaneous PET/MRI to compare the accuracy of diagnosing frontotemporal dementia by arterial spin labelling MRI and FDG-PET. *NeuroImage: Clinical* 17:405–414. <https://doi.org/10.1016/j.nicl.2017.10.033>
- Andersen FL, Ladefoged CN, Beyer T, et al (2014) Combined PET/MR imaging in neurology: MR-based attenuation correction implies a strong spatial bias when ignoring bone. *NeuroImage* 84:206–216. <https://doi.org/10.1016/j.neuroimage.2013.08.042>
- Aparicio J, Carreño M, Bargalló N, et al (2016) Combined 18F-FDG-PET and diffusion tensor imaging in mesial temporal lobe epilepsy with hippocampal sclerosis. *NeuroImage: Clinical* 12:976–989. <https://doi.org/10.1016/j.nicl.2016.05.002>
- Avants BB, Tustison NJ, Song G, et al (2011) A reproducible evaluation of ANTs similarity metric performance in brain image registration. *NeuroImage* 54:2033–2044. <https://doi.org/10.1016/j.neuroimage.2010.09.025>



- Basser PJ, Jones DK (2002) Diffusion-tensor MRI: theory, experimental design and data analysis – a technical review. *NMR Biomed* 15:456–467.  
<https://doi.org/10.1002/nbm.783>
- Bettus G, Bartolomei F, Confort-Gouny S, et al (2010) Role of resting state functional connectivity MRI in presurgical investigation of mesial temporal lobe epilepsy. *Journal of Neurology, Neurosurgery & Psychiatry* 81:1147–1154.  
<https://doi.org/10.1136/jnnp.2009.191460>
- Bettus G, Guedj E, Joyeux F, et al (2009) Decreased basal fMRI functional connectivity in epileptogenic networks and contralateral compensatory mechanisms. *Human Brain Mapping* 30:1580–1591. <https://doi.org/10.1002/hbm.20625>
- Blount JP, Cormier J, Kim H, et al (2008) Advances in intracranial monitoring. *FOC* 25:E18. <https://doi.org/10.3171/FOC/2008/25/9/E18>
- Boscolo Galazzo I, Mattoli MV, Pizzini FB, et al (2016) Cerebral metabolism and perfusion in MR-negative individuals with refractory focal epilepsy assessed by simultaneous acquisition of 18 F-FDG PET and arterial spin labeling. *NeuroImage: Clinical* 11:648–657. <https://doi.org/10.1016/j.nicl.2016.04.005>
- Brant-Zawadzki M, Gillan GD, Nitz WR (1992) MP RAGE: a three-dimensional, T1-weighted, gradient-echo sequence--initial experience in the brain. *Radiology* 182:769–775. <https://doi.org/10.1148/radiology.182.3.1535892>
- Burneo JG, Poon R, Kellett S, Snead OC (2015) The Utility of Positron Emission Tomography in Epilepsy. *Canadian Journal of Neurological Sciences* 42:360–371.  
<https://doi.org/10.1017/cjn.2015.279>
- Caciagli L, Bernhardt BC, Hong SJ, et al (2014) Functional network alterations and their structural substrate in drug-resistant epilepsy. *Front Neurosci* 8:411.  
<https://doi.org/10.3389/fnins.2014.00411>

- Cahill V, Sinclair B, Malpas CB, et al (2019) Metabolic patterns and seizure outcomes following anterior temporal lobectomy. *Annals of Neurology* 85:241–250.  
<https://doi.org/10.1002/ana.25405>
- Chamberland M, Bernier M, Fortin D, et al (2015) 3D interactive tractography-informed resting-state fMRI connectivity. *Front Neurosci* 9:275.  
<https://doi.org/10.3389/fnins.2015.00275>
- Coupé P, Manjón JV, Gedamu E, et al (2010) Robust Rician noise estimation for MR images. *Medical Image Analysis* 14:483–493.  
<https://doi.org/10.1016/j.media.2010.03.001>
- Coupé P, Yger P, Prima S, et al (2008) An optimized blockwise nonlocal means denoising filter for 3-D magnetic resonance images. *IEEE Trans Med Imaging* 27:425–441. <https://doi.org/10.1109/TMI.2007.906087>
- Crawford JR, Garthwaite PH (2012) Single-case research in neuropsychology: A comparison of five forms of t-test for comparing a case to controls. *Cortex* 48:1009–1016. <https://doi.org/10.1016/j.cortex.2011.06.021>
- de Tisi J, Bell GS, Peacock JL, et al (2011) The long-term outcome of adult epilepsy surgery, patterns of seizure remission, and relapse: a cohort study. *The Lancet* 378:1388–1395. [https://doi.org/10.1016/S0140-6736\(11\)60890-8](https://doi.org/10.1016/S0140-6736(11)60890-8)
- Didelot A, Manguiere F, Redoute J, et al (2010) Voxel-Based Analysis of Asymmetry Index Maps Increases the Specificity of 18F-MPPF PET Abnormalities for Localizing the Epileptogenic Zone in Temporal Lobe Epilepsies. *Journal of Nuclear Medicine* 51:1732–1739. <https://doi.org/10.2967/jnumed.109.070938>
- Finnema SJ, Nabulsi NB, Eid T, et al (2016) Imaging synaptic density in the living human brain. *Science Translational Medicine* 8:348ra96.  
<https://doi.org/10.1126/scitranslmed.aaf6667>

- Focke NK, Yogarajah M, Bonelli SB, et al (2008) Voxel-based diffusion tensor imaging in patients with mesial temporal lobe epilepsy and hippocampal sclerosis. *NeuroImage* 40:728–737. <https://doi.org/10.1016/j.neuroimage.2007.12.031>
- Fox MD, Greicius M (2010) Clinical Applications of Resting State Functional Connectivity. *Front Syst Neurosci* 4:19. <https://doi.org/10.3389/fnsys.2010.00019>
- Galovic M, Koepp M (2016) Advances of Molecular Imaging in Epilepsy. *Curr Neurol Neurosci Rep* 16:58. <https://doi.org/10.1007/s11910-016-0660-7>
- Güvenç C, Dupont P, Van den Stock J, et al (2018) Correlation of neuropsychological and metabolic changes after epilepsy surgery in patients with left mesial temporal lobe epilepsy with hippocampal sclerosis. *EJNMMI Res* 8:31. <https://doi.org/10.1186/s13550-018-0385-5>
- Helmstaedter C, Kurthen M, Lux S, et al (2003) Chronic epilepsy and cognition: A longitudinal study in temporal lobe epilepsy. *Ann Neurol* 54:425–432. <https://doi.org/10.1002/ana.10692>
- Henry TR, Mazziotta JC, Engel J, et al (1990) Quantifying Interictal Metabolic Activity in Human Temporal Lobe Epilepsy. *Journal of Cerebral Blood Flow & Metabolism* 10:748–757. <https://doi.org/10.1038/jcbfm.1990.128>
- Henry TR, Pennell PB (1998) Neuropharmacological imaging in epilepsy with PET and SPECT. *The Quarterly Journal of Nuclear Medicine; Torino* 42:199–210
- James JS, Radhakrishnan A, Thomas B, et al (2015) Diffusion tensor imaging tractography of Meyer’s loop in planning resective surgery for drug-resistant temporal lobe epilepsy. *Epilepsy Research* 110:95–104. <https://doi.org/10.1016/j.eplepsyres.2014.11.020>
- Jiang Y, Mao L, Yan X, et al (2017) Investigation of altered microstructure in patients with drug refractory epilepsy using diffusion tensor imaging. *Neuroradiology* 59:597–608. <https://doi.org/10.1007/s00234-017-1835-x>

- Jones DK, Cercignani M (2010) Twenty-five pitfalls in the analysis of diffusion MRI data. *NMR Biomed* 23:803–820. <https://doi.org/10.1002/nbm.1543>
- Kamm J, Boles Ponto LL, Manzel K, et al (2018) Temporal lobe asymmetry in FDG-PET uptake predicts neuropsychological and seizure outcomes after temporal lobectomy. *Epilepsy & Behavior* 78:62–67. <https://doi.org/10.1016/j.yebeh.2017.10.006>
- Knowlton RC (2006) The role of FDG-PET, ictal SPECT, and MEG in the epilepsy surgery evaluation. *Epilepsy Behav* 8:91–101. <https://doi.org/10.1016/j.yebeh.2005.10.015>
- Labate A, Cherubini A, Tripepi G, et al (2015) White matter abnormalities differentiate severe from benign temporal lobe epilepsy. *Epilepsia* 56:1109–1116. <https://doi.org/10.1111/epi.13027>
- Ladefoged CN, Benoit D, Law I, et al (2015) Region specific optimization of continuous linear attenuation coefficients based on UTE (RESOLUTE): application to PET/MR brain imaging. *Phys Med Biol* 60:8047–8065. <https://doi.org/10.1088/0031-9155/60/20/8047>
- Larsson A, Johansson A, Axelsson J, et al (2013) Evaluation of an attenuation correction method for PET/MR imaging of the head based on substitute CT images. *Magn Reson Mater Phy* 26:127–136. <https://doi.org/10.1007/s10334-012-0339-2>
- Le Bihan D (2006) Looking into the functional architecture of the brain with diffusion MRI. *International Congress Series* 1290:1–24. <https://doi.org/10.1016/j.ics.2006.04.006>
- Le Bihan D, Breton E, Lallemand D, et al (1986) MR imaging of intravoxel incoherent motions: application to diffusion and perfusion in neurologic disorders. *Radiology* 161:401–407. <https://doi.org/10.1148/radiology.161.2.3763909>

- Leemans A, Jeurissen B, Sijbers J, Jones DK (2009) ExploreDTI: a graphical toolbox for processing, analyzing, and visualizing diffusion MR data. *Proc Intl Soc Mag Reson Med* 17:3537
- Li W, An D, Tong X, et al (2019) Different patterns of white matter changes after successful surgery of mesial temporal lobe epilepsy. *NeuroImage: Clinical* 21:101631. <https://doi.org/10.1016/j.nicl.2018.101631>
- Lin JJ, Riley JD, Juranek J, Cramer SC (2008) Vulnerability of the frontal-temporal connections in temporal lobe epilepsy. *Epilepsy Research* 82:162–170. <https://doi.org/10.1016/j.eplepsyres.2008.07.020>
- Lippé S, Poupon C, Cachia A, et al (2012) White matter abnormalities revealed by DTI correlate with interictal grey matter FDG-PET metabolism in focal childhood epilepsies. *Epileptic Disorders* 14:404–413. <https://doi.org/10.1684/epd.2012.0547>
- Maier-Hein KH, Neher PF, Houde JC, et al (2017) The challenge of mapping the human connectome based on diffusion tractography. *Nature Communications* 8:1349. <https://doi.org/10.1038/s41467-017-01285-x>
- Moeller F, Maneshi M, Pittau F, et al (2011) Functional connectivity in patients with idiopathic generalized epilepsy. *Epilepsia* 52:515–522. <https://doi.org/10.1111/j.1528-1167.2010.02938.x>
- Mori S, Zhang J (2006) Principles of Diffusion Tensor Imaging and Its Applications to Basic Neuroscience Research. *Neuron* 51:527–539. <https://doi.org/10.1016/j.neuron.2006.08.012>
- Neher PF, Laun FB, Stieltjes B, Maier-Hein KH (2014) Fiberfox: Facilitating the creation of realistic white matter software phantoms: Realistic White Matter Software Phantoms. *Magnetic Resonance in Medicine* 72:1460–1470. <https://doi.org/10.1002/mrm.25045>

- Oldan JD, Shin HW, Khandani AH, et al (2018) Subsequent experience in hybrid PET-MRI for evaluation of refractory focal onset epilepsy. *Seizure* 61:128–134. <https://doi.org/10.1016/j.seizure.2018.07.022>
- Paldino MJ, Yang E, Jones JY, et al (2017) Comparison of the diagnostic accuracy of PET/MRI to PET/CT-acquired FDG brain exams for seizure focus detection: a prospective study. *Pediatr Radiol* 47:1500–1507. <https://doi.org/10.1007/s00247-017-3888-8>
- Pittau F, Grova C, Moeller F, et al (2012) Patterns of altered functional connectivity in mesial temporal lobe epilepsy. *Epilepsia* 53:1013–1023. <https://doi.org/10.1111/j.1528-1167.2012.03464.x>
- Rausch R, Henry TR, Ary CM, et al (1994) Asymmetric Interictal Glucose Hypometabolism and Cognitive Performance in Epileptic Patients. *Archives of Neurology* 51:139–144. <https://doi.org/10.1001/archneur.1994.00540140045013>
- Richardson MP, Strange BA, Thompson PJ, et al (2004) Pre-operative verbal memory fMRI predicts post-operative memory decline after left temporal lobe resection. *Brain* 127:2419–2426. <https://doi.org/10.1093/brain/awh293>
- Sarikaya I (2015) PET studies in epilepsy. *Am J Nucl Med Mol Imaging* 5:416–430
- Shang K, Wang J, Fan X, et al (2018) Clinical Value of Hybrid TOF-PET/MR Imaging-Based Multiparametric Imaging in Localizing Seizure Focus in Patients with MRI-Negative Temporal Lobe Epilepsy. *American Journal of Neuroradiology* 39:1791–1798. <https://doi.org/10.3174/ajnr.A5814>
- Sivakanthan S, Neal E, Murtagh R, Vale FL (2016) The evolving utility of diffusion tensor tractography in the surgical management of temporal lobe epilepsy: a review. *Acta Neurochirurgica* 158:2185–2193. <https://doi.org/10.1007/s00701-016-2910-5>
- Soares J, Marques P, Alves V, Sousa N (2013) A hitchhiker's guide to diffusion tensor imaging. *Front Neurosci* 7:31. <https://doi.org/10.3389/fnins.2013.00031>

- Téllez-Zenteno JF, Dhar R, Wiebe S (2005) Long-term seizure outcomes following epilepsy surgery: a systematic review and meta-analysis. *Brain* 128:1188–1198. <https://doi.org/10.1093/brain/awh449>
- Thivard L, Bouilleret V, Chassoux F, et al (2011) Diffusion tensor imaging can localize the epileptogenic zone in nonlesional extra-temporal refractory epilepsies when [18F]FDG-PET is not contributive. *Epilepsy Research* 97:170–182. <https://doi.org/10.1016/j.eplepsyres.2011.08.005>
- Tournier JD, Smith R, Raffelt D, et al (2019) MRtrix3: A fast, flexible and open software framework for medical image processing and visualisation. *NeuroImage* 202:116137. <https://doi.org/10.1016/j.neuroimage.2019.116137>
- Van Bogaert P, Massager N, Tugendhaft P, et al (2000) Statistical Parametric Mapping of Regional Glucose Metabolism in Mesial Temporal Lobe Epilepsy. *NeuroImage* 12:129–138. <https://doi.org/10.1006/nimg.2000.0606>
- Wang YH, An Y, Fan XT, et al (2018) Comparison between simultaneously acquired arterial spin labeling and 18F-FDG PET in mesial temporal lobe epilepsy assisted by a PET/MR system and SEEG. *NeuroImage: Clinical* 19:824–830. <https://doi.org/10.1016/j.nicl.2018.06.008>
- Wiest-Daesslé N, Prima S, Coupé P, et al (2008) Rician Noise Removal by Non-Local Means Filtering for Low Signal-to-Noise Ratio MRI: Applications to DT-MRI. In: Metaxas D, Axel L, Fichtinger G, Székely G (eds) *Medical Image Computing and Computer-Assisted Intervention – MICCAI 2008*. Springer Berlin Heidelberg, Berlin, Heidelberg, pp 171–179
- Woolrich MW, Jbabdi S, Patenaude B, et al (2009) Bayesian analysis of neuroimaging data in FSL. *NeuroImage* 45:S173–S186. <https://doi.org/10.1016/j.neuroimage.2008.10.055>

## Chapter 4

### 4 Conclusions and Future Directions

#### 4.1 Conclusions

The overall goal of this thesis was to develop a hybrid PET/MRI approach to non-invasively localize EF and assess structural integrity around EF for improving DRE surgical evaluation. Our first aim was to assess the diagnostic competence of hybrid PET/MRI against PET/CT, the current clinical standard for FDG-PET imaging in epilepsy, to evaluate whether quantitative PET biases from MRAC have any significant impact on clinical diagnosis of DRE. Our second aim was to develop a PET/DTI approach for assessing WM integrity around EF in MRI-negative DRE patients and to evaluate the potential clinical utility of PET/DTI in guiding clinical decision making in epilepsy surgery. These two research objectives were addressed in **Chapters 2 and 3**. Findings from both chapters will be summarized in this section.

In **Chapter 2**, we evaluated the diagnostic equivalency and clinical value of hybrid PET/MRI against PET/CT in DRE. Diagnostic equivalency was assessed by comparing regional MRAC biases in FDG-PET images between PET/MRI and PET/CT. Clinical value of hybrid PET/MRI in DRE localization was assessed by qualitatively and quantitatively comparing FDG-PET findings from PET/MRI against clinical reports and gold-standard post-surgical outcomes. We found that visual FDG-PET readings between PET/MRI and PET/CT were similar and yielded comparable diagnostic outcome. Likewise, we found that quantitative PET bias was low between PET/MRI and PET/CT, suggesting that PET/MRI can provide similar metabolic information as PET/CT. In general, PET/MRI with optimal MRAC can yield similar diagnostic performance as PET/CT. Indeed, hybrid PET/MRI is a reliable method for detecting EF in DRE and is a promising tool for improving epilepsy treatment and management.

In **Chapter 3**, we developed a PET/DTI approach combining FDG-PET and diffusion MRI to investigate WM integrity in the brains of MRI-negative DRE patients. We used AI mapping of FDG-PET to detect the EF and used diffusion tractography to assess WM



fiber integrity around the EF. We found that AI mapping of FDG-PET can successfully detect seizure-onset zones that are concordant with clinical reports, EEG findings, and visual FDG-PET assessment. PET/DTI revealed structural alterations around the EF in the majority of our MRI-negative epilepsy cohort. In general, PET/DTI combines PET and MRI information into one integrated platform and is a promising tool for improving surgical outcomes, especially in MRI-negative epilepsy where we can use FDG-PET to detect the EF. Specifically, PET/DTI can improve diagnostic confidence in DRE and could potentially impact clinical decision-making in epilepsy surgery. Indeed, multimodal brain imaging combining PET and MRI information can help advance epilepsy treatment and management, which could lead to improved surgical outcomes and better patient quality of life.

## **4.2 Future Directions**

The hybrid PET/MRI research discussed in this thesis showed the feasibility of PET/DTI in localizing EF and assessing WM integrity around EF in DRE. In the future, we plan to incorporate functional MRI (fMRI) into our PET/DTI approach to map out functional connections in the brain. Combining PET with DTI and fMRI could provide new insight into brain connectivity affected in epilepsy and may improve characterization of EF and surrounding brain regions to further enhance neurosurgical planning.

In this thesis, we found that AI mapping of FDG-PET can detect contralateral hypometabolism in some epilepsy patients, a finding that is consistent with past studies.<sup>1,2</sup> While a previous report has suggested that contralateral FDG-PET hypometabolism may be a compensatory mechanism against functional deficits in the ipsilateral lobe<sup>3</sup>, another study has shown that bilateral temporal lobe hypometabolism is associated with increased epilepsy duration and poorer surgical outcome.<sup>4</sup> It is evident that multi-focal hypometabolism is an issue, especially in patients who have multiple, non-continuous hypometabolic regions extending well beyond the seizure-onset zone and can lead to false lateralization of AI mapping. Hence, a course of future direction could further improve specificity of AI mapping in EF localization through statistical comparison of AI values between patients and an age-matched healthy control FDG-PET/MRI database.

There are a few interesting future avenues of epilepsy DTI research that should be noted. First, DTI scalar parameters can vary diurnally. Specifically, FA has been shown to decrease as the day progresses.<sup>5</sup> It would be interesting to investigate whether changes in DTI scalar values due to different patient scanning times can significantly affect FA and diffusion tractography results in epilepsy. Second, structural integrity of individual WM fiber pathways known to be affected in epilepsy, such as the uncinate fasciculus and fornix, and their potential relationships to FDG-PET metabolic alterations, especially around the EF, could be assessed to even better enhance characterization of EF and its relationships with surrounding neural networks. Finally, we plan to further improve our diffusion MRI image analysis pipeline by implementing automated quality control steps<sup>6</sup> to enhance detection of bad quality DWI data.

This thesis demonstrated the potential clinical utility of PET/DTI in epilepsy surgical evaluation. In the future, we plan to pilot a prospective study to assess the potential added value of PET/DTI in epilepsy surgical decision-making. Efforts are currently underway to extend this work to the pediatric population to gain new insight into functional and structural alterations that take place in different epilepsy patient groups. The goal is to provide clinicians with an interactive platform to non-invasively probe brain areas affected by seizures *in vivo* to determine whether a patient is suitable for surgery. This will further minimize potential risks associated with surgical resection, and in turn lead to better surgical outcomes and overall quality of life.

### 4.3 References

1. Aparicio J, Carreño M, Bargalló N, et al. Combined 18F-FDG-PET and diffusion tensor imaging in mesial temporal lobe epilepsy with hippocampal sclerosis. *NeuroImage: Clinical* 2016;12:976–89.
2. Cahill V, Sinclair B, Malpas CB, et al. Metabolic patterns and seizure outcomes following anterior temporal lobectomy. *Annals of Neurology* 2019;85:241–50.
3. Van Bogaert P, Massager N, Tugendhaft P, et al. Statistical Parametric Mapping of Regional Glucose Metabolism in Mesial Temporal Lobe Epilepsy. *NeuroImage* 2000;12:129–38.
4. Koutroumanidis M, Hennessy MJ, Seed PT, et al. Significance of interictal bilateral temporal hypometabolism in temporal lobe epilepsy. *Neurology* 2000;54:1811–21.
5. Jiang C, Zhang L, Zou C, et al. Diurnal Microstructural Variations in Healthy Adult Brain Revealed by Diffusion Tensor Imaging. *PLOS ONE* 2014;9:e84822.
6. Woolrich MW, Jbabdi S, Patenaude B, et al. Bayesian analysis of neuroimaging data in FSL. *NeuroImage* 2009;45:S173–86.

## **Appendix A: Empirical evaluation of diffusion tractography pipeline using whole-brain tractograms from a white matter phantom**

Before diffusion tractography, DWI images are preprocessed to remove noise, subject motion, and other image artifacts. Many different approaches exist for preprocessing DWI data which can impact the accuracy of WM fiber reconstruction. Here, we empirically evaluated our diffusion tractography pipeline (see **Figure A.1** below) using the ground-truth phantom from the ISMRM 2015 Tractography Challenge (<http://www.tractometer.org/>). Whole-brain WM fiber tracts (tractograms) from both the artifact-free phantom and the challenge phantom dataset were scored and compared to an online database of other tractograms. This work was accepted and presented at ImNO as a conference abstract:

**Poirier SE, Thiessen JD, Anazodo UC (2019).** Empirical evaluation of a DTI tractography pipeline using whole-brain tractograms from a white matter phantom. *17<sup>th</sup> Annual Imaging Network Ontario (ImNO) Symposium*, London, Canada. Abstract. Accepted – Oral Presentation.

### ***Methods: Phantom DWI data preprocessing and pipeline scoring***

The phantom DWI data, which contained noise, motion, and image artifacts, were generated using Fiberfox (Neher et al., MRM, 2014) from 25 computer-simulated WM bundles with the following parameters; 2 mm isotropic resolution, 32 contiguous slices, b-values = 0, 1000 s/mm<sup>2</sup> and 32 diffusion-encoding gradient directions. The phantom DWI data were preprocessed using our diffusion MR image analysis pipeline to generate whole-brain tractograms. Tractograms were scored using the scoring system from the ISMRM 2015 Tractography Challenge, which compared streamlines to the ground-truth bundles and generated the following parameters; valid bundles (VB) – scored out of 25, invalid bundles (IB) – number of bundles that did not exist in ground-truth phantom, valid connections (VC), invalid connections (IC), and no connections (NC).

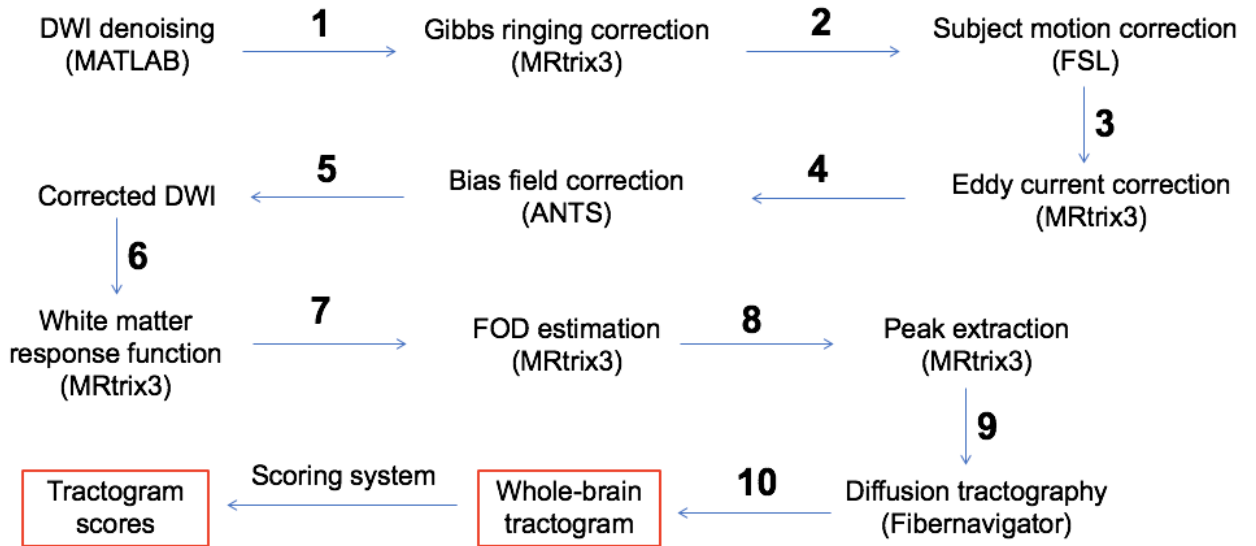


**Figure A.1: Diffusion tractography pipeline scoring.** Phantom DWI data were preprocessed to generate whole-brain tractograms. The whole-brain tractograms were scored using the scoring system from the ISMRM 2015 Tractography Challenge.

**Results: Pipeline scores**

Scores from the artifact-free phantom: VB = 24/25, IB = 76, VC = 85.78%, IC = 14.21%, NC = 0.00%. Scores from the challenge phantom data: VB = 23/25, IB = 70, VC = 70.37%, IC = 29.63%, NC = 0.00%. Whole-brain tractograms for the artifact-free and challenge phantom data are shown in **Figure A.2** below.

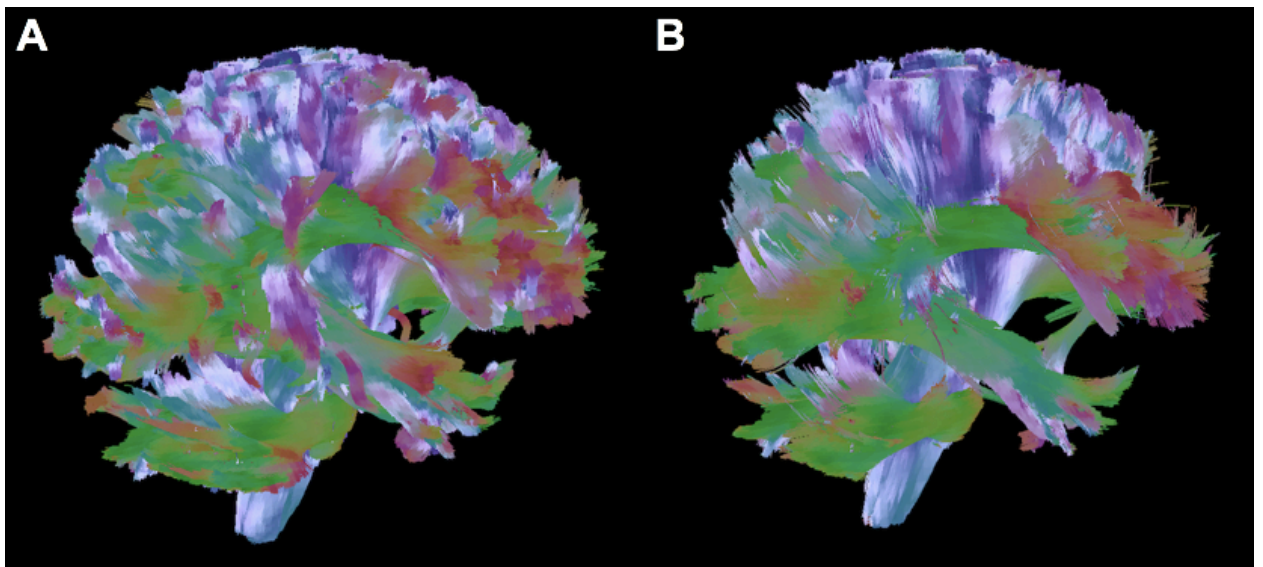


**Figure A.2: WM tractograms.** Whole-brain tractograms from (A) artifact-free phantom and (B) challenge phantom dataset.

### *Summary*

We empirically evaluated our diffusion tractography pipeline using a ground-truth diffusion phantom dataset. Comparing our whole-brain tractogram scores to the online submissions database ([http://www.tractometer.org/ismrm\\_2015\\_challenge/results](http://www.tractometer.org/ismrm_2015_challenge/results)), we found that our pipeline performed very well across all five scoring parameters (mean score percentile =  $76 \pm 24\%$ ) and this gives us confidence that our pipeline is indeed accurately reconstructing WM fiber pathways in the brain.

## Appendix B: Permission for Reproduction of Scientific Articles and Figures

### American Society of Neuroradiology - License Terms and Conditions

This is a License Agreement between Stefan Poirier ("You") and American Society of Neuroradiology ("Publisher") provided by Copyright Clearance Center ("CCC"). The license consists of your order details, the terms and conditions provided by American Society of Neuroradiology, and the CCC terms and conditions.

All payments must be made in full to CCC.

Order Date	29-Jun-2020	Type of Use	Republish in a thesis/dissertation
Order license ID	1045048-1	Publisher	WILLIAMS & WILKINS CO.;
ISSN	0195-6108	Portion	American Society of Neuroradiology Chart/graph/table/figure

### LICENSED CONTENT

Publication Title	AJNR, American journal of neuroradiology	Country	United States of America
Author/Editor	AMERICAN SOCIETY OF NEURORADIOLOGY., AMERICAN ROENTGEN RAY SOCIETY.	Rightholder	American Society of Neuroradiology
Date	01/01/1980	Publication Type	Journal
Language	English		

### REQUEST DETAILS

Portion Type	Chart/graph/table/figure	Distribution	Worldwide
Number of charts / graphs / tables / figures requested	1	Translation	Original language of publication
Format (select all that apply)	Print, Electronic	Copies for the disabled?	No
Who will republish the content?	Academic institution	Minor editing privileges?	No
Duration of Use	Life of current and all future editions	Incidental promotional use?	No
Lifetime Unit Quantity	Up to 499	Currency	CAD
Rights Requested	Main product		

### NEW WORK DETAILS

Title	A hybrid PET/MRI brain connectivity approach for improving epilepsy surgical evaluation	Institution name	Western University
Instructor name	Dr. Udunna Anazodo, Dr. Jonathan Thiessen	Expected presentation date	2020-08-06

## ADDITIONAL DETAILS

---

Order reference number	N/A	The requesting person / organization to appear on the license	Stefan Poirier
------------------------	-----	---	----------------

## REUSE CONTENT DETAILS

---

Title, description or numeric reference of the portion(s)	Figure 6	Title of the article/chapter the portion is from	Clinical Value of Hybrid TOF-PET/MR Imaging-Based Multiparametric Imaging in Localizing Seizure Focus in Patients with MRI-Negative Temporal Lobe Epilepsy
Editor of portion(s)	Dr. Jeffrey S. Ross	Author of portion(s)	AMERICAN SOCIETY OF NEURORADIOLOGY.; AMERICAN ROENTGEN RAY SOCIETY.
Volume of serial or monograph	39	Issue, if republishing an article from a serial	10
Page or page range of portion	1796	Publication date of portion	2018-09-20



## Elsevier Science & Technology Journals - License Terms and Conditions

This is a License Agreement between Stefan Poirier ("You") and Elsevier Science & Technology Journals ("Publisher") provided by Copyright Clearance Center ("CCC"). The license consists of your order details, the terms and conditions provided by Elsevier Science & Technology Journals, and the CCC terms and conditions.

All payments must be made in full to CCC.

<b>Order Date</b>	28-Jun-2020	<b>Type of Use</b>	Republish in a thesis/dissertation
<b>Order license ID</b>	1044804-1	<b>Publisher Portion</b>	Elsevier Chart/graph/table/figure
<b>ISBN-13</b>	9780123983985		

### LICENSED CONTENT

<b>Publication Title</b>	Introduction to Diffusion Tensor Imaging 2e : And Higher Order Models	<b>Country</b>	Netherlands
<b>Author/Editor</b>	Tournier, J-Donald, Mori, Susumu	<b>Rightsholder</b>	Elsevier Science & Technology Journals
<b>Date</b>	11/26/2013	<b>Publication Type</b>	Book
<b>Language</b>	English		

### REQUEST DETAILS

<b>Portion Type</b>	Chart/graph/table/figure	<b>Distribution</b>	Worldwide
<b>Number of charts / graphs / tables / figures requested</b>	2	<b>Translation</b>	Original language of publication
<b>Format (select all that apply)</b>	Print, Electronic	<b>Copies for the disabled?</b>	No
<b>Who will republish the content?</b>	Academic institution	<b>Minor editing privileges?</b>	No
<b>Duration of Use</b>	Life of current edition	<b>Incidental promotional use?</b>	No
<b>Lifetime Unit Quantity</b>	Up to 499	<b>Currency</b>	CAD
<b>Rights Requested</b>	Main product		

### NEW WORK DETAILS

<b>Title</b>	A hybrid PET/MRI brain connectivity approach for improving epilepsy surgical evaluation	<b>Institution name</b>	Western University
<b>Instructor name</b>	Dr. Udunna Anazodo, Dr. Jonathan Thiessen	<b>Expected presentation date</b>	2020-08-06

### ADDITIONAL DETAILS

Order reference number	N/A	The requesting person / organization to appear on the license	Stefan Poirier
------------------------	-----	---	----------------

## REUSE CONTENT DETAILS

---

Title, description or numeric reference of the portion(s)	Figure 9.3, Figure 9.5	Title of the article/chapter the portion is from	Chapter 9 - Fiber-Tracking: 3-Dimensional Tract Reconstruction
Editor of portion(s)	Susumu Mori and J-Donald Tournier	Author of portion(s)	Tournier, J-Donald; Mori, Susumu
Volume of serial or monograph	N/A	Issue, if republishing an article from a serial	N/A
Page or page range of portion	81-82	Publication date of portion	2013-11-26

## PUBLISHER TERMS AND CONDITIONS

Elsevier publishes Open Access articles in both its Open Access journals and via its Open Access articles option in subscription journals, for which an author selects a user license permitting certain types of reuse without permission. Before proceeding please check if the article is Open Access on <http://www.sciencedirect.com> and refer to the user license for the individual article. Any reuse not included in the user license terms will require permission. You must always fully and appropriately credit the author and source. If any part of the material to be used (for example, figures) has appeared in the Elsevier publication for which you are seeking permission, with credit or acknowledgement to another source it is the responsibility of the user to ensure their reuse complies with the terms and conditions determined by the rights holder. Please contact [permissions@elsevier.com](mailto:permissions@elsevier.com) with any queries.

## Copyright Agreement for *European Journal of Hybrid Imaging* (Chapter 3)

**18F-FDG PET-guided diffusion tractography reveals white matter abnormalities around the epileptic focus in medically refractory epilepsy: implications for epilepsy surgical evaluation**

Author: Stefan E. Poirier et al

**SPRINGER NATURE** Publication: European Journal of Hybrid Imaging

Publisher: Springer Nature

Date: Jun 25, 2020

Copyright © 2020, Springer Nature

---

### Creative Commons

This is an open access article distributed under the terms of the [Creative Commons CC BY](#) license, which permits unrestricted use, distribution, and reproduction in any medium, provided the original work is properly cited.

You are not required to obtain permission to reuse this article.

To request permission for a type of use not listed, please contact [Springer Nature](#)

## Curriculum Vitae

**Name:** Stefan Eric Poirier

**Post-secondary Education and Degrees:** Western University  
Schulich School of Medicine & Dentistry  
London, Ontario, Canada  
2018-2020  
Master of Science in Medical Biophysics  
Supervisors: Dr. Udunna Anazodo and Dr. Jonathan Thiessen  
*Thesis:* A hybrid PET/MRI brain connectivity approach for improving epilepsy surgical evaluation

Western University  
Schulich School of Medicine & Dentistry  
London, Ontario, Canada  
2013-2018  
Bachelor of Medical Sciences, Honours Specialization in Medical Biophysics (Clinical Physics Concentration)

**Honours and Awards:** Western Graduate Research Scholarship  
2018-2020  
\$9,000 (Canadian dollar)

Eastern Great Lakes Chapter Society of Nuclear Medicine and Molecular Imaging Annual Meeting – Abstract Oral Presentation Award Winner  
2019  
\$250 (U.S. dollar)

Lawson Internal Research Fund Studentship Award  
2018-2019  
\$15,000 (Canadian dollar)

Dean's Honour List  
2013-2018

Western Scholar  
2013-2018

CIS Academic All-Canadian/OUA Achievement Award Winner  
2014

Scholar's Electives – Social Science (*Declined*)  
Western University  
2013

Western Scholarship of Excellence  
2013  
\$2,000 (Canadian dollar)

**Related Work Experience:** Graduate Teaching Assistant  
Western University  
2018-2019

## PUBLICATIONS

### Manuscripts Submitted (1):

1. **Poirier SE**, Kwan BYM, Jurkiewicz MT, Samargandy L, Iacobelli M, Steven DA, Lam Shin Cheung V, Moran G, Prato FS, Thompson RT, Burneo JG, Anazodo UC, Thiessen JD. An evaluation of the diagnostic competence of hybrid PET/MRI in clinical management of drug-resistant epilepsy. Submitted to *Am J Neuroradiol* in June 2020. Under Review. Manuscript ID: AJNR-20-00760

### Manuscripts Published (1):

1. **Poirier SE**, Kwan BYM, Jurkiewicz MT, Samargandy L, Steven DA, Suller-Marti A, Lam Shin Cheung V, Khan AR, Prato FS, Burneo JG, Thiessen JD, Anazodo UC.  $^{18}\text{F}$ -FDG PET-guided diffusion tractography reveals white matter abnormalities around the epileptic focus in medically refractory epilepsy: implications for epilepsy surgical evaluation. *European J Hybrid Imaging*. 2020;4:10. DOI: <https://doi.org/10.1186/s41824-020-00079-7>

### Conference Publications (11):

1. **Poirier SE**, Kwan BY, Jurkiewicz MT, Samargandy L, Steven DA, Suller-Marti A, Lam Shin Cheung V, Khan AR, Prato FS, Burneo JG, Thiessen JD, Anazodo UC (2020). Positron emission tomography combined with diffusion tensor imaging reveals macrostructural breakdown around epileptic foci in non-lesional medically refractory epilepsy. *2020 North American Virtual Epilepsy Meeting*. Abstract. Accepted – Online Poster Presentation.
2. Dacey MT, **Poirier SE**, Gomes J, Anazodo UC, McIntyre C (2020). Hemodialysis can contribute to acute changes in cerebral volume and white matter structure. *2020 ISMRM Virtual Conference & Exhibition*. Abstract. Accepted – Online Poster Presentation.

3. **Poirier SE**, Kwan BY, Jurkiewicz M, Steven D, Pavlosky W, Romsa J, Prato FS, Thompson RT, Burneo J, Thiessen JD, Anazodo UC (2019). FDG PET-Guided Diffusion Tractography Reveals White Matter Abnormalities Around the Epileptic Focus in MRI-Negative Epilepsy and Can Be Used to Further Enhance Epilepsy Surgical Evaluation. *2019 Eastern Great Lakes Chapter Society of Nuclear Medicine and Molecular Imaging (EGLSNMMI) Annual Meeting*, London, Canada. Abstract. Accepted – Oral Presentation.
4. Anazodo UC, Dacey MT, **Poirier S**, Suskin N, McIntyre C, St. Lawrence KS, Shoemaker JK (2019). Cardiac rehabilitation is a potential potent neuromodulator of disrupted white matter macrostructure in adults with coronary artery disease. *JCBFM Volume 39 Issue 1\_suppl, PB03-F07*. Abstract. Published. DOI: <https://doi.org/10.1177/0271678X19851020>
5. **Poirier SE**, Kwan BY, Jurkiewicz M, Steven D, Pavlosky W, Romsa J, Prato FS, Thompson RT, Burneo J, Thiessen JD, Anazodo UC (2019). PET-guided DTI investigation of white matter integrity to improve surgical planning in medically refractory epilepsy. *Clinical Neurological Sciences (CNS) Departmental Research Day*, London, Canada. Abstract. Accepted – Oral Presentation.
6. **Poirier SE**, Kwan BY, Jurkiewicz M, Steven D, Pavlosky W, Romsa J, Prato FS, Thompson RT, Burneo J, Thiessen JD, Anazodo UC (2019). PET-guided DTI analysis of white matter integrity to improve epilepsy surgical planning. *London Health Research Day (LHRD)*, London, Canada. Abstract. Accepted – Poster Presentation.
7. **Poirier SE**, Kwan BY, Jurkiewicz M, Steven D, Pavlosky W, Romsa J, Prato FS, Thompson RT, Burneo J, Thiessen JD, Anazodo UC (2019). PET-guided DTI tractography reveals white matter abnormalities in medically refractory epilepsy: applications to epilepsy surgical planning. *17<sup>th</sup> Annual Imaging Network Ontario (ImNO) Symposium*, London, Canada. Abstract. Accepted – Poster Presentation.
8. **Poirier SE**, Thiessen JD, Anazodo UC (2019). Empirical evaluation of a DTI tractography pipeline using whole-brain tractograms from a white matter phantom. *17<sup>th</sup> Annual Imaging Network Ontario (ImNO) Symposium*, London, Canada. Abstract. Accepted – Oral Presentation.
9. Anazodo UC, **Poirier S**, Kwan, BYM, Pavlosky W, Steven D, Romsa J, Prato F, Thompson T, Burneo J, Thiessen JD (2017). PET-guided structural connectivity analysis of DTI applied to neurosurgical planning in medically refractory epilepsy. *ISMRM-SNMMI Co-Provided Workshop on PET/MRI*, Chicago, USA. Abstract. Accepted – Poster Presentation.
10. Anazodo UC, **Poirier S**, Kwan BYM, Pavlosky W, Moran G, Thompson RT, Stevens D, Prato FS, Burneo J, Thiessen JD (2016). Mapping structure and functional connectivity in hypometabolic brain regions of TLE patients using

simultaneous PET/MRI. *Epilepsy Research Day*, London, Canada. Abstract.  
Accepted – Oral Presentation.

11. Wang BT, **Poirier SE**, Guo T, Parrent AG, Peters TM, Khan AR (2016).  
Generation and evaluation of an ultra-high-field atlas with applications in DBS  
planning. *SPIE Medical Imaging, 97840H*. Paper. Published. DOI:  
<https://doi.org/10.1117/12.2217126>